博士論文

Modeling of thermally induced vibration of carbon nanotubes

(カーボンナノチューブの熱励起振動のモデリング)

高　嬉淵

Contents list

List of Figures

List of Tables

1. Introduction

1.1 Outline

Quasi-1D nano materials have been used for various applications. [De Volder et al., 2013; Eom et al., 2011] Among those, single walled carbon nanotubes (SWNT)[Iijima and Ichihashi, 1993], rolled up structure of graphene ribbon, has been studied for unique mechanical, thermal and electrical characteristics. [Saito et al., 1998; Dressellhaus et al., 2004]

From initial stage of expecting nano-electro-mechanical system application, [Craighead, 2000] to composite using SWNT as its ingredient [Davis et al., 2009], the possibility of the usage of SWNT has been expanded for various applications. The approach of using assembled structure of tubular molecules also has been studied due to the enhanced properties from the pristine 1-D material, as the patterned structure made of SWNT or other quasi-1D nano materials. [Cui et al., 2013; Volder et al., 2010; Duan and Berggren, 2010]

The advantage induced from structuring of tubes starts to present very promising applications recently such as the solar cell made from vertically aligned–SWNT [Cui et al., 2014] and the carbon nanotubes (CNT) computer using horizontally aligned-SWNT. [Shulaker et al., 2013] The study of morphology of the complex network of tubes will be getting more important than ever.

Morphological study has been studied for polyethylene and other bio molecules. [Noid, 2013] But those studies is related to the characteristics of entanglement within the solutions due to its given circumstances for bio-molecules. The bio-molecules are structured inside dense solutions such as water. Such condition has not been considered for the morphology of CNT so

that the study has suggested the entanglement by bundling and fully stabilized structure by minimizing potential energy between tubes. [Li and Kroger, 2012a, 2012b; Volkov and Zhigilei, 2010b; Won et al., 2012]

Multi-scaling model of thermal-mechanical motion for morphology has been shown that the effect of buckling inside of the complex makes the stabilized entanglement. [Li and Kroger, 2012a, 2012b, Volkov and Zhigilei, 2010b; Won et al., 2012] And such buckling might be decided not only by the static tube-tube interaction, but also by excessive dynamic collisions due to the thermal vibration during its growth. The structure built from real physical condition from its growth will contribute the study for the properties of materials [Volkov and Zhigilei, 2010a] and mass production for the networks of tubular or quasi-1D materials. Precise and efficient description for bending and buckling of SWNT in static and dynamics is the possible first step toward better and precise study of complex of molecular system. Better expression would also help bridging scale domain [Xiao et al., 2004; Sadeghirad et al., 2013] and better tuning for nano-electical devices. [Scheible et al., 2002; Lassagne et al., 2009; Castellanos-Gomez et al., 2012]

In this thesis, the bending motion of SWNT in various conditions is explored using molecular dynamics (MD) simulation. The nonlinear behavior of the free thermal vibration [Eom et al., 2009] in SWNT is observed and compared with nonlinear bending equation. Nonlinearity based on the classical Green-Lagrange strain tensor is adapted to confirm the applicability of continuum mechanics to the dynamics of molecular system. The beam models from the most advanced stress-strain definition for nano-poly-crystal system [Askes and Aifantis, 2011] are not included in this thesis because the focus of those models is the definition

of planar bending motion. Instead of the better expression for strain, more phenomenological condition of the motion in SWNT is studied intensively for practical reason. The comparison will show that the interplay between the displacements of two transverse waves in orthogonal axes of the SWNT system is the main contribution of peak broadening, i.e. relaxation time of the lowest transverse vibration mode of SWNT.

The importance of this motion for morphology is also briefly discussed and conventional coarse grained molecular dynamics (CGMD) is examined whether it can afford the nonlinearity of SWNT and other thermal-mechanical motion caused by the collision between other SWNT, forced excitation and thermally disturbed boundary condition.

In Chap 1, motivation of the study using continuum mechanical frame works and background of this thesis is explained briefly. Chap 2 will introduce the simulation by MD simulation for free thermal vibration of SWNT, forced excitation using mechanical excitation and colliding condition. Chap. 3 is dedicated for comparison the nonlinear motion of free thermal vibration to bending equations and the interpretation of each parameter is discussed. The derivation of the governing equation is attached as Appendix. Applicability of CGMD for the nonlinear response of SWNT revealed and analysed in Chap.3 is in Chap 4. The brief summary and suggestions is in Chap. 5.

1.2 Continuum frame works for SWNT

The frame works of continuum mechanics [Qian et al., 2002] has been used to describe enormous strength [Krishnan et al., 1998; Treacy et al., 1996; Ouyang et al., 2007] and high Q factor [Huang et al., 2006, Poncharal, 1999] of SWNT. Such properties profit many state-of-art experimental set ups for applications using SWNT such as mixers [Eichler et al., 2011; Sazonova V., 2004], sensors [Eom et al., 2011; Gil-Santos et al., 2010; Jensen et al., 2008; Sawano et al., 2010; Waggoner and Craighead, 2007] including pioneering researches on the motion of wave guide [Zhang et al., 2012; Chang et al., 2007] and quantum theory on macroscopic motion of SWNT [Carr et al., 2001; Katz et al., 2008], which are deeply related with low frequency transverse mode of SWNT. Cantilevered SWNT is, especially focused for scanning microscopy [Viani et al., 1999; Yu et al., 2002] and atomic force microscopy. [Hornstein and Gottlieb, 2012]

1.2.1 Stress and Strain for atomic system

While the discovered properties of CNT have been applied in experiments lively, the theory to describe its stress-strain condition for nano-micro-structure also has been advanced.

Conventionally, the strain-stress definition is a description of a line segment mapping in a deformed continuum body by transformation matrix from initial un-deformed body. The total length of a line segment in deformed body can be expressed using the combination of two matrices, the transformation matrix and its transpose matrix. When deformed condition is measured by strain, the stress is defined as same rank of matrix with strain so that projecting the eigen vector, normal vector of certain surface, to the matrix offers the force acting on that cross

section. The linear one-to-one relation between stress-strain is famous Lame constants, which are each component of 9x9 matrix. [Lai et al., 2009]

In case of macro-nano scale of deformation or stress, the target systems are composed of discretized mass and each mass is vibrating with their own thermal energy. Even the deformation or mechanical vibration are analyzed using continuum mechanics, the influence of thermal and quantum behavior is regarded as very important factor to excuse the discrepancies of result from analysis or to discover some unique features of nano materials. [Capaz et al., 2005; Lassagne et al., 2009; Peano et al., 2004; Werner and Zwerger, 2004]

There have been vast efforts on better stress-strain description, and the history and critical reviews are well organized in [Miller and Tadmor, 2003; Askes and Aifantis, 2011]. In the next paragraphs, the most advanced study for SWNT is briefly explored to distinguish the difference from what is used in Chap 3.

In case of strain, the specific mapping step for the curvature of cylinder shape of SWNT adjusts the strain energy from bending and torsional deformation at zero temperature. In this way, the deformation energy of SWNT, whose results had not fully explained by Born-rule is well matched with exponential mapping on tensor terms in statics [Arroyo and Belytschko, 2003; 2004]. In static condition, SWNT is following the same strain energy with Continuum mechanics until its Yielding point. [Yakobson et al., 1996] However, the bending motion of SWNT is out of scope from this approach.

The stress definition for molecules, the thermal energy is one reason causing the stress, therefore, it should be a part of stress source. In case of the virial or Hardy's definition [Zimmerman et al., 2004], which are most commonly adapted [Zhou, 2000; Gall et al., 2004],

the velocity of atoms in crystal at certain temperature are calculated in MD simulation and used as an ingredient of stress. In this way, the stress values are decided by empirical way as conducting the atomic simulations.

The continuum mechanics for describing the atomic structure and its behavior is still on going research for bridging atomic level to the conventional stress-strain field where Lame constants are valid. This is well known problem as multi-scale modeling [Eillot, 2011]. Direct link of atomic level simulation to continuum mechanical dynamics [Xiao, 2004; Sadeghirad and Tabarraei, 2013] needs quiet rigorous understanding about damping in both criteria and the achievement will offer the direct breakthrough to calculate multi-scale phenomena and the surface energy of nano materials.

In this sub section, some latest achievements from continuum frame works for SWNT were briefly introduced with their general differences from the strain condition which is adapted for this study.

1.2.2 Beam modeling

The validation of beam modeling in dynamics is not straight forward as static cases due to its kinetic energy directly related to thermal energy. [Feng and Jones, 2010; 2011; Schuster et al., 2008]

In the simulation [Feng and Jones, 2010] and measurement [Warner et al., 2011], Timoshenko beam is known to be more similar to SWNT in dynamics and statics than Euler -Bernoulli beam. For the nonlinear behavior of SWNT in FET system or cantilevered SWNT, the Euler-Bernoulli beam with additional higher order term has been adapted for a planar

bending motion. [Mitra, and Gopalakrishnan, 2007; Villanueva et al., 2013, Wang and Hu, 2005] The planar motion of nonlinearity is examined in other research for different purpose such as analyzing the simple higher order term [Kozinsky et al., 2007; Lifshitz and Cross, 2008], trials for tuning such behavior in frequency domain [Kozinsky et al., 2006; Verbridge et al., 2007] and predicting the reasonable range of dynamics [Villanueva,2013; Posta et al., 2005].

While the applicability of nano-electro-mechanical devices has been researched, the causality of the frequency response of the devices, which is supposed due to the macroscopic motion, also has been focused. In case of single peak broadening, the electron transport during the oscillating of suspended SWNT [Lulla et al., 2013], the tunneling of phonons through the substrate [Wilson-Rae, 2008] and its thermal noise influence [Feng and Jones, 2011] has been considered. Multiple resonances peaks which has been reported in suspended FET system, was studied right after its finding [Sazonova et al., 2004] and the slack condition tackled as the reason of jumping rope like motion in SWNT. [Ustunel et al., 2005; Conley et al., 2006] The model of slacks of suspended SWNT, with the range of slack controlled by gate voltage, has shown the very similar trend on frequency shift. Recently, the multiple peaks in various range of temperature is shown in only slacked condition in the experiment.[Eichler et al., 2011] Such result suggests the possibility of those multiple peaks from the resonance is caused by the nonlinear damping occurred during the forced excitation, however, specific description and detailed understanding how such motion is related to damping mechanism is still in veil.

1.3 Thermal-Mechanical motion

Thermal vibration is often regarded as an important characteristic with bio-molecules, such as protein folding and the formation between various shaped molecules. On the contrary, the motion with long wave length with low frequency, has been mostly focused on the forced excitation response to use such motion as sensors or mixers based on its high quality factor instead of the thermal-mechanical motion. High Q factor, which decides the sensibility of measuring masses or surface, of cantilevered CNT in vacuum chamber is easily degraded in various environments and temperature. [Sawano et al., 2012]

Separately from this problem in experiments, several theoretical modeling for energy dissipation from its 1st mode, which makes lower Q factor is pursued. [Lifshitz and Roukes, 2000; Banard et al., 2011; Wilson-Rae, 2008; Feng and Jones, 2011] Up to the writer's knowledge, yet, the direct contribution to peak broadening has not been fully elucidated. Understanding of the direct reason of peak broadening may not offer the direct solution to the applications, but would be fruitful for more advanced future devices.

Recently, the response of dynamics like transverse mode in SWNT is shown to have a good agreement with continuum bar theories. [Feng and Jones, 2010] This study showed the frequency and amplitude of cantilevered SWNT are predictable with righteous Young's modulus. Unlike frequency and amplitude, damping in beam theories are quiet different [Feng and Jones, 2011] from that of molecular vibration because the damping in continuum mechanics is defined to make the half of kinetic energy dissipated out during the relaxation time. [Cremer et al., 1990] The energy of the vibration in molecular system supposed to be remained but changes its state of standing wave, i.e. state of phase as a result of relaxation.[Ladd et al., 1960]

The state of the transverse mode in high temperature is easily varied and makes short relaxation time, as shown in many previous works. [Banard et al.,2012; Rhoads et al., 2010]

On the other hand, the recent experiment and theories on the response of SWNT [Eichler et al., 2011; Willson-Rae et al., 2011] with forced excitation, have suggested nonlinear damping which is emerged with multiple peaks in frequency domain. In this case, the conventional measurement of relaxation time i.e Q factor measured using Lorentzian fitting is difficult to be applied. Such multiple peaks in frequency range means the beating signals in time domain. This gives significant clue on how the macroscopic motion in low frequency around transverse mode should be. Nonlinearity of macroscopic motion like jumping rope [Conley et al., 2006; Ustünel et al., 2005] can be one possibility to have beating signal. Those result based on jumping rope motion has the closest match with experimental works in nonlinear continuum dynamics regime, which has beating including the frequency shift dependency with excitation level. The suggetions from these nonlinear models, yet, remained with missing parameters and precise description to stress-strain format.

To distinguish with other small wave length modes, 1st transverse mode is named as thermal-mechanical motion because it is thermally induced mechanical motion and its energy exchange with heat and macroscopic motion.

1.4 Molecular Dynamics (MD) simulation

As the boundary of classical mechanics based on Newton's equation of motion, physical characteristics, such as thermal transport, dynamics of molecules has been studied using MD simulation. From the detailed replica of molecular system, which is built using point mass for an atom and the network of potential wells for bonding structure between atoms, the simulation is expected to offer modal response of the molecular at certain temperature.

- Integration scheme

For the accuracy, the potential function, which decides atom-atom interaction should follow the real condition of the system. As such, enormous studied have been done after the basic concept of molecular potential function is established. Force calculated from potential well network can point out the location of the atom during certain time span by integrating the equation of motion. Since all the atoms are vibrating with its thermal energy, the integration algorithm should consider the displacement from velocity at the same time. The velocity verlet integration makes the time step between velocity and force same so that it minimize the accumulation error. The order of calculation for velocity verlet is as below:

1. Location of each atoms are integrated from given momenta and potential force

$$\vec{x}(t+\Delta t) = \vec{x}(t) + \vec{v}(t)\Delta t + \frac{1}{2}\vec{a}(t)\Delta t^2$$

2 Calculating acceleration $\vec{a}(t+\Delta t)$ from new location $\vec{x}(t+\Delta t)$

3 Velocity is updated using current acceleration $\vec{a}(t+\Delta t)$

$$\vec{v}(t+\Delta t) = \vec{v}(t) + \frac{1}{2}\left(\vec{a}(t) + \vec{a}(t+\Delta t)\right)\Delta t$$

After the molecule structure is designated by potential well network, filling the point mass with kinetic energy with certain temperature is essential. There are several algorithm of pouring the thermal energy to point masses in simulation, but in this thesis Langevin thermostat is mainly used.[Schneider, 1978]

- CGMD simulation

CGMD has lumped mass as a node with simplified network representing the full structure of molecules with same integration algorithm as described above. Less point mass mean the advantage in its efficiency. The same efforts with more efficient size of simulation covers the range between the atomic level of vibrations and continuum level of motion.[Foteinopoulou et al., 2008; Wang et al., 2012]

Thanks to its simplified structure, this method is suitable to run a simulation for large scale of number of molecules such as lipid [Noid, 2013] or massive network of SWNT. [Li and Kröger 2010a; 2010b] Morphology for complicated structure with SWNT or CNTs (Bucky paper) and its mechanical property has been studied using same method.[Buehler, 2006; Kim et al., 2008; Zhigilei et al., 2005] The main interest has been the structure and response of bunch of molecules with various thermal condition, rather than that of a single molecules. Inter-molecule potential and dissipation caused between the molecules, therefore, are more important.[Fritsch et al., 2013; Zhigilei et al., 2005] Yet, the real modal response of SWNT or quasi-1D system in CGMD is not fully considered. [Buechler, 2006; Jacobs et al., 2012]

2. MD simulation

As a tool of observation for the motion of SWNT with its thermal energy, MD is the one method which can afford such demmand. In this chapter, various simulation model is explored to measure the simuilarity of the dynamics of SWNT to the continuum beam models. In Sec. 2.1, cantilevered and suspended free thermal vibration is introduced. In Sec. 2.2, the response from the external mechanical excitation of SWNT is observed and briefly, the collision caused by other tube is calculated in Sec. 2.3.

2.1 Free thermal vibration

- Preparation

SWNTs with various aspect ratios is prepared as in Table 2.1~2.4 for free thermal vibration. On performing MD simulations, I used LAMMPS package. [Plimpton, 1995] and employed the Adaptive Intermolecular Reactive Bond Order (AIREBO) potential function [Stuart et al., 2000] to describe the carbon-carbon interaction. Schematic figure of the system used in this work is depicted in Fig. 2.1 (a). To realize the fixed-free/fixed-fixed boundary condition, the Lennard-Jones (12-6) potential is used instead of zero kevin condition. [Feng and Jones, 2010; 2011] This method is also known as phantom wall. The coefficients of this potential, ϵ_{LJ} and σ, are 20eV and 0.8909, respectively. The influence of rigidity of fixation also considered with three different ϵ_{LJ}, 5 eV, 20 eV, 80 eV and zero temperature case as in Table 2.2. This potential is applied with the coordinate to each atom in a ring at the bottom. The coordinate after energy minimization is used as its minimum potential energy point. The length in Table 2.1 is after the energy minimization condition.

The integration time step size is 0.5 fs.

A Langevin thermostat [Schneider et al., 1978] is used with damping coefficient of 0.01. I also examined Nose-Hoover thermostat [Nosé, 1984] and the results are not differed significantly. After thermostat process for 1 ns and another 1 ns under on NVE ensemble condition, the data from the system is gathered at the ring located at 7.5 nm and 22.8 nm from the bottom. Simulations are performed over 20 ns time span at 50, 100 and 300K, mainly. Higher temperature condition also explored as in Table 2.3. The total energy was conserved during the whole simulation time as well as the temperature.

The motion observed from the MD simulation shows non-planar and planar motion repeatedly as in Fig. 2.1 (b) and (c). These motions are occurred during the total energy is remained as constant. Unlike the reported 1st transverse motion of SWNT, the motion itself does not similar to the simple harmonic beam equations, [Feng and Jones, 2010; Cremer et al., 1990] the motion calculated from all the SWNTs shows circular motion with certain period. For better observation, the trajectory of tip location is drawn into Poincare map.

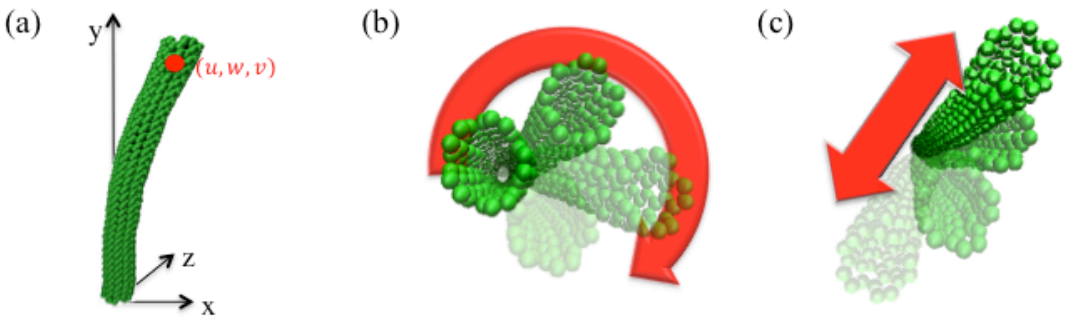

Fig. 2.1. Visualization of motion with the coordinate from MD simulation and poincare map for the trajectory of tip location. The averaged coordinate of each ring in perpendicular axis to tube axis is amplified 5 times to visualize the motion: (a) schematic figure of system, (b)non planar motion, (c)

planar motion.

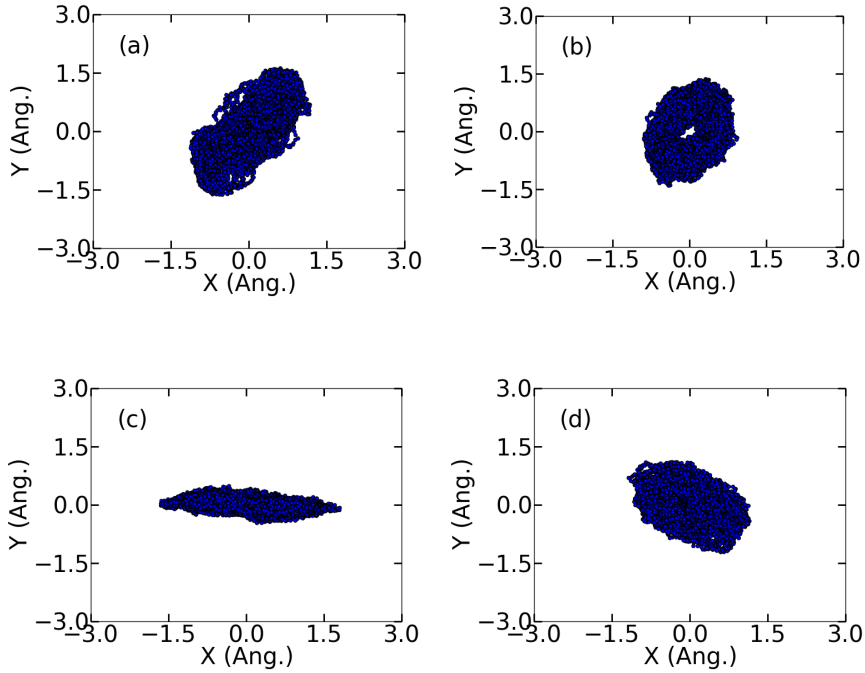

Fig. 2.2. Poincare map for free thermal vibration during 10 ns; (a) 1.2 ns~ 1.8 ns, (b),3.6 ns ~ 4.2 ns, (c)8.4 ns ~ 9.0 ns, (d) 6.0 ns~6.6 ns .

2.1.1 Cantilevered SWNT

- **Poincare map**

The poincaré map including the trajectory during 0.6 ns in Fig. 2.2 shows the motion of (5,5) 7.8 nm long SWNT, by free thermal vibration in simulation has highly nonlinear and non-planar characteristics despite of the constant total energy. The total displacement is varying as switching the motion between planar as in Fig. 2.2 (a) and non-planar as in Fig.2.2 (b). From the poincaré map, I found that the plane of the bending motion is changing after the appearance of whirling as shown in Fig. 2.2 (a) and (c). Results from higher temperature show more

frequent exchanging between planar and non-planar motion. This kind of non-planar motion has been shown in SiC nanowires during the experiment with the external force excitation in field emission method system. [Perisanu et al., 2010; 2011; 2007] The difference of the motion of SiC nanowire is that there is the motion exchange between planar and non planar in free thermal vibration of SWNT.

About the detailed trajectory of non-planar motion, it is on Fig. 2.2 (a) is divided into 0.06 ns resolution of 1st transverse mode as shown in Fig. 2.3. (a)~(c). There are clear small loops caused by higher frequency mode during big circular motion from 1st transverse mode.

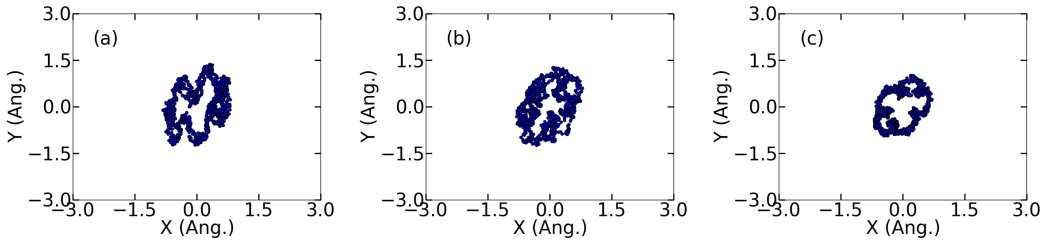

Fig. 2.3. Poincare map for free thermal vibration with fine resolution for the motion during (a) 3.66 ns ~ 3.72 ns, (b) 3.9 ns ~ 3.96 ns, (c) 4.08 ns ~ 4.14 ns.

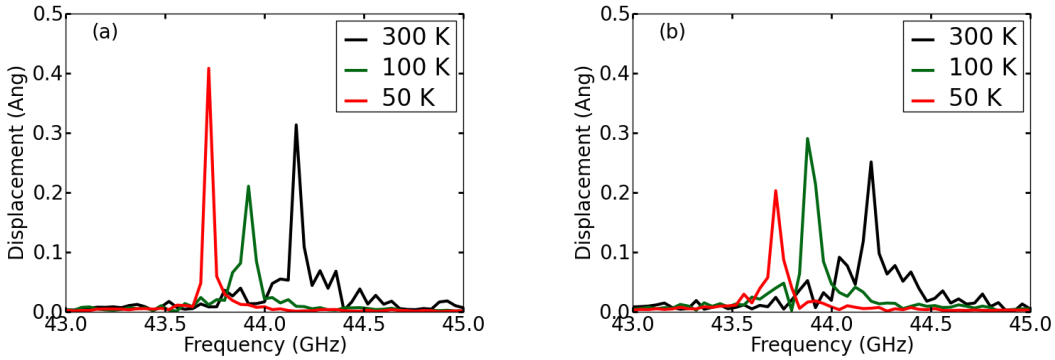

Fig. 2.4 Frequency response of free thermal vibration of (5,5) 7.8 nm: (a) along x axis and (b) y axis.

Especially, it is important to emphasize that the motion of rotation is also exchanging, for example, from clock-wise to counter-clockwise directions after its planar motion. Such condition is not well described in Fig. 2.3 with the Poincare map. However, it is not easy to quantify whether the motion is in planar or changing its rotation due to these small ripples from higher order transverse mode with the trajectory as in Fig. 2.3.

- Frequency response

The frequency response of the displacement along x and y axis is are Fig. 2.4 and Fig 2.5. The motion from non-planar to planar makes beatings in time signal and this beating signal gives several peaks in frequency range. All the simulations in Table 2.1~ Table 2.6 show two common features. One is the frequency shift as the temperature increasing and the other one is the peak shape with multiple peaks, as shown in Fig. 2.4 and Fig. 2.5.

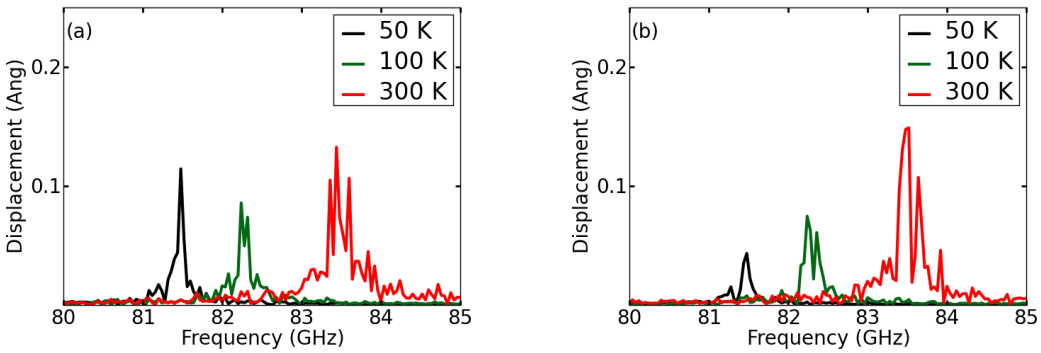

Fig. 2.5. Frequency response of free thermal vibration of (10,10) 7.8 nm: (a) along x axis and (b) y axis.

It should be noticed that this kind of multiple peaks is preventing to measure the right relaxation time which is equal to the inverse of Q factor using Lorentzian fitting [Ladd, 1986;

Wilson et al., 2011] In case of SWNT or other molecular system with thermal energy, it has a constant total energy during the relaxation process, which does not dissipate out the vibration energy as the definition of Lorentzian fitting with the damping mechanism in conventional beam theory. This difference will be discussed in Sec. 3 more.

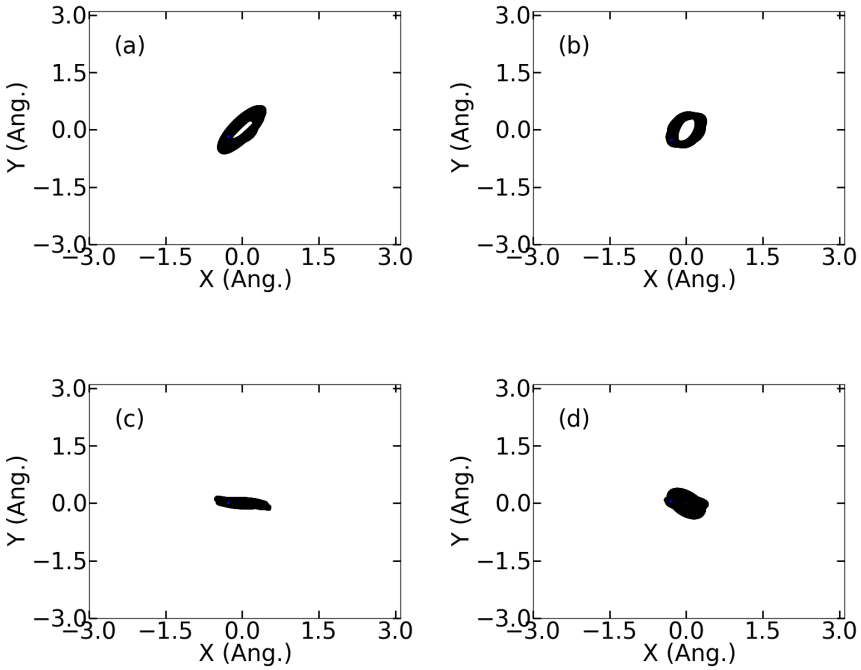

Fig. 2.6. Poincare map after IFFT process from Fig. 2.2: (a) 1.2 ns ~ 1.8 ns, (b) 3.6 ns ~ 4.2 ns, (c) 8.4 ns ~ 9.0 ns, (d) 6.0 ns ~ 6.6 ns.

As mentioned in Chap. 1, the purpose of the thesis is to study the motion of 1st transverse mode. The simple Inverse–FFT (IFFT) is used to quench out the other higher frequency components in time domain. With this process, more clear shape of trajectory caused by 1st transverse mode can be observed as in Fig. 2.6.

- Rotation exchange

While the motion is exchanging between planar and non-planar motion, the rotation direction also opposed from what it has, for instance, from clock-wise to counter clock wise or vice versa. To quantify such behavior of SWNT, the angle of the location of the tip is calculated and the increase is measured from IFFT-ed signal.

The angle is calculated by $\Theta = \tan^{-1} x/y$ as shown in Fig. 2.7 with the displacement signal treated with inverse-fft as in Fig. 2.6. The difference of $\Theta, \Delta\Theta$ is calculated for each 100 time steps, which is 50 fs. Basically, this is the angular velocity of the tip of SWNT during free thermal vibration. If $\Delta\Theta$ is bigger than 0, it is clockwise rotation and otherwise, it is counter clock-wise. The result for (5, 5) and (10,10) are presented in Fig. 2.7 and 2.8. The spikes as shown at 6 ns in Fig. 2.8 (c), are due to the planar-like motion. When the tip motion is on perfect planar motion, $\Delta\Theta$ should be close to zero, however, such condition is not observed in any of simulations. When tip has planar – like motion near the origin (0,0), $\Delta\Theta$ becomes maximum/minimum depends on its rotation direction.

As shown in Fig. 2.8 and Fig. 2.9, $\Delta\Theta$ keeps repeating its motion from positive value to opposite or vice versa. This indicates the rotation is exchanging its direction and one common trend could be pointed out from all the simulation results. The result at higher temperature has more exchange than lower temperature as Fig. 2.8 (a) and (c). And thick SWNT such as (10,10) SWNT in Fig.2.9 has more frequent exchange than relatively long and slender SWNT like (5,5) at same temperature. The figures like Fig. 2.8 for the rest of simulation models in Table I is contained in Appendix I.

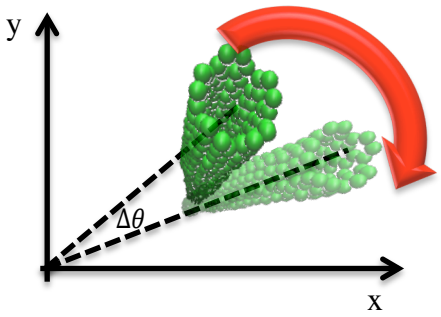

Fig. 2.7. Schematic figure to measure the rotation exchange.

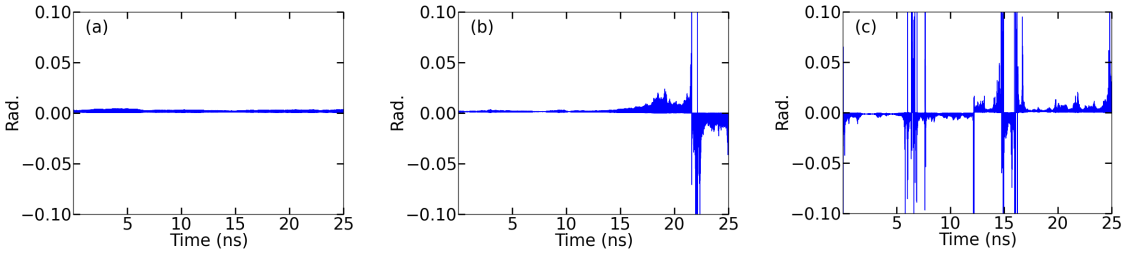

Fig. 2.8. Angle difference plot for (5,5) 7.6 nm; (a) 50 K, (b) 100 K, (c) 300 K.

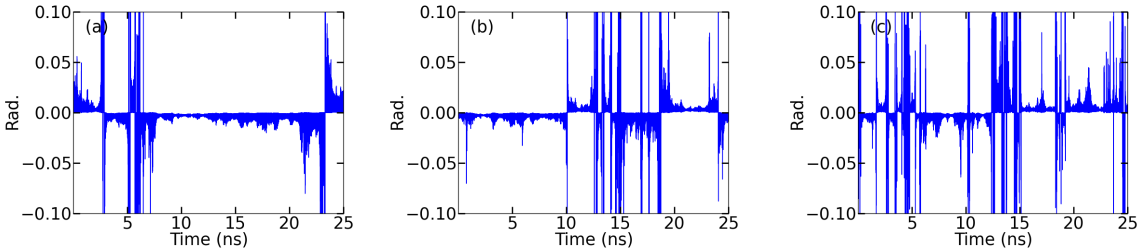

Fig. 2.9. Angle difference plot for (10,10) 7.6 nm; (a) 50 K, (b) 100 K, (c) 300 K.

2.1.2 Suspended case

Suspended condition with (5,5) 7.6 nm and 23.5 nm has been calculated to show its free thermal motion. It has same non-planar and planar motion exchange and rotation exchange as cantilevered condition. The list of simulation list is in Table 2.4.

As shown in Fig. 2.10 (a), which is calculated from (5,5) 7.6 nm at 300 K with fixed-fixed boundary condition, more frequent rotation exchange is observed than the cantilevered condition during same time span.

The trend suggested in Sec 2.1.1 for cantilevered case also valid in suspended simulation. Longer SWNT such as (5,5) 23.5 nm does not have the rotation exchange at all during the same number of osciallation and temperature with (5,5) 7.6 nm, so the higher temperature condition, 500 K is tried. The result in Fig. 2.10 (b) is the result at 500 K and both (a) and (b) has about 700 times of oscilaation. The motion of 50 nm is shown in Fig. 2.10 as the poincare map. This kind of motion with rotation exchange and motion exchange assure that the freuquency response of suspended simulation also has multiple peaks, so that Lorentzian fitting is not valid anymore.

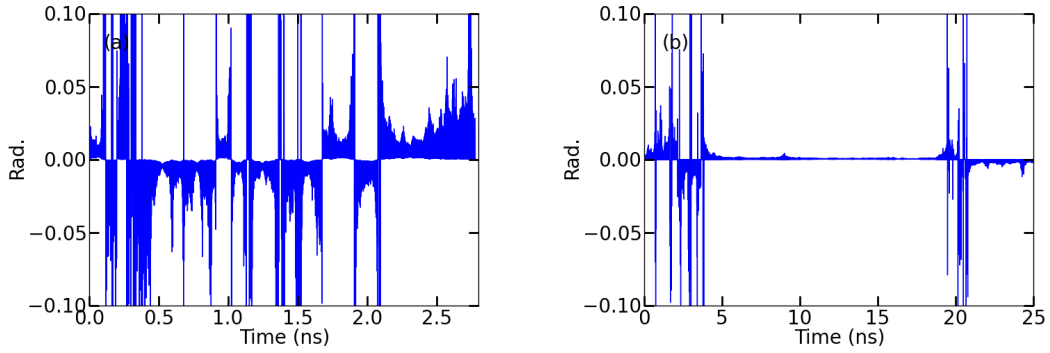

Fig. 2.10. Angle difference plot for suspended case during 700 times oscillation; (a) (5,5) 7.8 nm at 300K, (b) (5,5) 23.5 nm at 500 K.

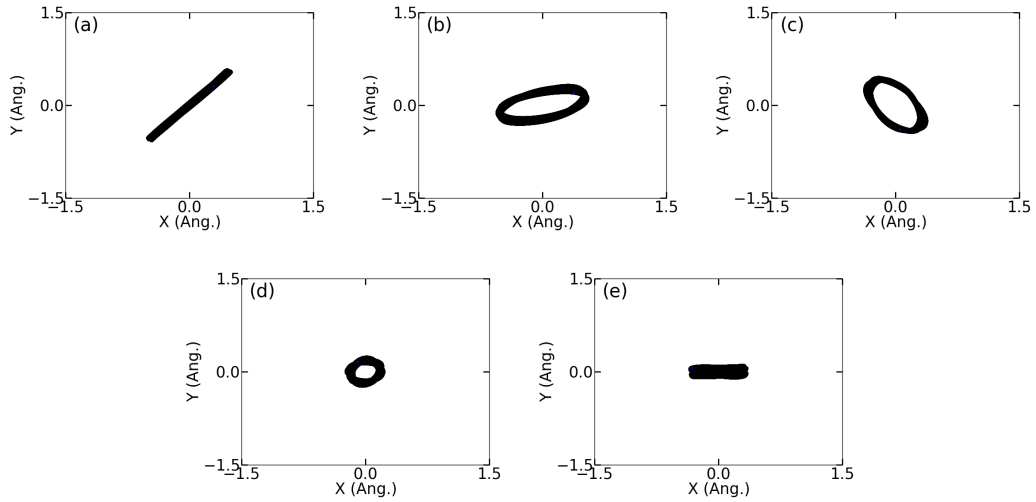

Fig. 2.11. Poincare map for suspended case of (5,5) 23.5 nm at 500K. Each figure has 0.6 ns duration; (a) 2.2 ns, (b) 7.2 ns, (c) 12.2 ns, (d) 17.2 ns, (e) 22.2 ns.

2.2 Forced Excitation

- Preparation

With the same configuration of free thermal vibration case, mechanical excitation by locating the bottom ring – a half unit cell, with the resonance frequency of a cantilevered SWNT is successfully performed. The schematic figure of the model is in Fig. 2.12. The list of simulation is in Table 2.5.

About this steady energy offering to the system, attachment of the thermostat for a unit cell including the bottom ring resolves the energy stacking situation. The simulation can not endure the resonance frequnecy excitation without thermostating for few steps. This thermostat does not work if the bottom ring fixed with zero temperature, which is perfect rigid boundary but operates well with phantom wall condition. This is the fixation explained in Sec. 2.1. The same condition of

phantom wall in Sec. 2.1. is used.

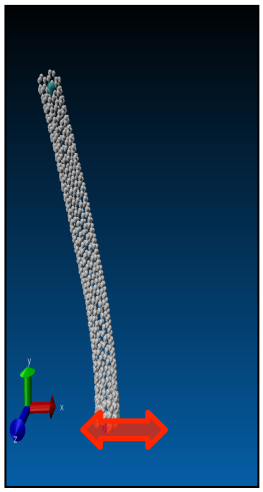

Fig. 2.12. Schematic view for forced excitation simulation.

Excitation with 0.01 Angstrom with 44.5 GHz is given to the (5,5) SWNT 7.8 nm based on the frequency plot in Fig. 2.3. The langevin thermostat is used with damping coefficient 0.001 for a unit cell including the fixed boundary part. Half unit cell langevin also tried with same condition. Total energy and temperature is remained as constant during the whole simulation time as shown in Fig. 2.13.

- Poincare map

The poincare map from the trajectory of top ring from three different temperature with mechanical exciation is presented in Fig. 2.14. With 0.01 Anstrong excitation along x axis, the non-planar motion becomes bigger but still has motion exchanging between non-planar to planar or vice versa.

- Frequency response

All three temperature conditions have a peak at 44.5 GHz, which is the frequency of excitation. And the original peaks observed in Fig. 2.4 with free thermal vibration condition remained with the same trend; higher temperature with higher frequency. Interestingly, except the existing peaks, the result of 300 K and 100 K shows another peaks in lower range in the Fig. 2. 15 (a). This additional peaks represent the time signal has more beating than free thermal vibration.

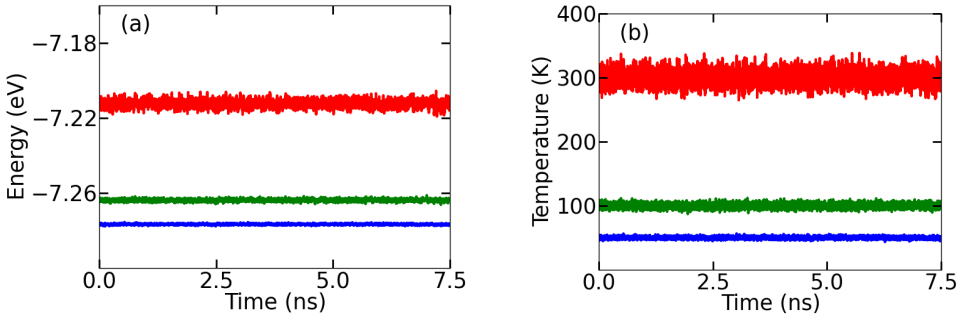

Fig. 2.13. Energy and temperature profile for forced excitation with langevin thermostat; (a) Total energy with 0.01 Ang excitation, (b) Temperature with 0.01 Ang excitation.

- Rotation exchange

As free thermal vibration, the rotation exchange is also observed, however, the trend of temperature with more rotation exchange is difficult to find as shown in Fig. 2.16. To exclude the influence of thermostatting at the bottom with random dissipation, the rotation exchange only with thermostatting is observed in Fig. 2.16. Thermostatting without forced excitation does not show the significant violation of trend found in free thermal vibration, but in case of forced excitation with thermostatting, 100 K has more exchange than 300 K, which means the rotation exchange is working differently as a part of damping.

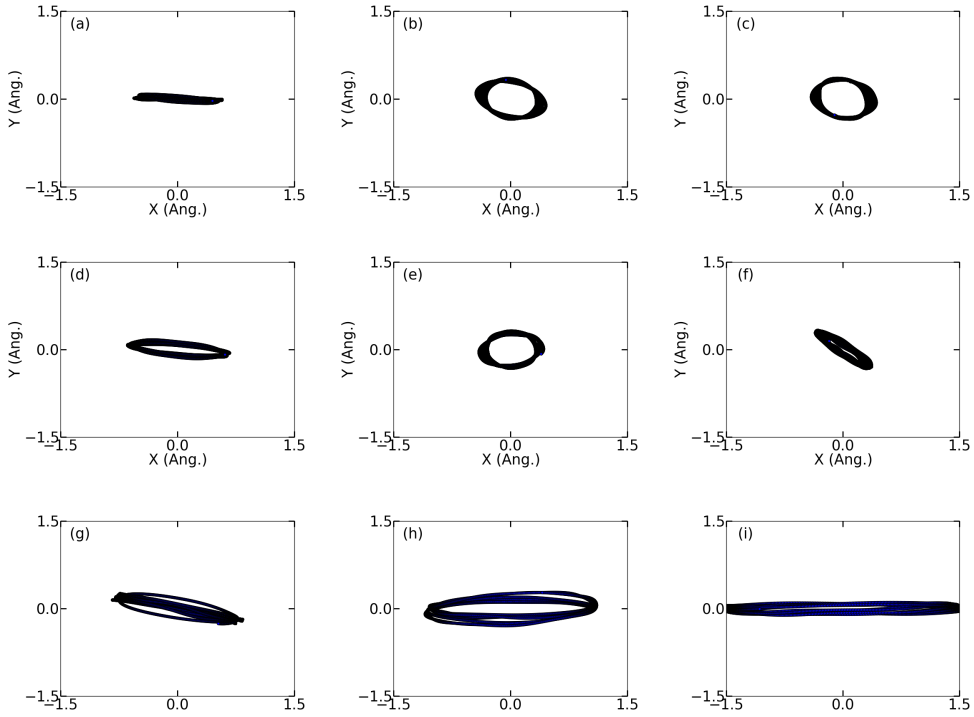

Fig. 2.14. Poincare map for forced excitation with 0.01 Ang.; (a) 0.7 ns ~ 0.8 ns at 50K, (b) 3.7 ns ~ 3.8 ns at 50K, (c) 6.7 ns ~ 6.8 ns at 50K, (d) 0.7 ns ~ 0.8 ns at 100K, (e) 3.7 ns ~ 3.8 ns at 100K, (f) 6.7 ns ~ 6.8 ns at 100K, (g) 0.7 ns ~ 0.8 ns at 50K, (h) 3.7 ns ~ 3.8 ns at 300K, (i) 6.7 ns ~ 6.8 ns at 300K.

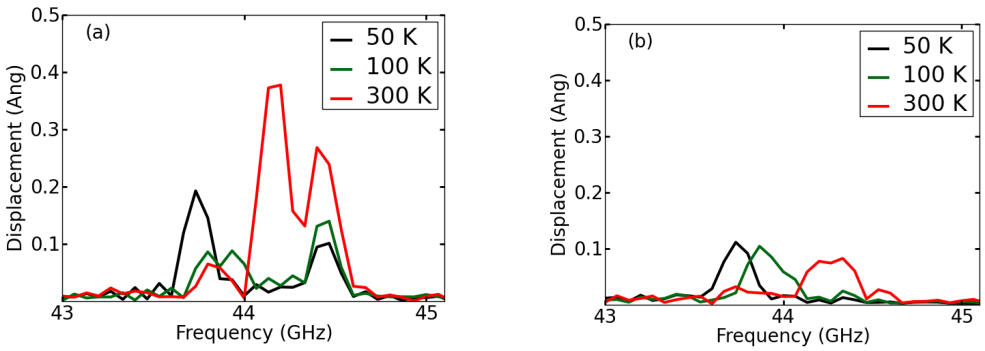

Fig. 2.15. Frequency response of forced excitation with 0.01 Ang along frequency (GHz) unit; (a) displacement along X axis, (b) displacement along Y axis.

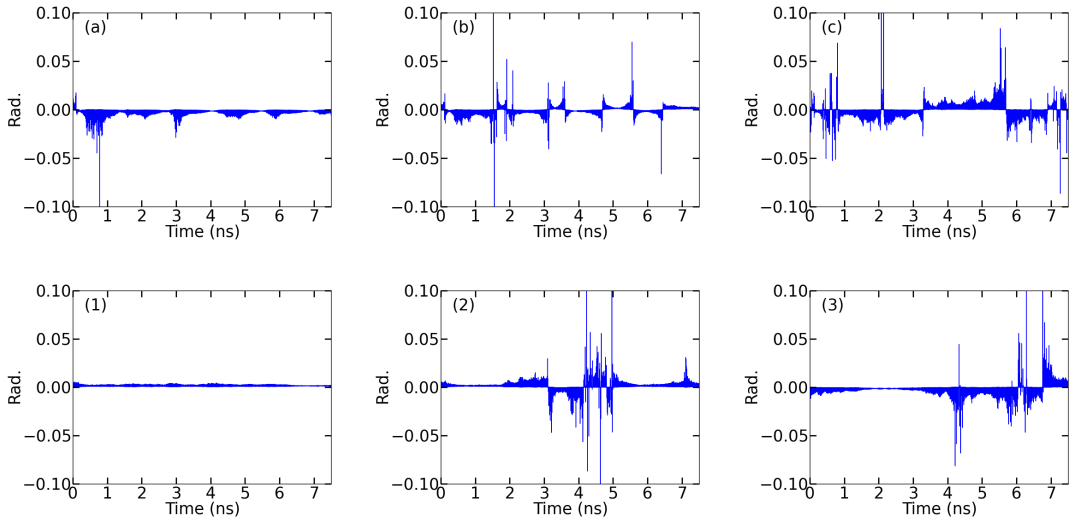

Fig. 2.16. Angle difference plot of forced excitation with 0.01 Ang; (a) 50K, (b) 100K, (c) 300K. Rotation exchange plot of thermostatted condition; (1) 50K, (2) 100K, (3) 300K.

2.3 Collisions between SWNT

The response of (5,5) 23.5 nm long SWNT from the collision is measured. The specific condition of simulation is in Table 2.6. Both tube are prepared in suspended fixation as Sec. 2.1.2 with 300 K. The tube which makes the collision, is given with artificial deformation with cosine fuction and arranged to meet at the middle each other, so the coordinate of this tube is rotated with 90 degree. The amplitude of this cosine function is 15 Ang. Both tubes have fixed-fixed boundary and located to be perpendicular with same center. More detailed condition is in Table 2.6. Further analysis will be discussed in Sec. 4. The analysis is performed only for the tube which is collided.

Table 2.1. Simulation condition with various aspect ratio

	r (nm)	Num. of Atoms	L (nm)	Temp. (K)	ε_{LJ} (eV)	σ (Å)	Total Simul. Time (ns)
(5,5)	0.34	400	4.28	50	20	0.89	25
				100			
				300			
		480	5.58	50			
				100			
				300			
		560	6.56	50			
				100			
				300			25/50
		660	7.6	50			25
				100			
				300			
		820	9.8	50			125
				100			
				300			
		1620	197.9	50			225
				100			
				300			
(10,10)	0.667	1320	7.6	50			25
				100			
				300			
		4000	25.3	50			22.5
				100			
				300			
(20,20)	1.36	8000	0.147	50			
				100			
				300			

Table 2.2. Simulation condition with various boundary rigidity

	r (nm)	Num. of Atom	L (nm)	Temp. (K)	ε_{LJ} (eV)	σ (Å)	Total Simul. Time (ns)
(5,5)	0.336	660	7.6	300	5	0.89	25
					20		
					80		
					0 K		

Table 2.3. Simulation condition with various termperature

	r (nm)	Num. of Atom	L (nm)	Temp. (K)	ε_{LJ} (eV)	σ (Å)	Total Simul. Time (ns)
(5,5)	0.336	660	7.6	50	20	0.89	25
				100			
				300			
				500			
				800			
(10,10)	0.67	1320	7.8	50			
				100			
				300			
				500			
				800			

Table 2.4. Simulation condition with suspended boundary

	r (nm)	Num. of Atom	L (nm)	Temp. (K)	ε_{LJ} (eV)	σ (Å)	Total Simul. Time (ns)
(5,5)	0.336	660	7.6	300	20	0.89	50
		2000	23.5	300/500			
(3,3)	0.23	1188	24.1	300			

Table 2.5. Simulation condition with external excitation

	r (nm)	Num. of Atom	L (nm)	Exci. (Ang)	Temp. (K)	ε_{LJ} (eV)	σ (Å)	Total Simul. Time (ns)
(5,5)	0.336	660	7.6	0	50	20	0.89	7.5
					100			
					300			
				0.01	50			
					100			
					300			
				0.1	50			
					100			
					300			

Table 2.6. Simulation condition for collision

	r (nm)	Num. of Atom	L (nm)		Temp. (K)	ε_{LJ} (eV)	σ (Å)	Total Simul. Time (ns)
(5,5)	0.336	2000 vs 2000	23.5	Suspended (1.5 nm)	0	20	0.89	5
					50			
					300			

3. Theoretical Analysis Based on Continuum Frame Works

In this section, the analytic approach for the bending motion of SWNT is compared with MD simulation in time and frequency domain. The approach based on the Green-Langrange strain tensor is adapted to confirm the applicability of continuum mechanics to the dynamics of molecular system. The comparison will show that the interplay between the displacements of two transverse waves in orthogonal axes of SWNT is describable using strain energy.

3.1 Nonlinear bending equation

Analytic solution to nonlinear bending equation without forced excitation has been done for suspended bar structure by C.-H Ho [Ho et al., 1975; 1976] using the equation of motion from the strain energy, which considers bending of the two orthogonal axis at the same time. Converting the governing equation to the cantilevered condition is the matter of parameters. The physical interpretation of the pre-strain ϵ_0 in suspended solution is changed to the thermal expansion coefficient. Brief derivation of nonlinear governing equation and its solution are included for the integrity of the thesis in Appendix I. The analytic solution has restricted to the inter-resonance between the same modes only, such as 1^{st} – 1^{st} transverse mode. Modifying the mode number can extend the scope of the analytic solution to let it consider the motion caused by inter-resonance between different mode numbers, but this approach is not included.

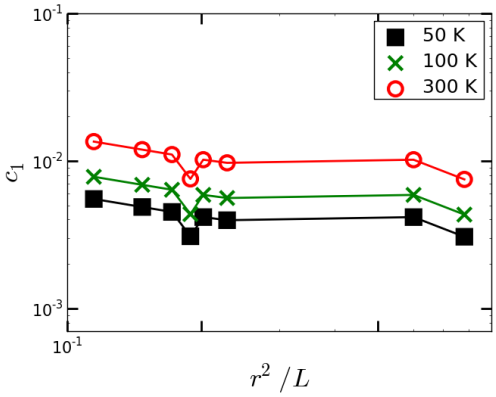

Fig. 3.1. Total amplitude $\mathbf{c_1}$ for cantilevered SWNT with temperature at 50 K (blue), 100 K (green) and 300 K (red).

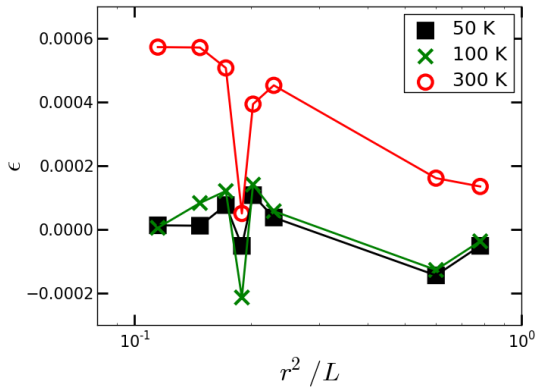

Fig. 3.2 Thermal expansion coefficient ε for each SWNT model with temperature at 50 K (blue), 100 K (green) and 300 K (red).

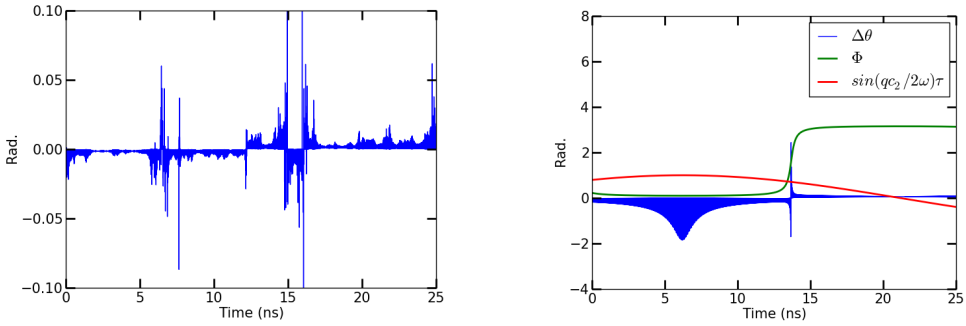

Fig. 3.3 Fitting of (5,5) 7.6 nm 300K case using $\Delta\Theta$, (a) MD result, (b) C_0 fitted $\Delta\Theta$.

From the newly interpreted parameters, I decide the specific values for each parameter in the analytic solution, which fit well with the result from MD. The motion of equation from derivation is as below [Ho et al., 1976]:

$$u_{,\tau\tau} + \frac{I}{AL^2}(u_{,ssss} - \beta\pi^2 u_{,ss}) - \frac{1}{2}u_{,ss}\int_0^1 \{(u_{,s})^2 + (v_{,s})^2\}ds = 0, \tag{3.1}$$

$$v_{,\tau\tau} + \frac{I}{AL^2}(v_{,ssss} - \beta\pi^2 v_{,ss}) - \frac{1}{2}v_{,ss}\int_0^1 \{(u_{,s})^2 + (v_{,s})^2\}ds = 0, \tag{3.2}$$

where, u, v, w and τ are non-dimensionalized coordinates along x, y, z axis and time, in non-dimensionalized form. The definition for non-dimensionalization is in Appendix 1. The amplitude along time and location of displacements are separated using Galerkin Method as u=$\xi(\tau)$sin[πs/2] and v= $\eta(\tau)$sin[πs/2] like planar bending motion. It is supposed that the displacement caused by 1st transverse mode is very large so that the higher frequency terms and other wave vector higher than π/2 are ignored. Time varying amplitude and phase, $\xi(\tau)$ $=x(\tau) \cong a(\tau)\cos(\omega\tau + \theta(\tau))$, and $\eta(\tau)=y(\tau) \cong b(\tau)\sin(\omega\tau + \phi(\tau))$, is assumed due to the nonlinearity and derived as follows:

$$a^2(\tau) = \frac{c_1^2}{2} + c_1^2\sqrt{(1 - C_0^2)}\sin\left(\frac{qc_1^2}{4\omega}C_0\tau\right), \tag{3.3}$$

$$b^2(\tau) = \frac{c_1^2}{2} - c_1^2\sqrt{(1 - C_0^2)}\sin\left(\frac{qc_1^2}{4\omega}C_0\tau\right), \tag{3.4}$$

$$\theta(\tau) = \left(\frac{3qc_1^2}{8\omega} + \Gamma\right)\tau + \Phi_1(\tau), \tag{3.5}$$

$$\phi(\tau) = \left(\frac{3qc_1^2}{8\omega} + \Gamma\right)\tau + \Phi_2(\tau). \tag{3.6}$$

ϵ_0 denotes the thermal expansion coefficient, A is cross-sectional, L is the length of SWNT. I represents the momentum of inertia. q is the constant $\pi^4/64$. The differences of solutions for cantilevered and suspended are the value of q and the natural frequency which should be non-dimensional constant ω defined as $\pi^2/8\sqrt{I/AL^2}$ for cantilevered and $\pi^2\sqrt{I/AL^2}$ for suspended, where 0.706 nm was used as the thickness of each SWNT.[Huang et al., 2006] $\Phi_1(\tau)$ and $\Phi_2(\tau)$ are in Appendix I.

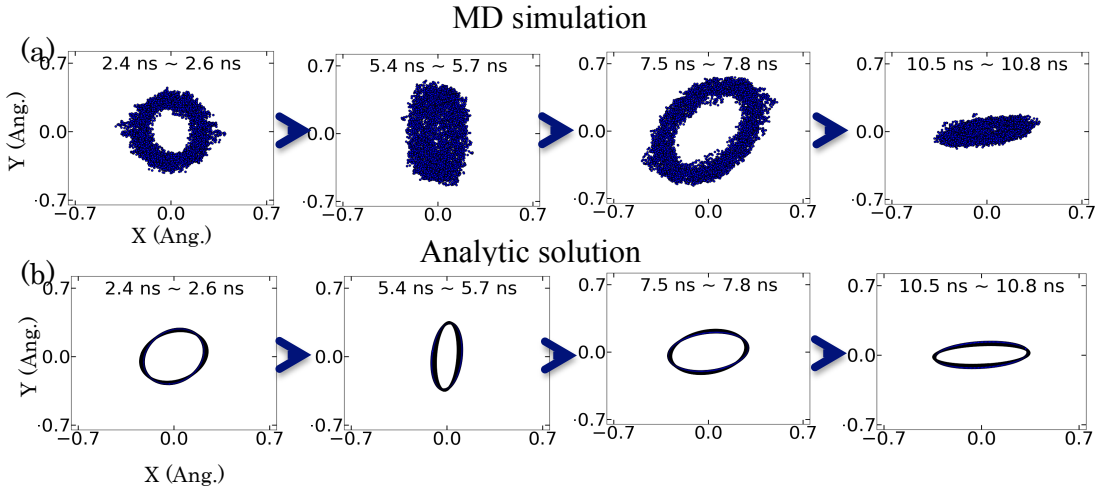

Fig. 3.4. Comparison of motion exchange in Poincare map; (a) MD simulation and (b) analytic solution.

3.2 Fitting method

To compare the results between MD and nonlinear continuum equation, proper fitting of the parameters is essential. Except the parameters ignored from original paper [Ho et al., 1976], there are 3 unknowns, c_1, Γ and C_0.

- c_1 and Γ

From the attentive following on analytic derivation, c_1 is interpretated as total amplitude of bending motion. As mentioned in Chap. 1, the amplitude of beam motion of SWNT is already figured out to follow the Gibbs-Boltzmann distribution. c_1, the amplitude of flexural displacements, is decided directly from the probability distribution derived from the Boltzmann-Gibbs distribution, as $Z^{-1}e^{-KU^2/(2k_BT)}$, where the ensemble average, $\langle U^2 \rangle = k_BT/K$. The result from those formulations gives a reasonable value of c_1, which is U/L. $K = 3EI/L^3$ is spring constant. Young's modulus, E is from the empirical formulation. [Zhigilei et al., 2005] In case of (10,10) 7.6 nm and (20,20) 23.5 nm like Timoshenko beam, the poisson ratio of 0.03 is applied for $K = \frac{3EI}{L^3(1+\frac{3\kappa}{\epsilon})}$. $\kappa = E/kG$ and $\epsilon = L/\sqrt{I/A}$. k is the Timoshenko beam factor and G is shear modulus. Approaximately, c_1 is twice larger than Euler beam. The value of c_1 from this approach is in Fig. 3.1.

And Γ is thermal expansion coefficient, ε multiplied with $\pi^2/4$. It is very straight to have its value unless Gruneissen parameter [Schellin and Keblinski, 2003], is adapted. In this thesis, the DC value came from the FFT is used and the initial length is came from the energy minimized structure. Fig. 3.2 has Γ along the inverse of aspect ratio.

Its negative value, known is Negative Thermal Expansion (NTE), has been reported from other MD simulation [Kwon et al., 2004] or theoretical approach using Green function. [Jiang et al., 2009] The negative value in this thesis is also shown for thick SWNT in low temperature in couple of SWNT.

- C_0 fitting

The last parameter left is C_0, which decides the motion and the rotation exchange as the beating frequency of $c_1^2 C_0/2\omega$ in Eq. (3) ~ Eq. (6). Since the shape of motion in Poincare map is difficult to measure and to compare, C_0 is measured by matching the angle difference of MD and that of analytic solution as shown in Fig. 3.3. With proper fitting of C_0, the motion and rotation exchange can be followed up as the result of MD as in Fig. 3.4 with right sequence of planar and non-planar motion. The exact physical interpretation of this parameter is still missing such as why the motion should be exchanged. The theoretical approach, however, can offer how C_0 influence to beating and rotation exchange as the research next to this thesis. In this sub-section, the fitting method is introduced and some discussion is dealt in Sec. 3.3.

Theoretically, the opposite rotation direction occurred when the Φ, the difference between ϕ and θ is flipped from 0 to π because the phase is reversed between x and y. With the same procedure to derive Eq. (A36) and Eq. (A37) in Appendix I, Φ is expressed as below:

$$\Phi = \tan^{-1} \frac{\sqrt{1-C_0}\cos(qc_1^2 C_0/4\omega\tau)}{C_0} + \pi/2 \qquad (3.7)$$

,here, $\pi/2$ is integration constant to make the Φ same with the result of substituting Eq. (3.5) from Eq. (3.6).

When C_0 is small enough, Φ in Eq. (3.7) is remained either of 0 or π as shown in Fig. 3.3 (c). Rotation direction is reversed at the moment when the value of Φ is flipped. The frequency of rotation exchange is, therefore, equal to $qc_1^2C_0/4\omega$, in analytic solution. Only the 1st-1st mode interaction is dealt as IFFT process in this thesis based on the assumption that the displacement of tube is most highly dependent on the lowest mode. If the rotation exchange is occurred by the interaction between two different modes, the influence of other modes can be another reason of such motion or rotation exchange.

As the fitting result using the comparison of rotation exchange is in Appendix 1.3 and the result is in Fig. 3.5. Strong tendency along the aspect ratio is shown in log-log scale. The value used for fitting is in Table 3.1~3.4.

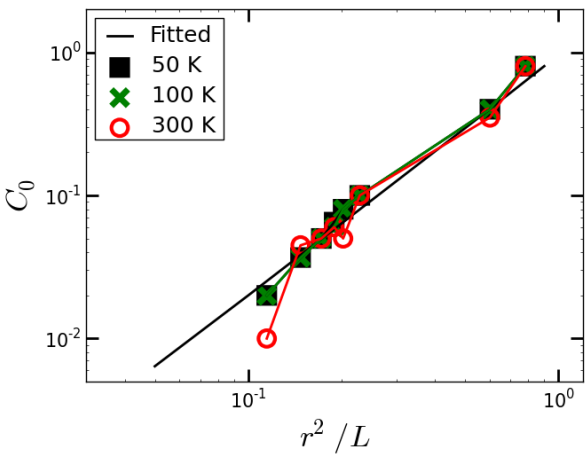

Fig. 3.5. Beating frequency coefficient C_0 for each SWNT model with temperature at 50 K (blue), 100 K (green) and 300 K (red).

The major discrepancy is that the rotation direction once turned into opposite, it undergoes some recovery state several times, in which is shown in Fig.3.3 (b) around 15 ns. This is supposed mainly due to the condition of $\frac{d\Phi}{d\tau} = \infty$ is out of scope of Eq. (A.44) and Eq. (A.45). Therefore, the solution in Eq. (3.3)~Eq.(3.6) does not afford this recovery from the change because a and b do not have their value when $\frac{d\Phi}{d\tau} = \infty$. Interestingly, the infinite value of $sec\,\Phi$ in Ho et al.'s paper, $csc\,\Phi$ in Appendix, is unavoidable to have rotation change from clockwise to counter-clockwise or vice versa when $\frac{d\Phi}{d\tau} = \infty$. The influence of this extreme value of $\frac{d\Phi}{d\tau}$ which is sort of phase velocity of 1st mode, should be compensated by another momentum condition for better dictation of nonlinear motion.

In case that the profile of $\Delta\Theta$ is too complicated, the comparison of the motion exchange in Poincare map is used. Each displacement data is split with several cycles in the poincare map and the change from planar to non-planar motion or the opposite is observed. Precisely, the duration for one cycle of motion is firstly checked by its resonance frequency, and several cycles are duplicated in one map for easier comparison with analytical cases. The whole signal from MD calculation and analytic solution are split with the same time span, which includes the same number of cycles, so that the change from planar to non planar motion can be observed.

Then, with c_1 from the Gibbs-Boltzmann distribution, C_0 is decided. So far, high C_0 produces high beating frequency which alters the motion from planar to non-planar more frequently. The each 300 K case for (5,5) and (10,10) SWNT is shown in Fig. 3.6 and in Fig. 3.7 which are the result with fitted parameter and arranging to show same sequence of motion

exchange. The amplitude and motion exchange sequence are agreeable with that of MD result, which is IFFT processed.

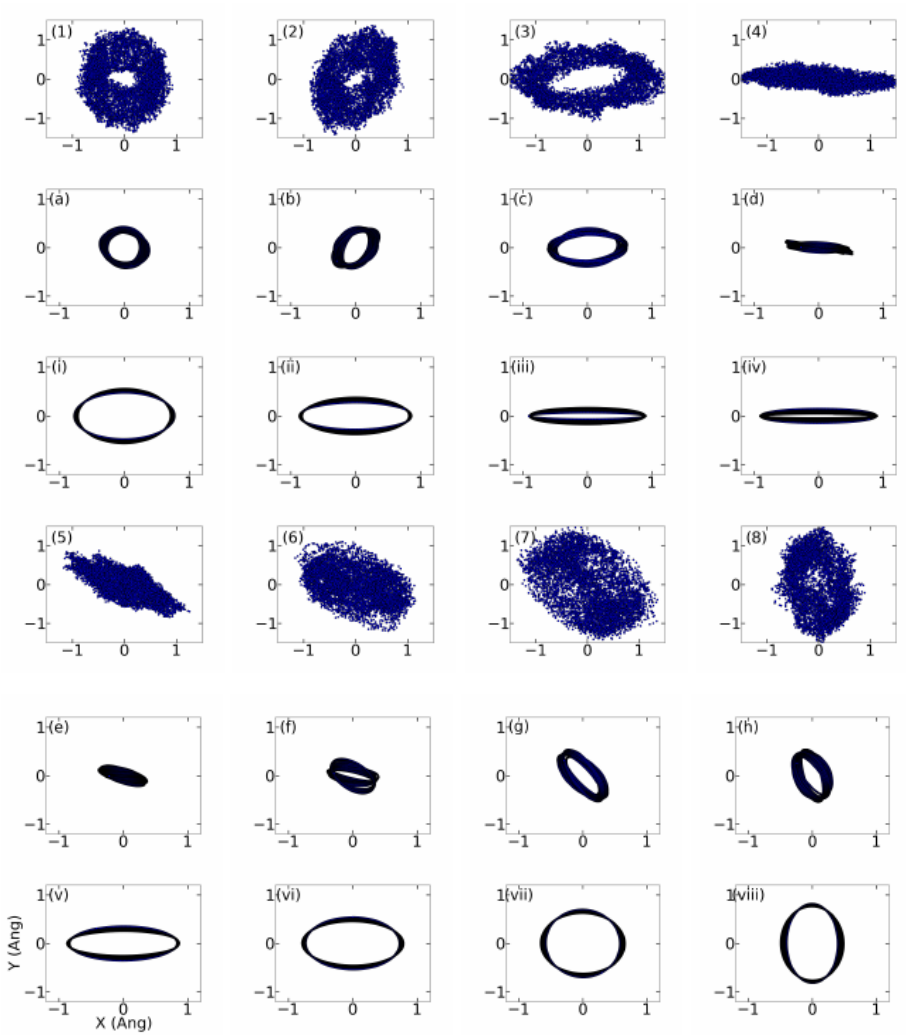

Fig. 3.6. Poincare map of (5,5) 7.6 nm case at 300 K from MD (1~8), ifft result (a~h) and analytic solution (i~viii); (1,a,i) 0.6 ns ~1.2 ns, (2,b,ii) 1.8 ns ~2.4 ns, (3,c,iii) 3 ns ~3.6 ns, (4,d,iv) 5.4 ns ~ 6 ns, (5,e,v)6.6 ns ~ 7.2 ns, (6,f,vi) 8.4 ns ~9 ns, (7,g,vii) 9.6 ns~ 10.2 ns, (8,h,viii) 10.8 ns~ 11.2 ns.

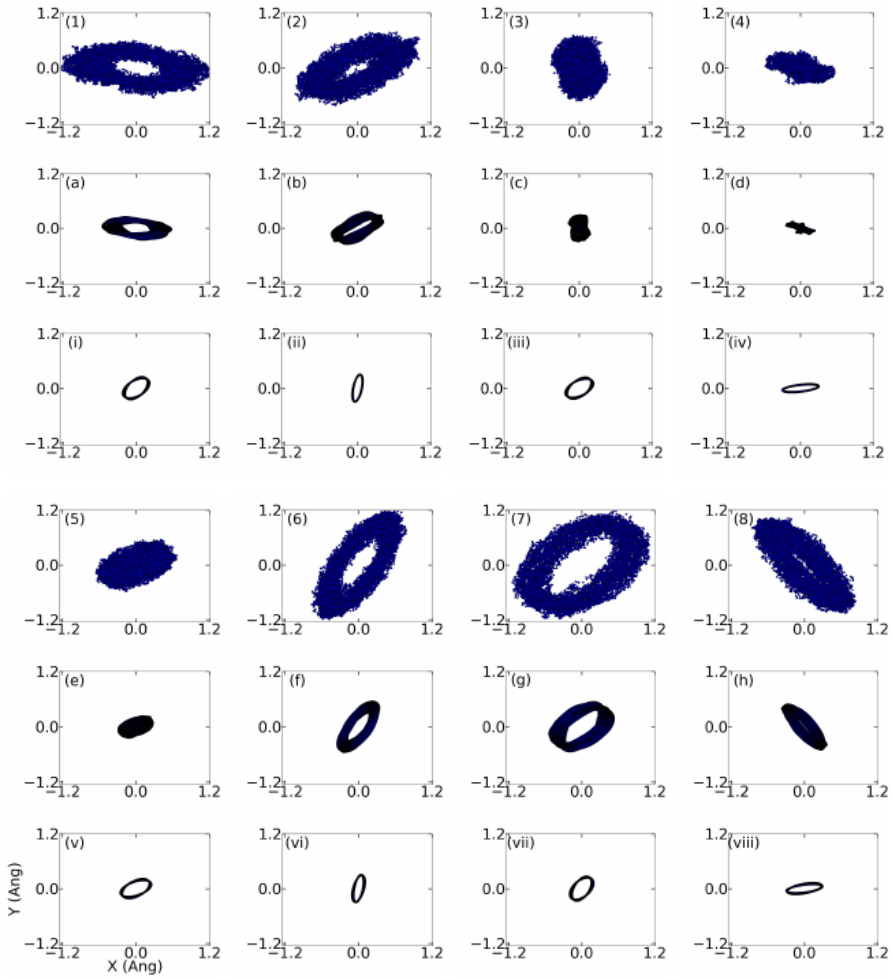

Fig. 3.7. Poincare map of (10,10) 8nm case at 300K from MD (above), ifft result (middle) and analytic solution (below), (1,a,i) 0.6 ns ~1.2 ns, (2,b,ii) 1.8 ns ~2.4 ns, (3,c,iii) 3 ns ~3.6 ns, (4,d,iv) 5.4 ns ~ 6 ns, (5,e,v)6.6 ns ~ 7.2 ns, (6,f,vi) 8.4 ns ~9 ns, (7,g,vii) 9.6 ns~ 10.2 ns, (8,h,viii) 10.8 ns~ 11.2 ns.

Other calculation results such as (5,5) for 23.5 nm length are not displayed in this thesis. Especially slender SWNTs than the SWNT in Table 2.1 have their resonance in very low frequency range, therefore, the calculation time should be much longer than 75 ns, to observe

the full motion change cycle. When the simulation time is not enough for fitting, C_0 for these cases is chosen to have maximum C_0 ,which can maintain the motion during the full calculation time.

In this way, the non-dimensionalized analytic solution can be compared with the MD result whose components in higher than 1st transverse mode is eliminated. The comparison in frequency domain is shown in Fig. 3.8 and Fig. 3.9. Each location of peaks is matched with managing Young's Modulus in Table. 3.1 ~ 3.4.

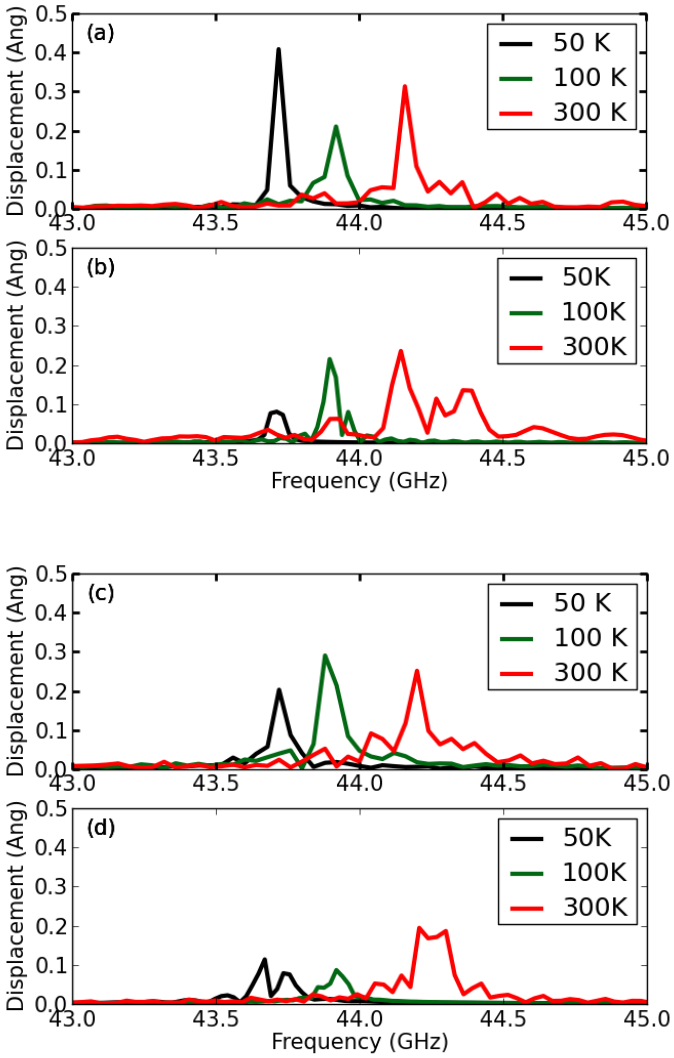

Fig. 3.8. Frequency response of 1st transverse mode of analytic solution and MD result along x (upper) and y (lower) axis, black line is 50 K, green line is 100 K and red line is 300 K of (5,5) 7.6 nm case: (a) displacement along x axis in MD simulation, (b) along x axis by analytical solution, (c) along y axis in MD simulation, (d) along y axis by analytic solution.

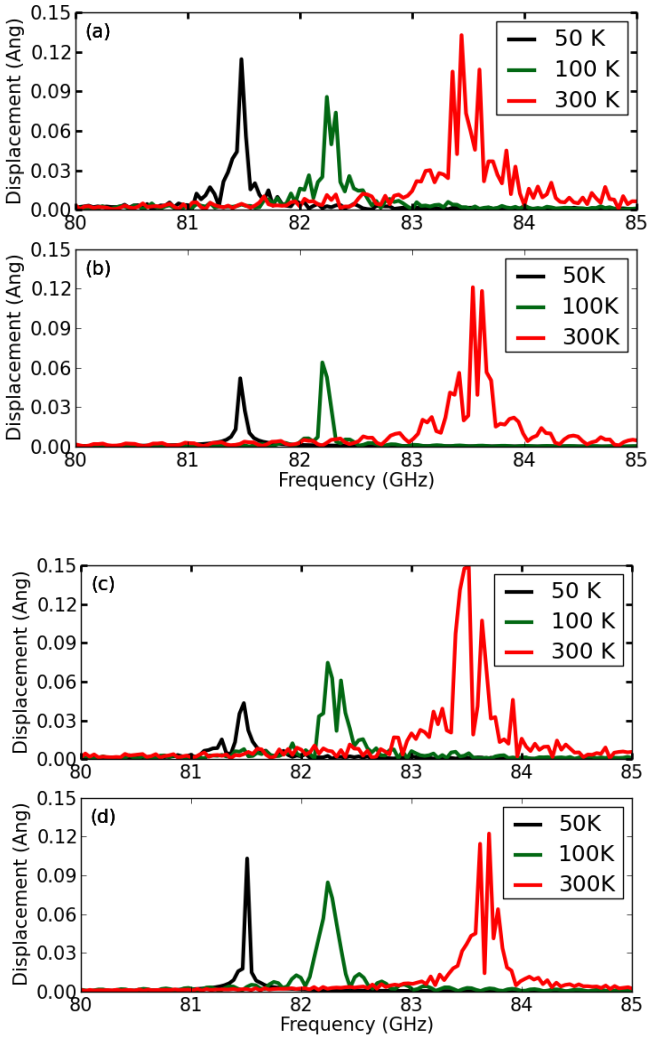

Fig. 3.9. Frequency response of 1st transverse mode of analytic solution and MD result along x (upper) and y (lower) axis, black line is 50 K, green line is 100 K and red line is 300 K of (10,10) 7.6 nm case: (a) Displacement along x axis in MD simulation, (b) along x axis by analytical solution, (c) along y axis in MD simulation, (d) along y axis by analytic solution.

3.3 Parameter study

- c_1

Unlike the elastic wave as mentioned to have no phase velocity change due to the magnitude of eigenmode, [Ziman, 1960] analytic solution of 1st transverse mode response of quasi-1D system should have its phase as a function of c_1. Especially, the frequency shift for each temperature and model is directly caused by c_1 in Eq. (3.5) and Eq. (3.6). Also the beating frequency in Eq. (3.3) and Eq. (3.4) is dependent on c_1.

- Γ

The Γ, the thermal expansion coefficient in Fig. 3.2, which is came from the amplitude of 1st longitudinal mode, plays its role for the frequency shift as revealed in Eq.(3.5)~(3.6). Its influence on whirling motion, however, is negligible and the location of peaks is re-adjusted with time constant from Young's modulus later. In Fig. 3.9 and Fig. 3.10, the FFT results from each case matches well with that of MD and shows similar tendency with temperature. The frequency of peaks is fitted at that of simulation results by applying slightly different Young's modulus as in Table 3.1~4.

- C_0

Interestingly, the value of C_0 shows the linear tendency in log-log scale on the aspect ratio. Those conditions are represented from c_1 and C_0. Unlike c_1, C_0 seems not significantly disturbed as the temperature. The more peaks from the signal at high temperature, which is

produced from more beating and longer distance between peaks in frequency response, is because the beating frequency, $\frac{qc_1^2C_0}{4\omega}$, dependent on c_1. Therefore, c_1 is also an important factor which decides the peak shape.

Three different rigidity boundaries are examined as shown in Table. 2.3. The fitted parameter is in Table 3.3 and the trend is quiet obvious. Less rigid boundary has more frequent rotation exchange. The zero temperature, i.e. frozen boundary is also considered, however, this case does not fitted into the revealed trend. C_0 can be related to the rigidity of fixation, too.

- Young's Modulus

Young's modulus has two roles for the comparison process; one is suggesting c_1 from the Boltzmann-Gibbs distribution and the other one is manipulating the peak location for comparison in frequency domain, the value used for each case is not exactly same but has same order. It is difficult to conclude that the Young's modulus is altered by temperature in real system. The exact value of Γ from the 1st longitudinal mode seems necessary instead of fitting Young's modulus.

- Q factor

The reason why Green Lagrange strain can be a common feature linking continuum mechanics and molecular systems, is mainly due to the entanglement by the anharmonicity which makes the bending in one plane coupled with orthogonal vibrations. The strain condition used in this paper, represents the longitudinal displacement sharing its portion with transverse

modes, could mimic the scattering process for 1st transverse modes. Theoretically, other scattering of higher modes whose wave length is longer than optical mode is also applicable to this approach.

Since full analytic solutions of 1st transverse mode is offered with the abstract motion trend and frequency response, but in quiet rigorous quantitative agreement, the meaning of the relaxation time of such motion and nonlinear damping, which is closely related to the interaction with higher phonon modes is still beyond the scope of this paper because the expression of the solution of nonlinear equation is not standing in parallel with the the expression of the direct approximation of relaxation time [Ladd, 1986], $e^{-i(\omega - i\tau_0/2)t}$ for τ_0, the phonon life time. The relaxation process for 1st transverse mode, which have known as the dissipation of kinetic energy in continuum mechanics should be reconsidered as energy exchange between transverse modes in two orthogonal planes in case of molecular system.

3.4 Validation with Experiment

The same formulae with different parameters for suspended case compared with the simulation explained in Chap. 2.1. Using the fitting method fully explained in Sec. 3.2, C_0 for suspended SWNT condition, shows the same trend with that of cantilevered SWNT as shown in Fig. 3.5. The empirical formulation as in Eq. (3.7) is emerged as below and it is examined with experimental results.

$$C_0 = 0.82\left(\frac{r^2}{L}\right)^{1.67} \qquad (3.7)$$

The value of C_0 is decided from the empirical formulation above with the radius and length in experimental report, as shown in Fig. 3.10, and the thermal expansion is simply ignored. c_1 is initially given as same way of free thermal vibration. As a result, the location and peak shape is not consistent with the experimental data provided from Eichler et al. shown in Fig. 3.11 (a).

The experimental condition has external forced excitation, therefore, it is difficult to say the total amplitude is in the same range with Gibbs-Boltzmann distribution. Fig. 3.11 (b) is the result with 4 times larger. C_0 in Eq. (3.7) is used, again.

Another frequency response at 300 K with other experimental conditions [Sazonova et al., 2004] is checked and the location of peaks and numbers are in very close agreement in Fig. 3.12. In this case, free thermal vibration fitting is fine. It is also possible that the temperature in Fig. 3.11 is too low.

The Young's modulus used in Fig. 3.11 and 3.12 has its value around the empirical

formulation [Zhigilei et al., 2005], except the Fig. 3.11 (a) case. The parameters used are included in Table 3.4.

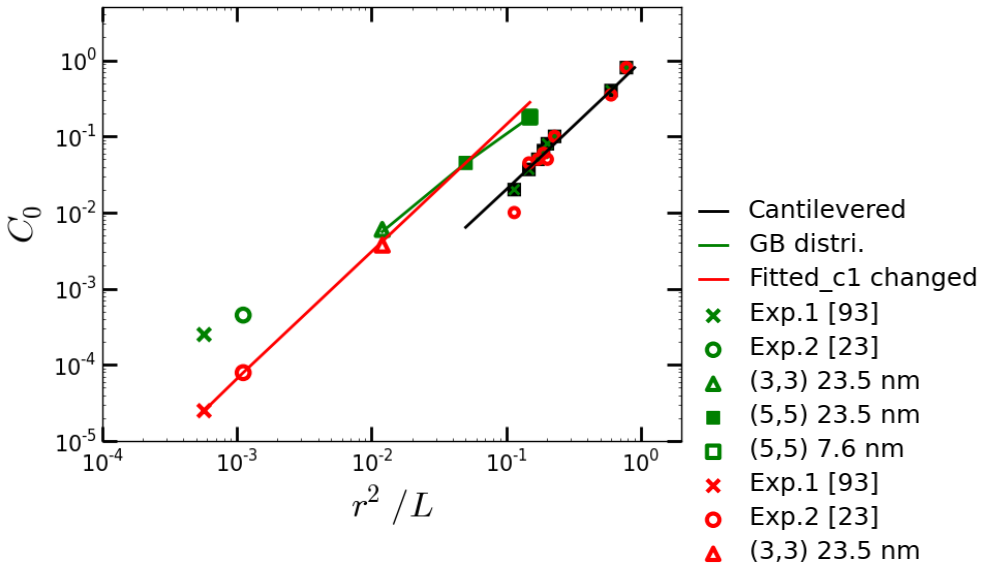

Fig. 3.10 C_0 plot for suspended case with experiement result.

The frequency response from free vibration, having same peaks with forced condition means that the damping process might not be the main cause, but it has to be multiple peaks because the vibration energy at 1st mode is contained with mode coupling as producing beating signal which is composed of several peaks.

The multiple peaks appeared with minimized excitation in the experiment [Eichler et al., 2011] also bolster the hypothesis that the signal from the macroscopic motion of suspended SWNT could have the appearance of planar and non planar motion like free thermal vibration. The result of Fig. 3.11 and Fig. 3.12, therefore, shows the possible existence of the periodic order of non-planar and planar motion in experiment and provides a decent explanation of multiple resonances with analytic solution as a part of natural resonance not from the nonlinear damping.

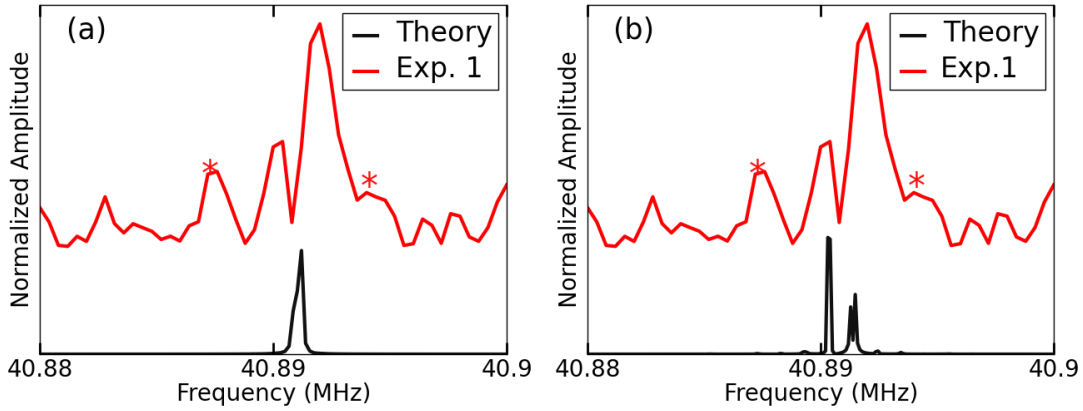

Fig. 3.11. Comparison of frequency response for Exp 1[Eichler et al.,2011]. The suspended CNT with L=2 μm and diameter = 1.5 nm. Fitting parameters are in Table 3.4. * mark represents the peak from noise: (a) c_1 from Gibbs-Boltzman, (b) c_1 fitted to peak distance, 4 times larger than the value from Gibbs-Boltzmann distribution.

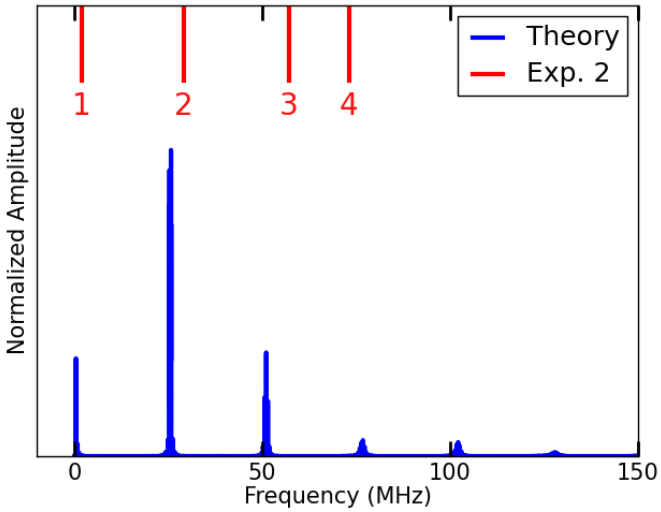

Fig. 3.12. Comparison of frequency response for experiment 2, [Sazonova et al., 2004] from FET system. The suspended CNT with L=1.75 μm and diameter = 1 nm. Parameter for analytic solution is in Table 3.4.

3.5 Instability condition

Instability is examined using same governing equation of Ho et al. [Ho et al., 1976] There are two kinds of instability. One is the existence of the steady planar motions. The other one is the durability to the external disturbance, like the status on the saddle point like condition. The former case, the governing eq. (3.1) and (3.2) is simplified into the Mathieu equation, whose solution is numerically decided based on the constants used in equation. In case of the latter one, the planar motion's homogeneous solutions is substituted as follows:

$$u = A\ \cos\omega\tau,\ v = 0 \tag{3.8}$$

$$A(P-\omega^2)+\frac{3\pi^4}{16}A^3=0 \quad \xrightarrow{P-\omega^2<0} \quad A=\sqrt{\frac{16}{3\pi^4}(P-\omega^2)}$$
$$P=\omega^2(1-\epsilon_0)$$

ϵ_0 is thermal expansion coefficient.

When epsilon zero is less than zero, the amplitude of A can be existed. Theoretically, such condition is achievable with Negative Thermal Expansion (NTE) of SWNT. [Jiang et al., 2009; Miller et al., 2009; Kwon et al., 2009] Among the MD simulations, which this thesis is presenting, such condition has been appeared in most of simulation results except (10,10) and (20,20) SWNT. NTE is found in (10,10) and (20,20) SWNT with 50 K and 100 K.

Theoretically, those tubes can make perfect planar motion with proper initial conditions, which never could be offered from Lagevin thermostatting, so the tubes is still shown with motion and rotation exchange.

3. 6 Summary

In this section, the analytic model from Lagrange strain tensor with 1st order cantilever motion of SWNT shows the consistency with the nonlinear motion observed from MD simulation. The peak broadening calculated from MD simulation result has shown to have the exact similarity with the frequency response of 1^{st}-1^{st} transverse mode analytic solution. This means the reason of the degeneration of Q factor of SWNT is mainly caused by its nonlinearity not its thermal noise. Another interesting point is the frequency shift by temperature increasing. Unlike well knwon characteristics of elastic wave, [Ziman, 1960] the phase velocity is decided by the magnitude of wave vector, here it is 1^{st} mode in the analytic solution has the total amplitude in every beating frequency and the result is well matched with MD simulation and experiment.

The same analytic model is applied to suspended boundary condition results calculated from MD simulation and measured in experimental set up. [Eichler et al.,2011; Sazonova et al. 2004] The multiple peaks reported in the experiments are in the free thermal vibration response with same number of peaks and distance. This result signifies the multiple resonance peaks can be the response from the natural characteristic of quasi-1D system rather than its dissipating mechanism.

Further steps should build a theoretical connection between the anharmonicity and strain function for the better explanation of the relation between temperature and the motion exchange expressed by C_0. More specifically, the mechanism how higher temperature allows the tube to repeat the non-planar motion and planar motion appearance more frequently, why C_0 is

dependent on aspect ratio and why rigidity of fixation should be strongly related to the process of relaxation time i.e. the Q factor. Lastly, the inter-resonance with the higher modes is also essential step to describe the accurate limitation of the continuum mechanical approach to molecular system.

Table 3.1. Simulation results for various aspect ratio

	Num. of Atom	r^2/L (nm)	Temp. (K)	C_0	c_1	Γ_0	E (TPa)
(5,5)	400	0.23	50	0.10	0.004	$3.75\text{x}10^{-5}$	1.81
			100	0.16	0.0056	$5.72\text{x}10^{-5}$	1.83
			300	0.10	0.0102	$4.52\text{x}10^{-4}$	1.99
	480	0.20	50	0.08	0.0042	$1.08\text{x}10^{-4}$	2.03
			100	0.10	0.0059	$1.41\text{x}10^{-4}$	2.05
			300	0.06	0.0102	$3.94\text{x}10^{-4}$	2.20
	560	0.17	50	0.05	0.0045	$7.65\text{x}10^{-5}$	2.10
			100	0.05	0.0064	$1.21\text{x}10^{-4}$	2.10
			300	0.05	0.0110	$5.07\text{x}10^{-5}$	2.44
	660	0.15	50	0.037	0.0049	$1.17\text{x}10^{-5}$	2.10
			100	0.037	0.0069	$8.30\text{x}10^{-5}$	2.10
			300	0.045	0.0119	$5.71\text{x}10^{-4}$	2.70
	820	0.11	50	0.020	0.0055	$1.30\text{x}10^{-5}$	2.26
			100	0.020	0.0078	$5.17\text{x}10^{-6}$	2.40
			300	0.030	0.0135	$5.72\text{x}10^{-4}$	3.63
(10,10)	1320	0.60	50	0.4	0.0017	$-1.44\text{x}10^{-4}$	1.48
			100	0.4	0.0024	$-1.27\text{x}10^{-4}$	1.51
			300	0.4	0.0041	$1.61\text{x}10^{-4}$	1.57
	4000	0.19	50	0.065	0.0031	$-5.16\text{x}10^{-5}$	1.93
			100	0.06	0.0044	$-2.14\text{x}10^{-4}$	2.05
			300	0.06	0.0075	$5.02\text{x}10^{-5}$	2.09
(20,20)	8000	0.78	50	0.65	0.0010	$-5.14\text{x}10^{-5}$	1.50
			100	0.65	0.0014	$-3.70\text{x}10^{-5}$	1.54
			300	0.65	0.0025	$1.35\text{x}10^{-4}$	1.63

Table 3.2. Simulation results for various boundary rigidity

	Num. of Atom	r^2/L (nm)	ε_{LJ} (eV)	σ (Å)	C_0	c_1	Γ	E (TPa)
(5,5)	660	4.28	5	0.89	0.153	0.0119	$4.06\text{x}10^{-4}$	-
			20		0.045		$5.71\text{x}10^{-4}$	0.65
			80		0.019		$2.76\text{x}10^{-4}$	-
			0 K		0.03		$4.34\text{x}10^{-4}$	-

Table 3.3. Simulation results for various termperature

	Num. of Atom	r^2/L (nm)	Temp. (K)	C_0	c_1	Γ	E (TPa)
(5,5)	660	0.15	50	0.037	0.0049	$1.17\text{x}10^{-5}$	0.50
			100	0.037	0.0069	$8.30\text{x}10^{-5}$	0.50
			300	0.045	0.0119	$5.71\text{x}10^{-4}$	0.65
			500	0.065	0.0153	$1.19\text{ x}10^{-3}$	0.94
			800	0.07	0.0194	$1.91\text{ x}10^{-3}$	1.60

Table 3.4. Simulation results with suspended boundary

	Num. of Atom	r^2/L (nm)	Temp. (K)	C_0	c_1	Γ	E (TPa)
Exp. 1. [Eichler et al., 2011]	-	-	0.005	$7.9\text{x}10^{-5}$	$4.0\text{x}10^{-4}$	0	4.47
					$1.6\text{ x}10^{-3}$		1.45
Exp. 2. [Sazanova et al., 2004]	-	-	300	$2.5\text{x}10^{-5}$	0.022	0	0.25
(5,5)	660	0.15	300	0.089	0.012	0	-
	2000	0.05	500	0.045	0.027	0	-
(3,3)	1188	0.012	300	0.006	0.061	0	-

4. Modeling thermal-mechanical motion into CGMD

In biology molecule's morphology study where the CGMD method is adapted seriously, the amount of dissipation is considered as more important fact for coalguation of molecules [Noid, 2013; Ortiz et al., 2005] than the modal behavior of molecules.[Yang et al., 2011] For that, the dissipating conditions realized by DPD, Langevin thermostat and the damping parameter are regarded as molecules thermal characteristics.[Fritsch et al., 2012] For bio-molecules, DPD potential which is including the random motion and dissipation between nodes is used to follow the motion from thermal vibrations.

Unlike the bio-molecules which is packed with high density from the initial stage so that the dissipation between molecules is all the priority to be considered, the morphology of SWNT during its generation, such as CVD process should have different prospectives because its morphology is surely decided during its length on growing from the distributed catalyst on the substrate. This means the size of cantilevered motion and the collision between tubes during the growth becomes more important. Therefore, in this chapter, the amplitude resulted by its internal energy and dissipation process occurred from the collisions of SWNT is considered separately using couple of numerical tools.

The capability of CGDM algorithm can be tested in many ways, including its statistical condition whether the beam like nonlinear motion is its part of ergodic ensembles. In this study, more simple and intuitive method is selected.

- Preparation : Beads model from Classical MD simulation

The modal energy for its acoustic damping process against given initial strains is, surely, lose their path to be transformed into heat bath energy by simplified structure. [Rudd and Broughton, 1998; 2005; Sadeghirad and Tabarraei, 2013]

As the simplified model of SWNT, coarse grained SWNT including its simplified radial structure has been studied [Jacobs et al., 2012] instead of a complete one dimensional model like other bio molecules or polymers. [Foteinopoulou et al., 2008] In this study, however, completely simplified into one dimensional string like coarse grained bio molecules [Ortiz et al., 2005] is adapted.

From the nonlinear motion of SWNT described by nonlinear beam equation whose variable is identical to the one-dimensional string, proper derivation from the Eq. (3.1) and Eq. (3.2) would help the simple string to have the nonlinear vibrational behavior in CGMD simulation. Theoretically, there would be no losing quantities to describe the motion.

To examine the capability of the most simplified continuum, firstly, the result of classical MD simulation is converted into the one dimension string by averaging the each half unit cell's displacements and velocity into one lumped mass. This string will be called as beads model in following sub sections. And this simplified model is analyzed using the algorithm of CGMD and normal mode decomposition.

In this way, it would be much easier to suggest the characteristics of coarse grained model for SWNT's thermal-mechanical motion should have. Another reason of this simplification is to discard the modal response of small wave length which lumped mass model is not able to calculate when the certain mechanical motion of tube is appeared. However, the

main focus of this section is on observation of the macroscopic motion of SWNT caused by thermal energy and its compatibility to simpler model, therefore, the vibration from the smallest wave length in beads model is also compared with the long wave length, mainly 1st mode for each axis.

Free thermal motion of (5,5) 7.6 nm and 23.5 nm long SWNT, each tube has 660 and 2000 atoms respectively, are simplified into one single string by averaging the displacement and velocity for each half unit cell. This result is applied to various analysis, such as normal mode projection and the algorithm of CGMD simulation. More specific explanation is on the followings.

- Analysis I : CGMD algorithm

In conventional CGMD, the nodes represent a lumped mass of certain part of molecule and the spring constants for distance and angle between each node define the structure of simplified model with harmonic potential energy. The spring constants for axial and bending deformation of SWNT are thoroughly studied.[Zhigilei et al, 2008] For (5,5) SWNT, they are 445 (eV/ang) and 2235 (eV ang) for axial and bending spring constants, respectively.

The data converted into beads model from classical MD is analyzed in two ways using CGMD algorithm.

One is, **Analysis I (a)**, is using the beads model's displacement and velocity as the initial condition for CGMD simulations. The comparison of poincare map between CGMD with initial condition from classical MD and CGMD calculation with langevin thermostatting gives good reason why the m odal response of molecular structure is important. This is in Sec. 4.1.

The other one is, **Analysis I (b),** that calculating the amount of work done, W by spring forces from bead's model's displacement versus the potential energy differences, ΔE for each time step by following definition:

$$W = \sum_{i,j}^{N,3} \vec{F}_{angle\ or\ length,i}(\overrightarrow{dl}_{j,i+1} - \overrightarrow{dl}_{j,i}) \quad (4.1)$$

$$\Delta E = \sum_{i}^{N}(E_{i+1} - E_i) \quad (4.2)$$

, here, $\vec{F}$ is force calculated using CGMD spring constant and displacement of beads model, $\overrightarrow{dl}_{i+1}$ is the difference of displacement during a time step calculation, i is the time iteration number, j is the node number and N is total number of nodes. It is obvious that W and ΔE should have the opposite sign with identical absolute value if the spring constant has applied correctly for the motion of beads model.

- Analysis II : Normal Mode Decomposition (NMD)

NMD is projecting the unit vector to the displacement of waves by following [McGaughey and Keviani, 2004]:

$$S_i(\kappa, v) = N^{-1/2} \sum_j M_j^{1/2} exp\left(-i\kappa \cdot r_{j,\omega}\right) e_i^*(\kappa \cdot v) \cdot u_j \quad (4.3)$$

Normal mode $S_i(\kappa, v)$ is the projected value with each wave vector, $exp\left(-i\kappa \cdot r_{j,\omega}\right)$ to the displacement of each j-th mode, u_j, which is $r - r_0$. $e_i^*(\kappa \cdot v)$ is a vector to describe the mode polarization. With N nodes in beads motion, there could be N modes for each Cartesian coordinate. Due to the fixed free boundary, the sine function is used for projecting. The

projection to cosine wave vectors also has its value because the boundary condition in simulation is not perfectly rigid but its influence is ignored in this thesis. Applying this method to beads model will offer the information about the energy distribution along the one dimensional string is varying as the motion of SWNT.

In this section, 1st mode and Nth mode in 3 Cartesian axis is shown. 1st mode along x and y axis are transverse modes and 1st mode along z axis is 1st longitudinal mode. The n-th mode, which is called the optical mode, is the out of limit to be described from continuum frame works because it is not differentiable any longer. Therefore, the high intensity of n-th mode signifies the difference between molecular system and continuum modeling. Lastly, the each line along the tube axis of full structured SWNT is also decomposed using NMD to confirm the influence of averaging process as beads model.

For the validation of the projection with simplified version of tube, the graph of $\Delta\Theta$, which is measured from iffted signal in free thermal vibration in Fig. 4.1 (a) is compared with the $\Delta\Theta$ calculated from NMD amplitude with the wave vector of 1st transverse mode in Fig. 4.1 (b). Both showed the almost same rotation exchange, so the NMD analysis of beads model is regarded to decompose the normal modes, correctly.

4.1 Free thermal motion analysis

As the most un-disturbed condition from external sources, free thermal vibration is the standing point to distinguish the influence of forced mechanical excitation, thermal disturbance and the response from Collisions.

The compatibility of the motion calculated by MD dynamics with CGMD harmonic potential is examined in Analysis 1, whether the work done by the force from the spring constant with given displacement for each time step from beads model can reveal whether the harmonic spring constants can follow up the nonlinear motion of SWNT. Then, the energy distributed to 1st and Nth mode is observed in Analysis 2.

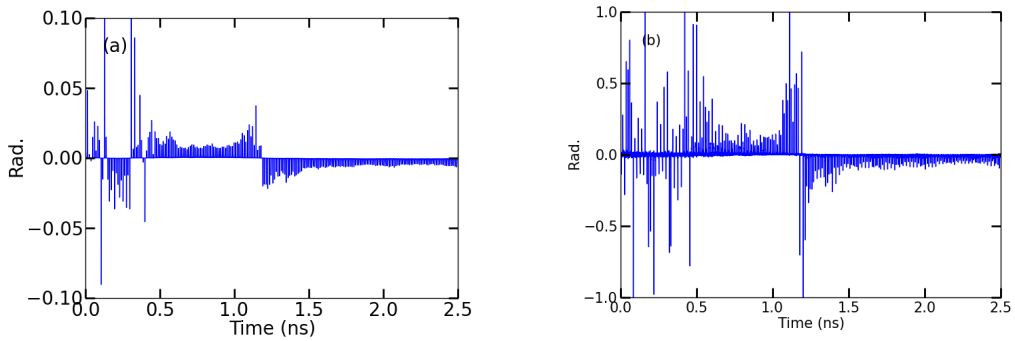

Fig. 4.1. Angle difference measured from IFFT signal and NMD; (a) angle measured from IFFT signal, (b) angle measured from 1st mode decomposition using NMD.

In this section, free thermal motion of (5,5) 7.6 nm length SWNT at 300 K is converted into beads model to provide the data to Analysis I. This SWNT has 660 atoms in total, so the number n in n-th mode is 66. Preparation of this analysis using beads model is averaging the displacement and velocity for each half unit cell. To adapt this data, however, as the initial

condition to CGMD string, proper node length of coarse grained string needs extra the observation of the distance between beads. The result is differed a lot from the node length calculated from the energy minimized structure of SWNT at zero temperature. Mismatch of this condition provokes significant level of excessive energy. The process to decide this node length for initial condition from classical MD simulation is in Appendix II.

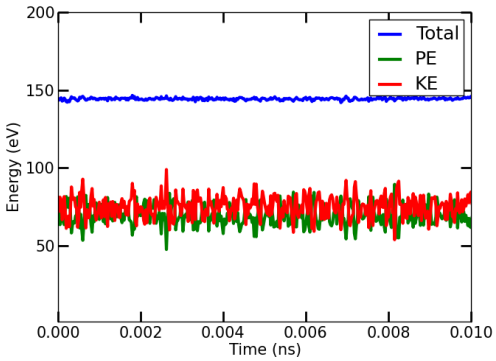

Fig. 4.2. Energy profile from the beads model with CGMD spring constants.

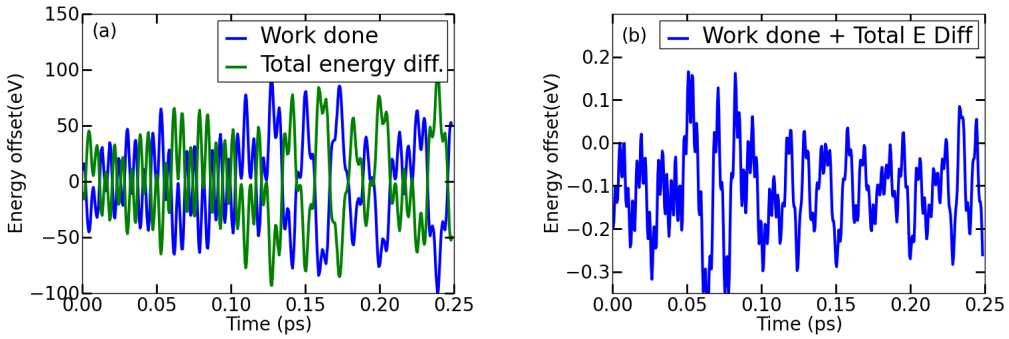

Fig. 4.3. Energy profile for analys I, (a) The work done by spring constant and energy from the given displacement of beads model, (b) sum of the work done and total energy of a lumped mass .

Result of Analysis I (a) : As shown in Fig. 4.2, the energy profile shows the constant level of total energy. The significant fluctuation of potential energy does not exist, even in its initial stage of simulation. This means potential energy and kinetic energy is well balanced and the given initial state from Classical MD simulations is compatible to CGMD algorithm.

The poincare maps from CGMD simulation with initial condition by beads model is in Fig. 4.4. Unlike that from the CGMD calculated with constant application of Langevin thermostat, the displacement has similar level with that of Classical MD simulation.

Result of Analysis I (b) : The energy profile of CGMD simulation using the displacement of beads model is calculated using Eq. (4.1) and Eq. (4.2). The work from the spring constants and the total energy deviation for each time step is in Fig. 4.3 (a) and (b). The result from Analysis I opens an interesting possibility that the potential energy defined by spring constants is righteous, but the way of force exerted from that amount of energy might be different from simple static condition. The exertion can be nonlinear as the motion of MD has proved in Sec 3 or some other force caused the thermal energy like n-th mode can be come into play. One suggestion from the strain condition for the derivation of governing equation will be followed at the end of this subsection.

Result of Analysis II : NMD is performed for 1^{st} and n -th mode in beads model and in each line of full structure of MD simulation. The result is in Fig. 4.5 ~ Fig. 4.7. Fig. 4.5 (a) shows the amplitude of the 1^{st} mode, and nth mode of beads model in Fig. 4.6. (b) is rather following the frequency and phase of 1^{st} transverse mode in Fig. 4.5. (a). And the displacement along tube

axis are negligible for both modes. This is exactly what assumed during the derivation of Eq. (3.1) ~ (3.2), as mentioned in Appendix I. To confirm this crucial assumption, NMD is directly measured as shown in Fig. 4.7, in which a line, i.e. 66 atoms, along tube axis is projected with n-th mode wave vector. Interestingly, this result shows the displacement along tube axis in a line, before they are averaged out, actually has very same level of displacement with that of other perpendicular axis. This is same for 1st mode projection to tube axis.

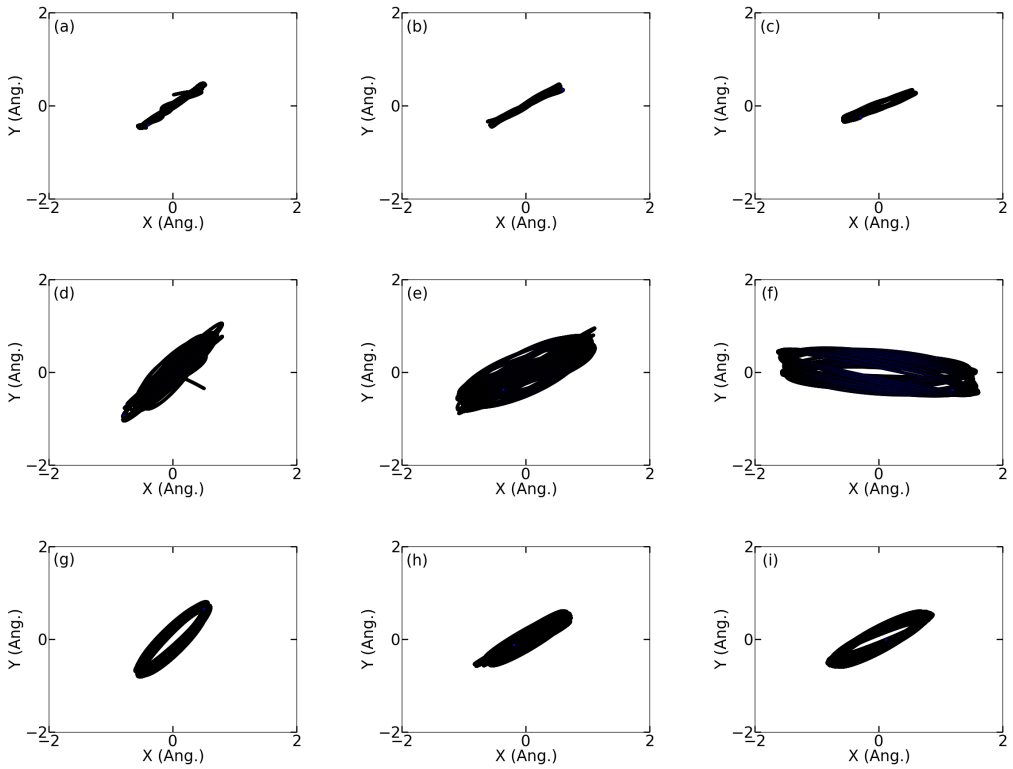

Fig.4.4. Poincare map from MD and CGMD for free thermal vibration; MD simulation (a) 0.6 ns ~ 1.2 ns, (b) 1.8 ns ~ 2.4 ns, (c) 3.0 ns ~ 3.6 ns; CGMD modeled with 10 atoms per node (d) 0.6 ns ~ 1.2 ns, (e) 1.8 ns ~ 2.4 ns, (f) 3.0 ns ~ 3.6 ns; CGMD modeled with 60 atoms per node, (g) 0.6 ns ~ 1.2 ns, (h) 1.8 ns ~ 2.4 ns, (i) 3.0 ns ~ 3.6 ns.

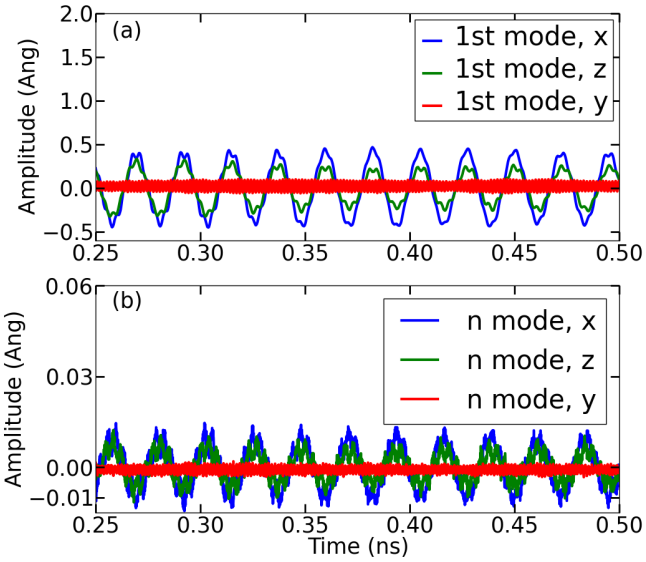

Fig. 4.5. Amplitude of 1st mode and Nth mode along each Cartesian axis, (a) 1st mode, (b) Nth mode in beads model.

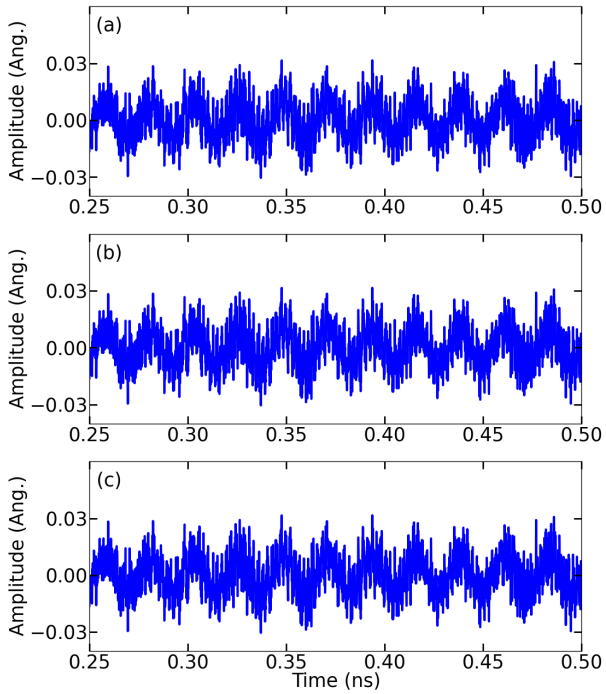

Fig. 4.6. Amplitude of 1st mode from nth mode from a line of tubes full structure along each Cartesian axis; (a) X axis, (b) Y axis, (c) Z axis.

The noticeable displacement along the tube axis means the significant dissemblance to the continuum frame-works, the Euler beam theory. The reason that the beads model has negligible level along tube axis in Fig. 4.6 is well explained in Fig 4.7, where all 10 lines of (5,5) SWNT has projected to 1st and n-th mode wave vector. While the displacement along x axis, sharing the same phase for the amplitude between all lines in Fig. 4.7 (a), the displacement along the tube axis in Fig. 4.7 (c) has opposite phase with neighbor lines. Particularly, line #1~#3 and line #6 and #8 are revealing such condition as modulating in the frequency and phase of 1st transverse mode shown in Fig. 4.7 (a).

Fortunately, the phase with the opposite for half of lines to the other half of 5 lines as shown in Fig. 4.7 (c) is the same assumption on the strain distribution of tube axis in continuum beam theories as described in Fig. 4.8.

The n-th mode is checked, which is the measure how much the motion is out of range of continuum frame as mentioned in former paragraphs. From this view point, the phase of n-th mode following the 1st mode trend, as shown in Fig. 4.8(b) and Fig. 4.8 (d), indicates the motion of SWNT is following continuum beam condition very well. The dependency of n-th mode to the lowest frequency motion is started to be disturbed in other dissipative condition in following sections and is discussed at the end of this section.

The Analysis I and II gives two conclusions. One is mechanical motion of SWNT is convertible to beam like motion with CGMD spring constant except its nonlinear behaviour. From what have been learned, the suggestions for CGMD will be in next sub section. The other conclusion is that the n-th mode is acting in same condition with transverse mode for free thermal vibrations.

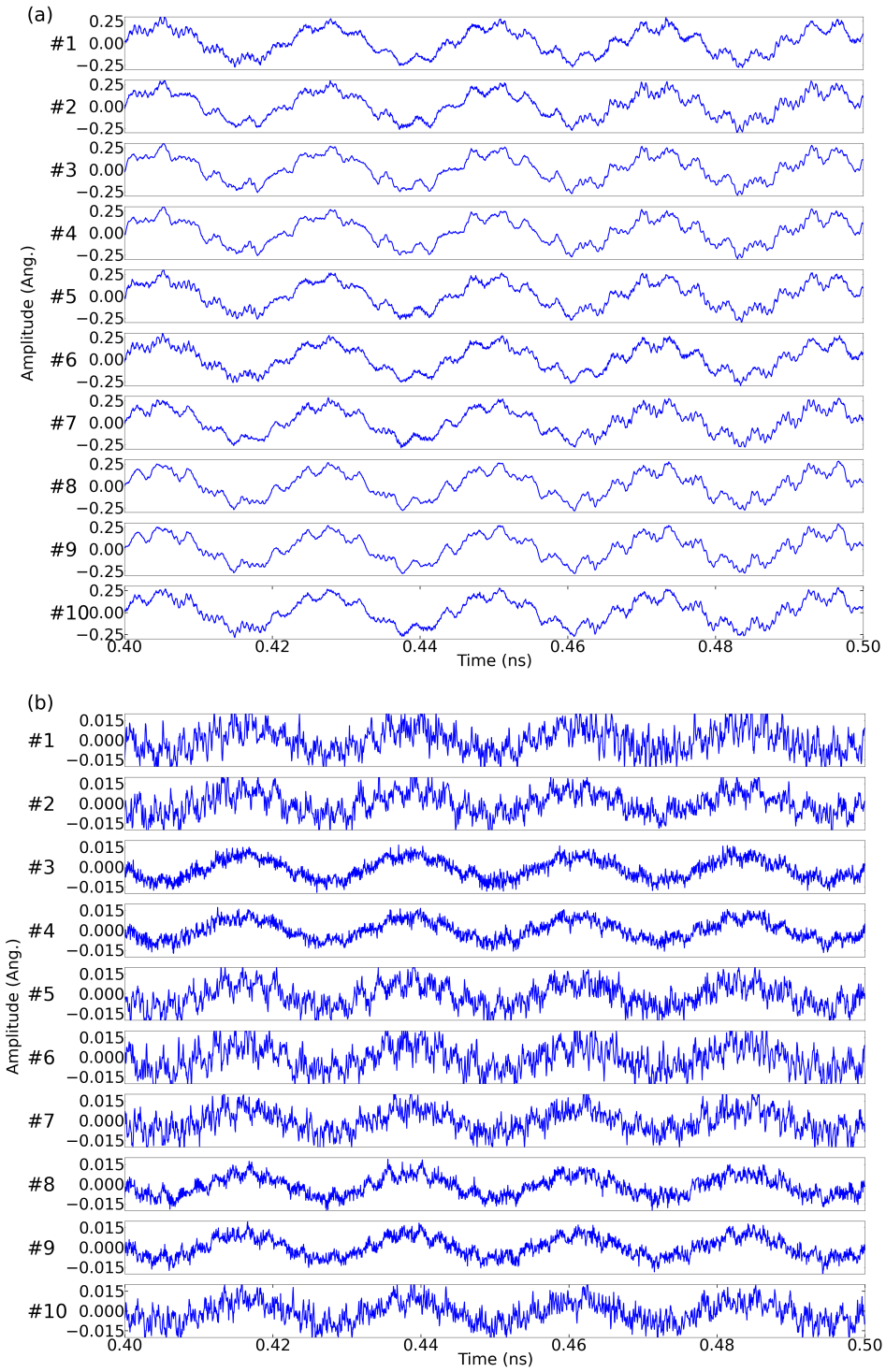
(a)
#1
#2
#3
#4
#5
#6
#7
#8
#9
#10
0.25
0.00
−0.25
Amplitude (Ang.)
0.40
0.42
0.44
0.46
0.48
0.50
Time (ns)
(b)
0.015
0.000
−0.015
Amplitude (Ang.)
Time (ns)

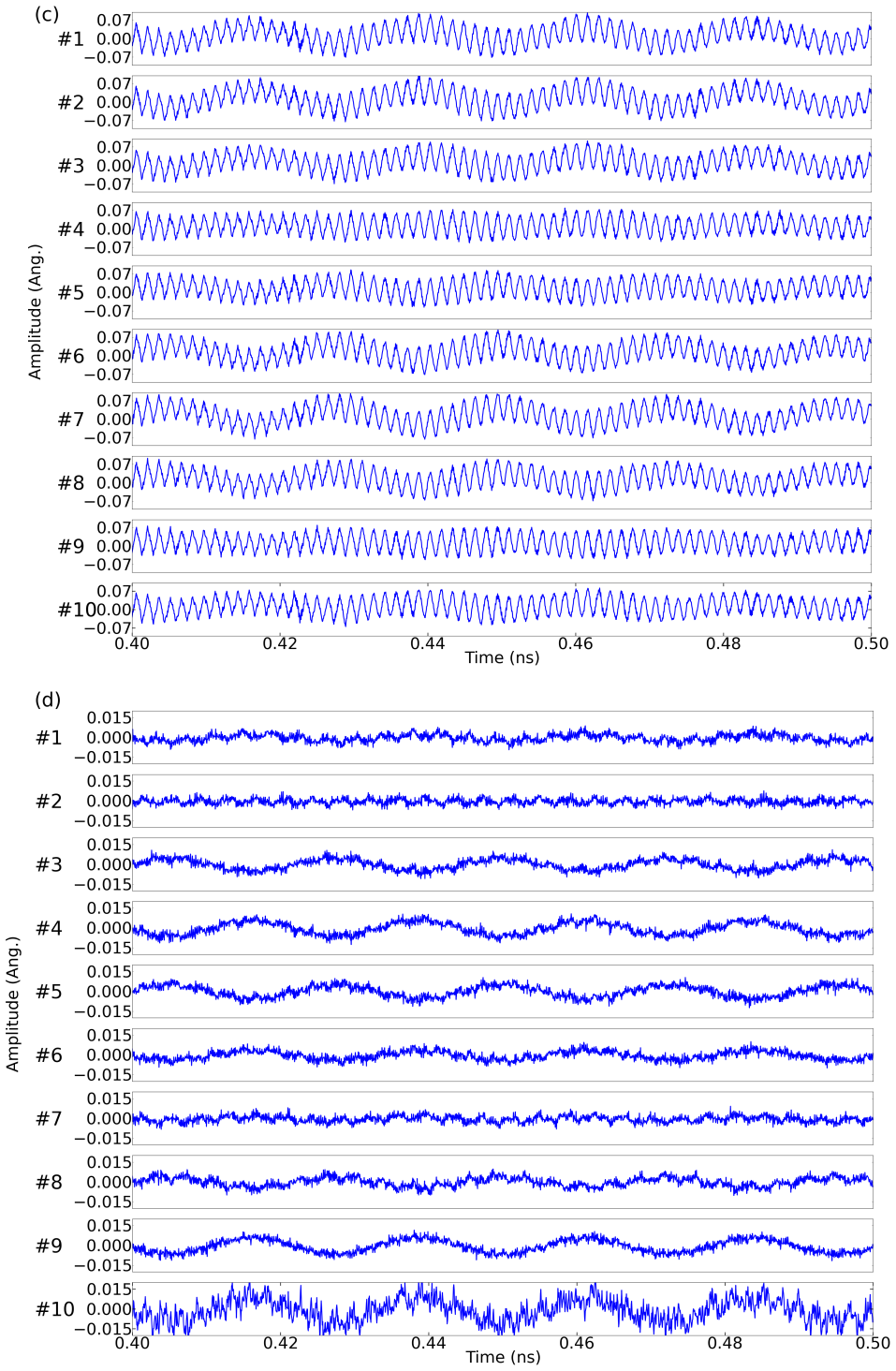

Fig.4.7. Amplitude of motion of 1st and n-th mode measured from each line of SWNT, (a) projection with 1st mode of x axis displacement, (b) projection with Nth mode of x axis displacement, (c)projection with 1st mode of y axis displacement (d)projection with Nth mode of y axis displacement.

4.1.1 Amplitude and thermostatting

The status of SWNT at certain temperature is revealed to have quiet level of amplitude for 1st transverse mode, which is from 1 Ang. to 6 Ang. for 7.6 nm~ 23.5 nm length tubes at 300 K, including on the temperature dependency by Gibbs-Boltzmann distribution and radius of SWNT. The area of the tip of SWNT can have about 1.2 to 3.2 nm as its diameter at 800K for 7.6 nm and 23.5 nm respectively. These diameters can be even larger when the fixation of end point is weak. The distance of catalyst is at least 1~2 nm. The possibility to make a collision with neighbor tubes is increasing with the square of the radius of trajectory and it is $\pi r/2r_0$ times bigger when the motion is in whirling than a simple planar motion. r_0 is the radius of tube and r is the radius of whirling of tube. CGMD simulation with initial data from beads model has its motion as Fig. 4.10. The poincare map has same amount of displacement as MD simulation but whirling does not appeared.

The conventional CGMD with the thermostat is essential due to the constant energy disturbance as increasing its length and colliding from other tubes in relatively high temperature. And as mentioned above, this dissipative condition is very important for coagulation of molecules. The turning off the thermostatting after the energy is stabilized may gives certain level of displacements, however, this is not the proper maneuver to the constant source of increase of energy during the growing process. Better thermostatting mechanism is essential.

Langevin thermostatting attached to the string for SWNT modeling, however, disturbs the modal behavior of string severely, so that it does not show neither of the same range of displacement nor the same level of appearance of whirling motion as shown in Fig. 4.10 (b). Even if the conventional CGMD with the initial values from beads model has used for

morphology study with compromised colliding number, the possibility to have collision between SWNT should be more compromised due to the influence of the thermostat.

4.1.2 Strain CGMD with initial value from classical MD

As discussed in Analysis I (a) and (b), the exertion of energy as the force would be different way from the CGMD algorithm. To compensate the absence of the mechanism for mode coupling between two orthogonal displacement in conventional CGMD, the different energy exertion is explored in this subsection, adapting the Green-Lagrange strain instead of length spring constants. The force along the tube axis is calculated as below:

$$\epsilon_{zz} = \bar{w}_{,z} + \frac{1}{2}\left(\bar{u}_{,z}^2 + \bar{v}_{,z}^2 + \bar{w}_{,z}^2\right) \tag{4.4}$$

$$F_z = E \int \epsilon_{zz}\, dA \tag{4.5}$$

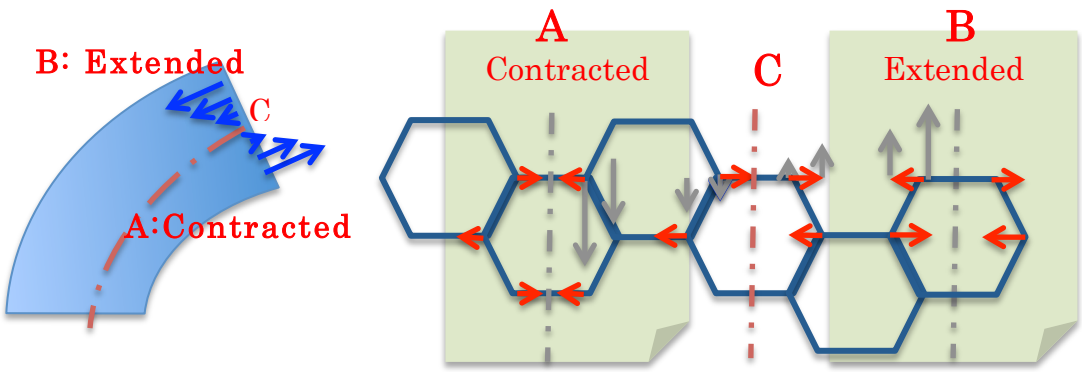

Fig.4. 8. Schematic figure for strain in bending condition, (a) notation for each condition, (b) the strain supposed to be exerted on each side, gray arrows are strain condition from continuum beam theory, red arrow is the strains supposed to be realized for SWNT network.

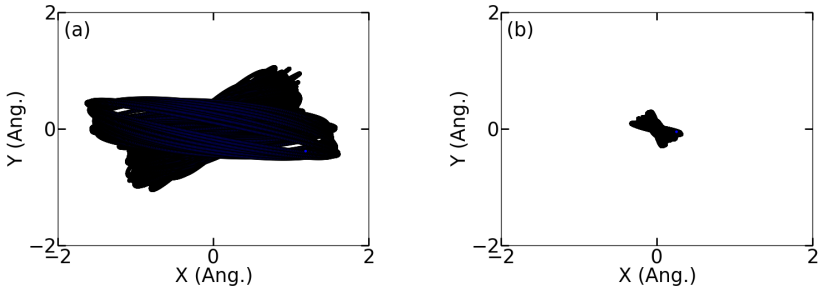

Fig. 4.9 Poincare map of tip location of (5,5) SWNT at 300K, (a) CGMD with initial condition from beads model, (b) Langevin thermostatted CGMD calculation.

Fig. 4.10 is the Poincare map with the strain-CGMD calculation with the initial condition from beads model. The motion of string is maintaining the whirling motion and does not have the motion or the rotation exchanging like full structured SWNT does. Since the exact longitudinal strain condition or the nonlinear term to the angle spring are yet applied, the motion itself does not have the mode coupling completely, but this result implies the one simple dimensional string in CGMD can have nonlinear behavior with different forcing mechanism.

From next sections, the role of optical mode during the various external excitation is observed and further study will be discussed.

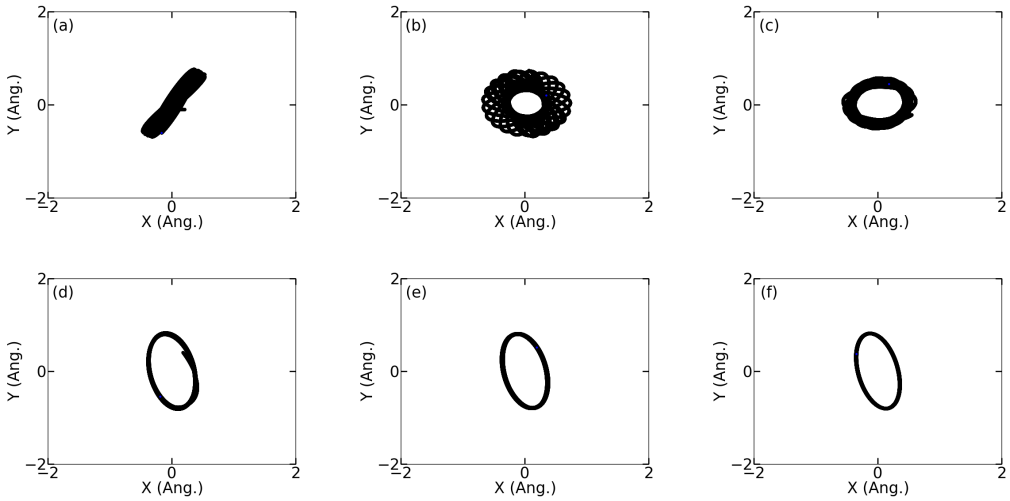

Fig. 4.10 Poincare map of CGMD with strain energy instead of spring constant along tube axis; (a)~(c) Strain-CGMD with 10 atoms per node and initial condition from MD simulation; (a)0.6 ns ~ 1.2 ns, (b)2.4 ns ~ 3.0 ns, (c)4.2 ns ~ 4.8 ns, (d)~(f) Strain-CGMD with 60 atoms per nodes and initial condition from MD simulation; (d) 0.6 ns ~ 1.2 ns, (e)2.4 ns ~ 3.0 ns, (f)4.2 ns ~ 4.8 ns.

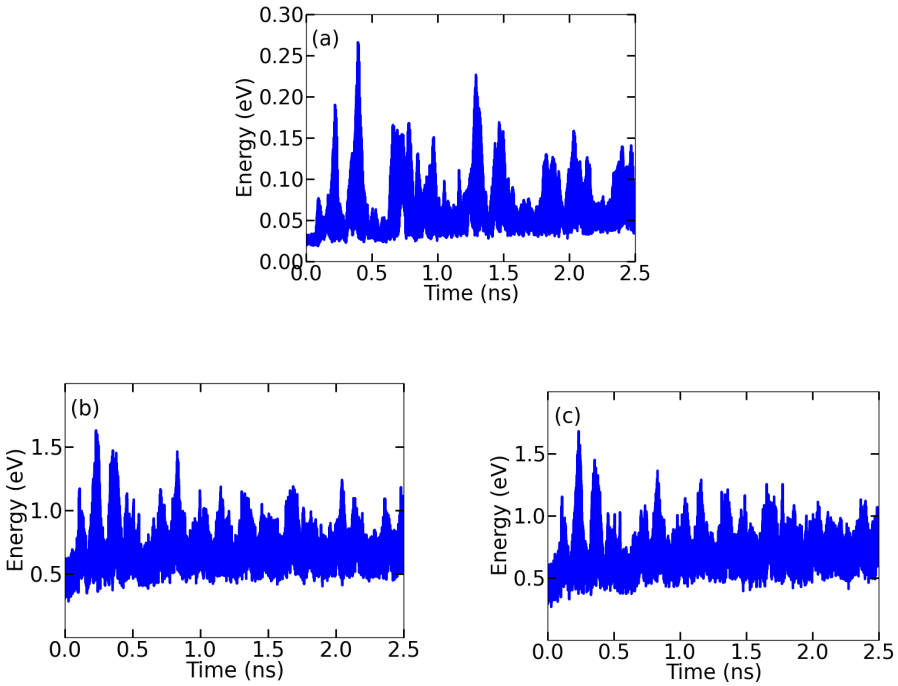

Fig. 4.11. Kinetic energy of collision simulations, (a) beads model from collided SWNT at 300K, (b) Collided CGMD string from the initial condition of 300K, (c) Collided CGMD string from the zero temperature.

4.2 Collision

- Collision algorithm

The advantage of using the most simplified structure like one dimensional string is that the node length can be extended until the CFL (Courant-Friedrich-Levy) boundary condition allows for targeted wave length. Meanwhile the interaction between tubes can be transparent each other with long node length because the distance between tubes can be longer than the cut off length of inter-tube potential functions, which is calculated by the distance between nodes belong to each tube. To prevent the transparent tube-tube interaction, the minimum distance, D_{min} between the lines defined by the two nodes for each tube is calculated for the force from LJ potential function. The calculated force is applied to four nodes, i.e. lumped mass, with the weighting proportional to the distance from the point where the D_{min} is measured. The sigma and epsilon is from the LJ potentials between C60 and SWNT. [Girifalco et al., 2000]

- Beads model

For the control condition, the full structured MD is calculated using (5,5) 23.5 nm length SWNT as described in Sec. 2.6. Firstly, the two suspended tube using phantom wall condition described in Sec. 2 is prepared at 300K with Langevin thermostat during 1 ns. Then, one of them is added with the bending strain defined as 15 Ang. amplitude with sine function, which has the length of SWNT as its half wave length. The other tube is rotated with 90 degree and arranged to meet with the artificially strained tube at its middle point. The purpose of this comparison is for the observation of the response after the collisions, therefore, any specific effort to smooth the artificial bending strain condition is not considered and only the tube,

which is collided by another tube's reaction, is analyzed.

Result of Analysis I (b)

Simulation time is 2.5 ns with 0.5 fs of time step. Each 5 fs, the displacement and velocity for all atoms in the SWNT, total 4000, is gathered to make beads model. CGMD has same time step and sampling frequency with MD simulation. Total simulation step is also same. The spring constants are same with (5,5) 7.6 nm case.

The kinetic energy after the collision is in Fig. 4.1a (a). The first peak in Fig. 4.11(a) is identical to the moment of 1st recovery from the hit by another tube. The bottom line of kinetic energy is monotonically increasing after the first shock. The kinetic energy profile from CGMD simulations are in Fig. 4.13 (b). For the better observation, the zero temperature condition also examined as not offering the initial velocity condition into CGMD simulation. Its kinetic energy profile is in Fig. 4.13 (c).

Result of Analysis II : Damping process from the collision

Beads model and CGMD result are analyzed using NMD. The results of 1st mode and n-th mode for each case are in Fig. 4.14~ Fig. 4.16. The major difference is that there is a sudden increase of n-th mode in case of MD simulation. On the contrary, there are no spikes of nth mode for CGMD case.

The 1st mode decays faster in beads model as in the Fig. 4.12 than that of CGMD in the Fig. 4.13-14. In MD case, severe spike of nth mode is followed for each collision between tubes. These shock waves in nth mode are not appeared in the result of CGMD simulation. The decay

of 1st mode of CGMD are much longer than MD result. Clear spikes of nth mode induced by the impact force seems to be very obvious reason of faster decay in full structure, because nth modes should be much easier to be immersed into the thermal energy. The kinetic energy in both cases, however, shows the same amount of monotonic increase in Fig. 4.13. This is very identical with the free thermal motion of beads model. The amount of energy is same, but the proportion of energy in each mode is not.

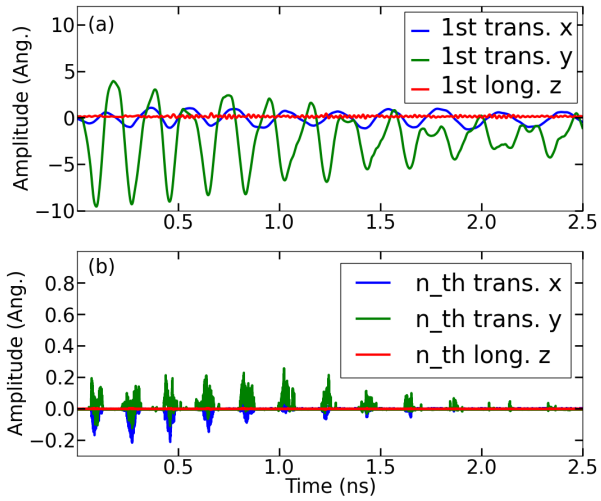

Fig. 4.12. Amplitude of 1st mode and nth mode of beads model from collided SWNT at 300K; (a) 1st mode, (b)n-th mode.

MD result in Fig. 4.12 and CGMD result in Fig. 4.13-14, which are calculated with the initial condition from MD simulation, has the same number of nodes. If CGMD does not have n-thl mode shock like the beads model from the response of full structure, this shock can be said it came from the modal behavior of finer wave length mode like radial or torsional mode, which are beyond the continuum mechanics can have.

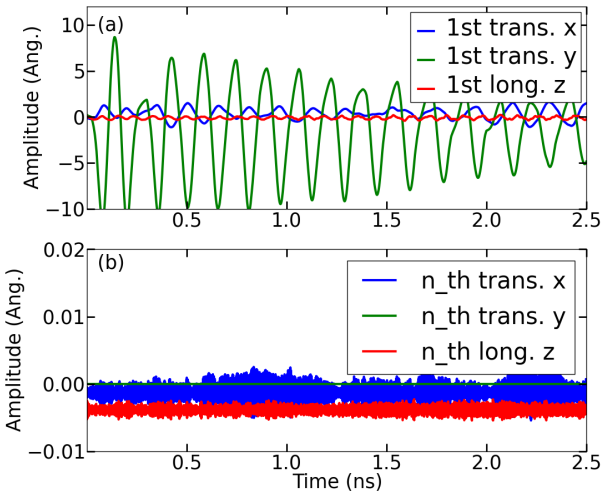

Fig. 4.13. Amplitude of 1st mode and nth mode of beads model from collided CGMD string of SWNT at 300 K; (a) 1st mode, (b)n-th mode.

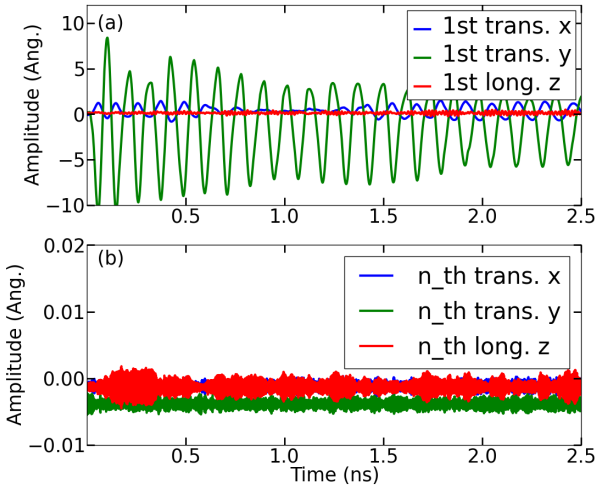

Fig. 4.14. Amplitude of 1st mode and optical mode of beads model from collided CGMD string of SWNT at 0 K; (a) 1st mode, (b)n-th mode.

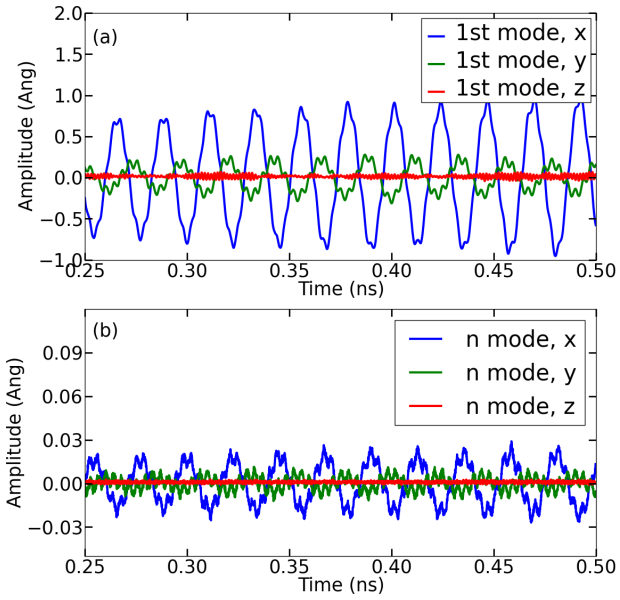

Fig. 4.15. Amplitude of 1st mode and optical mode of beads model from forced excited with 0.01 Ang cantilevered SWNT at 300 K; (a) 1st mode, (b) n-th mode.

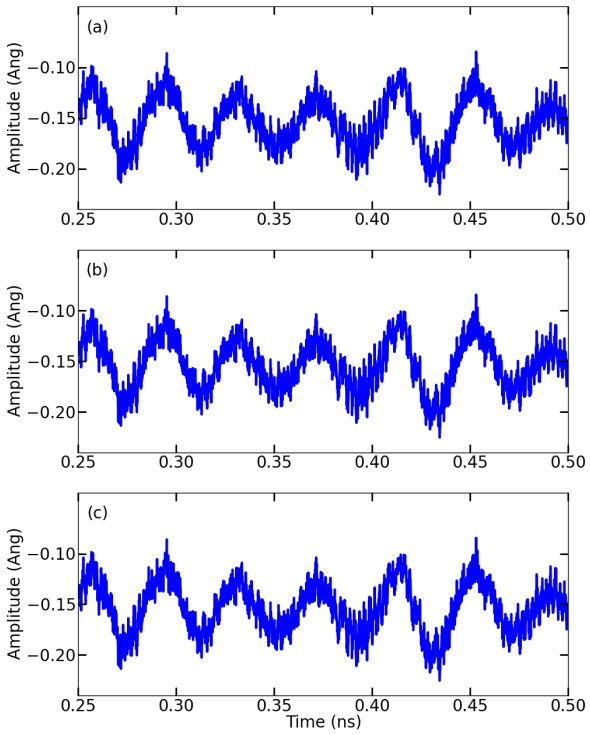

Fig. 4.16. Amplitude of nth mode from a line in full structure of forced excited SWNT with 0.01 Ang; (a) projection to x axis, (b) projection to y axis, (c) projection to z axis.

4.3 Constant dissipation condition

In following subsections, the response of SWNT from steady external disturbance is studied. This analysis is for checking the 1st mode behavior of SWNT in such harsh condition is still in the range of continuum beam models. The active n-th mode response, differed from 1st mode is regarded as the indication for the response of SWNT beyond the continuum-mechanical response.

4.3.1 Forced excitation

The result of Table 2.5 in Sec. 2 is analyzed using Analysis I (a). Sampling frequency is 50 fs. Tube is excited with 0.01 Ang along x axis as introduced in Sec. 2.

As briefly discussed in Sec. 2, external excitement in mechanical source – shaking the bottom of cantilevered tube with slightly off- resonance frequency, which is 44.5 GHz for (5,5) 7.6 nm SWNT is performed with the dissipation source with a length of unit cell The motion added as big wave lengths should be scattered out to be absorbed through the small thermostatting region. The motion itself shows rotation exchange with some whirling motion like the free thermal vibration had shown with losing the trend of rotation exchange.

The modal response for 1st and Nth mode in Fig. 4.17-18 is revealed with the enlarged amplitude of n th mode. Comparing with free thermal vibration results, the amplitude of n th mode is about 2 times larger, but that of 1st mode has very weak increasemnt. N th mode is activated with little off-phased with 1st transverse modes as shown in Fig. 4.19, but still the motion of 1st mode is in the range of continuum mechanical regime based on the similarity of displacement along y axis.

4.3.2. Thermally Disturbed Boundary

If the forced excitation with 1st mode frequency is inducing the acoustic mode scattering into the small waves, the thermal conduction situation with two thermostatting at both ends makes the tube packed with small waves. To consider the 1st mode motion severely influenced by small waves, the data from the paper written by S. Maruyama in 2002[Maruyama, 2002] is converted to beads model and analyzed with NMD. The some data has merely one cycle or less time span, so the trend of 1st mode is very difficult tracking. The motion of he short SWNT like (5,5) 6 nm long, which is effected by the thermal conduction, can be analyzed thanks to its high resonance frequency.

Its amplitude of n-th mode from beads model has no resemblance with 1st mode unlike the free thermal vibration. The optical mode of each line in along x and z axis is separated by half to share the same phase with same frequency of 1st transverse mode. The other half has the opposite phase. In case of same mode along y, each neighbor has opposite phase like forced excitation in Fig. 4.21, but they have more random frequency.

4.3.3. Boundary of continuum frame works in SWNT

The n th mode, which has same wave profile with the 1st transverse mode in free thermal vibration, shows the different results from collision, dissipation from the resonance and thermal conduction simulation. With additional displacement of 1st mode during collision, intensive n th mode amplitude is appeared. As n th mode is activated, the mechanical motion such as 1st transverse mode becomes to get less influence by excitation or more rotation exchange.

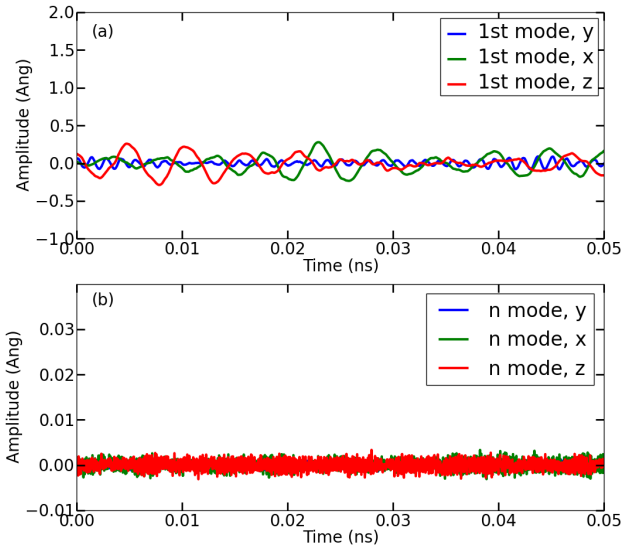

Fig. 4.17. Amplitude of 1st mode and nth mode from beads model averaged from 5 nm length SWNT with temperature difference; (a) 1st mode, (b)n-th mode.

This signifies that the mechanical motion like 1st mode can be easily influenced by the state of n th mode according to NMD analysis. This sensibility of 1st mode to thermal vibration whose wavelength is out of range for continuum mechanics is the difference between continuum media and molecular system. The unique structure of SWNT, which has only one layer and has cylinderical shape may have more sensibility than MWNT or other quasi-1D molecular system.

5. Summaries and Discussion

5.1 Summaries

In this thesis, thermal-mechanical motion of SWNT is studied using Molecular dynamics simulation and the analysis from elastic continuum beam theory. The thermal- mechanical motion is restricted to the 1st transverse vibration mode of SWNT in this thesis.

Firstly, free thermal vibration is observed. The motion is appearing as the planar or the non-planar motion, i.e. whirling like jumping rope, with rotation exchange. The nonlinear beam theory [Ho et al., 1976] offers the exact same condition using the derivation with the strain energy from two Cartesian axes, which are perpendicular to tube axis. The parameters fitted to the nonlinear motion of SWNT from MD simulation shows the strong tendency along the temperature and its geometry.

The analytic solution derived from 1st-1st normal mode coupling explains other characteristics such as; 1) Frequency shift dependent on the total amplitdue, 2) Periodic motion exchange between non-planar and planar motion, 3) Rotational direction exchange of non-planar motion. While the motion is changing its rotational direction, however, it is not always remained as predicted with the solution, this is supposed due to the mode interaction limited only to 1st-1st mode. Normal mode energy transfer between other modes should be included for the accuracy.

The frequency response of the thermal-mechanical motion of tubes happens to have the multiple peaks for a single resonance mode due to the nonlinear motion. This response is compared with the similar results reported from the state of art experiments using suspended

SWNT with forced excitation conditions. [Eichler et al., 2013, Sazonova et al., 2004] For the analytic solutions for free thermal vibration provides the same number of peaks and the distance between peaks in the frequency response of experiments, the nonlinearity of structural condition is suggested as the reason of multiple peaks instead of nonlinear damping or slacking. The brief formulation as a function of geometric condition of tubes is offered for the trend of parameters in the analytic solution.

The solution of free vibration of SWNT, therefore, gives new viewpoint that such multiple peaks are its natural characteristics, not its nonlinear response from the forced excitement. The relaxation process for 1st transverse mode, which have known as the reason of peak broadening in continuum mechanics should be reconsidered as the result of the energy exchange between transverse modes in two orthogonal planes in case of quasi-1D molecular system.

From the agreement between the motion of SWNT observed from MD simulation and nonlinear beam theory, the possibility of the perfect one dimensional mass-spring model for SWNT is examined with the CGMD algorithm. Since the algorithm with conventional angle spring only affords torques in one plane, the strain condition used for the derivation of nonlinear bending equation is applied and succeed to make whirling motion except the motion or rotation exchange.

The other characteristics for the simplified one dimensional mass-spring model of SWNT is suggested from various MD simulations such as mechanical resonance excitation, collisions from another tube and thermally disturbed boundary. For each condition, the following features are observed from the beads model, i.e. averaged model from MD simulation into one

dimension string. These responses are supposed to be realized into CGMD algorithm for better morphology and the characteristic study of the complex of SWNT.

- Free thermal vib. : non-planar and planar motion exchange and rotation exchange at high temperature
- Forced excitation : bigger amplitude in nth mode by NMD analysis. The rotation exchange loses its trend with forced excitation case
- Collisions : Collided tube is analysized with NMP. More rapid damping than simple CGMD string due to optical mode propagation from the collision.
- Thermally disturbed boundaries : thermostat attached to the ends of tubes with and without temperature gradient. Less rotation exchange is observed without temperature gradient and activated optical mode is found in other case.

5.2 Discussions

Relaxation process i.e. damping of 1st mode has been measured using the peak shape. Multiple peaks found from simulation and experiments make difficulties for fitting of Lorentzian as rising one question on its physical meaning. Theoretical work for periodic appearance between **n**on-planar and planar motion of free thermal vibration of SWN**T** includes the rotation exchange from clock-wise and counter clock-size without damped out energy, which should return to 1st mode motion because of energy conservation. This is not Lorentzian shape peak can suggest.

Another interesting point is the tendency of C_0 with the geometry of tube. This trend covers well the experimental result from suspended FET system by SWNT. Multiple resonances found from the experiments can be explained with mode coupling without including the damping process mechanism directly. For very low temperature case, however, the amount of total amplitude should be fitted to have same result as experiment. This represents the peak location of forced excitation is not always identical to that of free thermal vibration response. The amplitude from forced excitation can differ the peak locations. With the compensation of the governing equation adapted in this thesis to consider the another significant factor for beating i.e. the rigidity and the amplitude from forced excitation, more precise prediction of multiple resonance peak would be possible.

CGMD and CGMD with strain force have been examined based on what have been found from nonlinear dynamics regime. CGMD motion with strain forces has converged into whirling state. CGMD with strain terms shows whirling motion whose appearance is not from

conventional CGMD, but none of both has exchange motion. The reason of this discrepancy, the n-th mode tendency in free thermal vibration, forced excitation, collisions and thermal boundary condition is considered. There is a high expectation to reveal the proper dissipation mechanism for quasi-1D system. The achievement is supposed not only to make proper entanglement between many strings of CGMD but also to offer the clue to link the continuum frame works to atomic vibration for the multi-scale simulations. For its initial trials, the role of n-th mode for damping for SWNT in collision and forced excitation is suggested.

Thermal conduction condition with short (5,5) SWNT cases is additionally checked the state of low frequency motion with temperature gradient. Indeed, the n th mode of beads model showed no tendency like it has for free thermal vibration condition. The role of n-th mode to make the thermal-mechanical motion is a unique characteristic only can be found in molecular system. How much those two are related and where is the key to control one and another seems very interesting question to be answered.

Reference

Arroyo, M., & Belytschko, T. (2003). Nonlinear mechanical response and rippling of thick multiwalled carbon nanotubes. *Physical Review Letters*, *91*(21), 1–4.

Arroyo, M., & Belytschko, T. (2004). Finite crystal elasticity of carbon nanotubes based on the exponential Cauchy-Born rule. *Physical Review B*, *69*(11), 1–11.

Askes, H., & Aifantis, E. C. (2011). Gradient elasticity in statics and dynamics: An overview of formulations, length scale identification procedures, finite element implementations and new results. *International Journal of Solids and Structures*, *48*(13), 1962–1990.

Ayari, A., Vincent, P., Perisanu, S., Choueib, M., Gouttenoire, V., Bechelany, M., Cornu, D. & Purcell, S. T. (2007). Self-oscillations in field emission nanowire mechanical resonators: a nanometric dc-ac conversion. *Nano Letters*, *7*(8), 2252–7.

Barnard, A. W., Sazonova, V., Zande, A. M. Van Der, & McEuen, P. L. (2011). Fluctuation broadening in carbon nanotube resonators, *PNAS, 109*(47), 19093-6.

Buehler, M. J. (2006). Mesoscale modeling of mechanics of carbon nanotubes : Self-assembly, self-folding, and fracture. *Journal of Material Research., 21(11)*, 2855–2869.

Cao, G., Chen, X., & Kysar, J. W. (2006). Thermal vibration and apparent thermal contraction of single-walled carbon nanotubes. *Journal of the Mechanics and Physics of Solids*, *54*(6), 1206–1236.

Capaz, R., Spataru, C., Tangney, P., Cohen, M., & Louie, S. (2005). Temperature Dependence of the Band Gap of Semiconducting Carbon Nanotubes. *Physical Review Letters*, *94*(3), 036801.

Carr, S., Lawrence, W., & Wybourne, M. (2001). Accessibility of quantum effects in mesomechanical systems. *Physical Review B*, *64*(22), 1–4.

Castellanos-Gomez, A., Meerwaldt, H. B., Venstra, W. J., van der Zant, H. S. J., & Steele, G. A. (2012). Strong and tunable mode coupling in carbon nanotube resonators. *Physical Review B*, *86*(4), 041402.

Chang, C., Okawa, D., Garcia, H., Majumdar, A., & Zettl, A. (2007). Nanotube Phonon Waveguide. *Physical Review Letters*, *99*(4), 1–4.

Conley, W. G., Raman, A., Krousgrill, C. M., & Mohammadi, S. (2008). Nonlinear and nonplanar dynamics of suspended nanotube and nanowire resonators. *Nano Letters*, *8*(6), 1590–5.

Craighead, H. G. (2000). Nanoelectromechanical Systems. *Science*, *290*(5496), 1532–1535.

Cremer, L., Heckl, M., & Ungar, E. (1990). *Structural Borne Sound: Structural Vibrations and Sound Radiation at Audio Frequencies*. Verlag: Springer.

Cui, K., Chiba, T., Omiya, S., Thurakitseree, T., Zhao, P., Fujii, S., Kataura, H., Einarsson, E.,, Chiashi, S., Maruyama, S. (2013). Self-Assembled Micro-Honeycomb Network of Single-Walled Carbon Nanotubes for Solar Cell, *Journal of Physical Chemistry Letters*, 4, 2571-2576.

Cui, K., Anisimov, A. S., Chiba, T., Fujii, S., Kataura, H., Nasibulin, A. G., Chiashi, S., Kauppinen, E. I., Maruyama, S., (2014). Air-Stable High-Efficiency Solar Cells with Dry-Transferred Single-Walled Carbon Nanotube Films, Journal of Material Chemistry, A, 2, 11311-11318.

Davis, V. A, Parra-Vasquez, A. N. G., Green, M. J., Rai, P. K., Behabtu, N., Prieto, V., Booker, R. D., Schmidt, J., Kessellman, E., Zhou, W., Fan, H., Adams, W.W., Haugel, R.H., Fischer, J., Cohen, Y., Talmon, Y., Smalley, R.E., Pasquali, M. (2009). True solutions of single-walled carbon nanotubes for assembly into macroscopic materials. *Nature Nanotechnology*, *4(12)*, 830–4.

De Volder, M. F. L., Tawfick, S. H., Baughman, R. H., & Hart, a J. (2013). Carbon nanotubes: present and future commercial applications. *Science*, *339*(6119), 535–9.

Dresselhaus, M. S., Dresselhaus, G., & Jorio, A. (2004). Unusual Properties and Structure of Carbon Nanotubes. *Annual Review of Materials Research*, *34*(1), 247–278.

Duan, H., & Berggren, K. K., (2010) Directed self-assembly at the 10 nm scale by using capillary force-Induced nanocohesion, *Nano Letters, 10*(9), 3710–3716.

Eichler, A., Moser, J., Chaste, J., Zdrojek, M., Wilson-Rae, I., & Bachtold, a. (2011a). Nonlinear damping in mechanical resonators made from carbon nanotubes and graphene. *Nature Nanotechnology*, *6*(6), 339–42.

Elliott, J. A. (2011). Novel approaches to multiscale modelling in materials science. *International Materials Reviews*, *56*(4), 207–225.

Eom, K., Park, H. S., Yoon, D. S., & Kwon, T. (2011). Nanomechanical resonators and their applications in biological/chemical detection: Nanomechanics principles. *Physics Reports*, *503*(4-5), 115–163.

Feng, E. H., & Jones, R. E. (2010). Equilibrium thermal vibrations of carbon nanotubes. *Physical Review B*, *81*(12), 1–5.

Feng, E., & Jones, R. (2011). Carbon nanotube cantilevers for next-generation sensors. *Physical Review B*, *83*(19), 1–6.

Foteinopoulou, K., Karayiannis, N., Laso, M., Kröger, M., & Mansfield, M. (2008). Universal Scaling, Entanglements, and Knots of Model Chain Molecules. *Physical Review Letters*, *101*(26), 265702.

Fritsch, S., Poblete, S., Junghans, C., Ciccotti, G., Delle Site, L., & Kremer, K. (2012). Adaptive resolution molecular dynamics simulation through coupling to an internal particle reservoir. *Physical Review Letters*, *108*(17), 170602.

Gall, K., Diao, J., & Dunn, M. L. (2004). The Strength of Gold Nanowires. *Nano Letters, 4*(12), 2431-6.

Garcia-Sanchez, D., San Paulo, a., Esplandiu, M., Perez-Murano, F., Forró, L., Aguasca, a., & Bachtold, A. (2007). Mechanical Detection of Carbon Nanotube Resonator Vibrations. *Physical Review Letters*, *99*(8), 1–4.

Gil-Santos, E., Ramos, D., Martínez, J., Fernández-Regúlez, M., García, R., San Paulo, A., … Tamayo, J. (2010). Nanomechanical mass sensing and stiffness spectrometry based on two-dimensional vibrations of resonant nanowires. *Nature Nanotechnology*, *5*(9), 641–5.

Girifalco, L. A., Hodak, M., & Lee, R. S. (2000). Carbon nanotubes, buckyballs, ropes and a universal graphitic potential. *Physical Review B*, *62*(19), 104–110.

Ho, C., Scott, R. A., & Eisley, J. G. (1975). Non-Planar, non-linear oscillations of a beam - I.Forced motions. *International Journal of Non-Linear Mechanics*, *10*, 113–127.

Ho, C.-H., Scott, R. A., & Elsley, J. G. (1976). Non planar nonlinear oscillations of a beam : II Free motions. *Journal of Sound and Vibration*, *47*(3), 333–339.

Hornstein, S., & Gottlieb, O. (2012). Nonlinear multimode dynamics and internal resonances of the scan process in noncontacting atomic force microscopy. *Journal of Applied Physics*, *112*(7), 074314.

Huang, Y., Wu, J., & Hwang, K. (2006). Thickness of graphene and single-wall carbon nanotubes. *Physical Review B*, *74*(24), 1–9.

Iijima. S & Ichigashi, T. (1993).Single-shell carbon nanotubes of 1 nm diameter, *Nature*, 363, 603-605.

Jensen, K., Kim, K., & Zettl, A. (2008). An atomic-resolution nanomechanical mass sensor. *Nature Nanotechnology*, *3*(9), 533–7.

Jiang, J.-W., Wang, J.-S., & Li, B. (2009). Thermal expansion in single-walled carbon nanotubes and graphene: Nonequilibrium Green's function approach. *Physical Review B*, *80*(20), 205429.

Katz, I., Lifshitz, R., Retzker, A., & Straub, R. (2008). Classical to quantum transition of a driven nonlinear nanomechanical resonator. *New Journal of Physics*, *10*(12), 125023.

Kim, J. M., Keffer, D. J., Kröger, M., & Edwards, B. J. (2008). Rheological and entanglement characteristics of linear-chain polyethylene liquids in planar Couette and planar elongational flows. *Journal of Non-Newtonian Fluid Mechanics*, *152*(1-3), 168–183.

Kozinsky, I., Postma, H. W. C., Bargatin, I., & Roukes, M. L. (2006). Tuning nonlinearity, dynamic range, and frequency of nanomechanical resonators. *Applied Physics Letters*, *88*(25), 253101.

Kozinsky, I., Postma, H. W. C., Kogan, O., Husain, A., & Roukes, M. L. (2007). Basins of Attraction of a Nonlinear Nanomechanical Resonator. *Physical Review Letters*, *99*(20), 8–11.

Krishnan, A., Dujardin, E., Ebbesen, T. W., Yianilos, P. N., & Treacy, M. M. J. (1998). Young's modulus of single-walled nanotubes. *Physical Review B*, *58*(20), 13–19.

Kwon, Y.-K., Berber, S., & Tománek, D. (2004). Thermal Contraction of Carbon Fullerenes and Nanotubes. *Physical Review Letters*, *92*(1), 1–4.

Ladd, A. J. C., Moran, B., & Hoover, W. G. (1986).Lattice thermal conductivity: A comparison of molecular dynamics and anharmonic lattice dynamics, *Physical Review 34*(8), 5058–5064.

Lai, W. M., Rubin, D., & Krempl, E. *Introduction to Continuum mechanics 3rd.,* Mc-Graw Hill, (2009)

Lassagne, B., Tarakanov, Y., Kinaret, J., Garcia-sSanchez, D., Garcia-Sanchez, D., & Bachtold, A. (2009). Coupling mechanics to charge transport in carbon nanotube mechanical resonators. *Science*, *325*(5944), 1107–10.

Li, Y., & Kröger, M. (2012a). A theoretical evaluation of the effects of carbon nanotube entanglement and bundling on the structural and mechanical properties of buckypaper. *Carbon*, *50*(5), 1793–1806.

Li, Y., & Kröger, M. (2012b). Viscoelasticity of carbon nanotube buckypaper: zipping–unzipping mechanism and entanglement effects. *Soft Matter*, *8*(30), 7822.

Lifshitz, R., & Roukes, M. L. (2000). Thermoelastic damping in micro- and nanomechanical systems. *Physical Review B*, *61*(8), 5600–5609.

Lulla, K. J., Defoort, M., Blanc, C., Bourgeois, O., & Collin, E. (2013). Evidence for the Role of Normal-State Electrons in Nanoelectromechanical Damping Mechanisms at Very Low Temperatures. *Physical Review Letters*, *110*(17), 177206.

Maruyama, S. (2003). Molecular Dynamics Simulation of Heat Conduction of a Finite Length Single-Walled Carbon Nanotube. *Microscale Thermophysical Engineering*,7, 41–50.

Matheny, M. H., Villanueva, L. G., Karabalin, R. B., Sader, J. E., & Roukes, M. L. (2013). Nonlinear mode-coupling in nanomechanical systems. *Nano Letters*, *13*(4), 1622–6.

McGaughey, A., and Kaviany, M. (2004). Quantitative validation of the Boltzmann transport equation phonon thermal conductivity model under the single-mode relaxation time approximation. *Physical Review B*, *69*(9), 1–13.

Miller, R. E. & Tadmor, E. B. (2002). The Quasicontinuum Method : Overview, applications and current, *Journal of Computer-Aided Materials Design*, 9: 203–239.

Mitra, M., & Gopalakrishnan, S. (2007). Vibrational characteristics of single-walled carbon-nanotube: Time and frequency domain analysis. *Journal of Applied Physics*, *101*(11), 114320.

Noid, W. G. (2013). Perspective: Coarse-grained models for biomolecular systems. *Journal of Chemical Physics, 139,* 090901.

Nosé, S. (1984). A molecular dynamics method for simulations in the canonical ensemble. *Molecular Physics*, *52*(2), 255–268.

Ortiz, V., Nielsen, S. O., Discher, D. E., Klein, M. L., Lipowsky, R., & Shillcock, J. (2005). Dissipative particle dynamics simulations of polymersomes. *The Journal of Physical Chemistry. B*, *109*(37), 17708–14.

Ouyang, G., Li, X., Tan, X., & Yang, G. (2007). Anomalous Young's modulus of a nanotube. *Physical Review B*, *76*(19), 1–4.

Peano, V., & Thorwart, M. (2004). Macroscopic quantum effects in a strongly driven nanomechanical resonator. *Physical Review B*, *70*(23), 1–5.

Perisanu, S., Barois, T., Ayari, A., Poncharal, P., Choueib, M., Purcell, S. T., & Vincent, P. (2010). Beyond the linear and Duffing regimes in nanomechanics: Circularly polarized mechanical resonances of nanocantilevers. *Physical Review B*, *81*, 165440.

Perisanu, S., Barois, T., Poncharal, P., Gaillard, T., Ayari, A., Purcell, S. T., & Vincent, P. (2011). The mechanical resonances of electrostatically coupled nanocantilevers. *Applied Physics Letters*, *98*(6), 063110.

Perisanu, S., Vincent, P., Ayari, a., Choueib, M., Purcell, S. T., Bechelany, M., & Cornu, D. (2007). High Q factor for mechanical resonances of batch-fabricated SiC nanowires. *Applied Physics Letters*, *90,* 043113.

Plimpton, S. (1995). Fast Parallel Algorithms for Short-Range Molecular Dynamics. *Journal of Computational Physics*, *117*, 1–42.

Poncharal, P. (1999). Electrostatic Deflections and Electromechanical Resonances of Carbon Nanotubes. *Science*, *283*(5407), 1513–1516.

Postma, H. W. C., Kozinsky, I., Husain, A., & Roukes, M. L. (2005). Dynamic range of nanotube- and nanowire-based electromechanical systems. *Applied Physics Letters*, *86*(22), 223105.

Jacobs, W. M., Nicholson, D. A., Zemer, H., Volkov, A. N., & Zhigilei, L. V. (2012). Acoustic energy dissipation and thermalization in carbon nanotubes: Atomistic modeling and mesoscopic description. *Physical Review B*, *86*(16), 165414.

Qian, D., Wagner, G. J., Liu, W. K., Yu, M.-F., & Ruoff, R. S. (2002). Mechanics of carbon nanotubes. *Applied Mechanics Reviews*, *55*(6), 495.

Rhoads, J. F., Shaw, S. W., & Turner, K. L. (2010). Nonlinear Dynamics and Its Applications in Micro- and Nanoresonators. *Journal of Dynamic Systems, Measurement, and Control*, *132*(3), 034001.

Rudd, R., & Broughton, J. (1998). Coarse-grained molecular dynamics and the atomic limit of finite elements. *Physical Review B*, *58*(10), R5893–R5896.

Rudd, R., & Broughton, J. (2005). Coarse-grained molecular dynamics: Nonlinear finite elements and finite temperature. *Physical Review B*, *72*(14), 144104.

Saito, R., G. Dresselhaus, M.S. Dresselhaus, (1998) *Physical Properties of Carbon Nanotubes*, Imperial College Press, London.

Sadeghirad, A., & Tabarraei, A. (2013). A damping boundary condition for coupled atomistic–continuum simulations. *Computational Mechanics*, *52*(3), 535–551.

Sawano, S., Arie, T., & Akita, S. (2010). Carbon nanotube resonator in liquid. *Nano Letters*, *10*(9), 3395–8.

Sazonova, V., Yaish, Y., Ustünel, H., Roundy, D., Arias, T. A, & McEuen, P. L. (2004). A tunable carbon nanotube electromechanical oscillator. *Nature*, *431*(7006), 284–7.

Scheible, D. V, Erbe, A., & Blick, R. H. (2002). Tunable coupled nanomechanical resonators for single-electron transport. *New Journal of Physics*, *4*, 86–86.

Schelling, P., & Keblinski, P. (2003). Thermal expansion of carbon structures. *Physical Review B*, *68*(3), 1–7.

Schneider, T., Stoll, E. P., & Morf, R. (1978). Brownian motion of interacting and noninteracting particles subject to a periodic potential and driven by an external field. *Physical Review B*, *18*(3), 1417–1424.

Schuster, H. G., Lifshitz, R., & Cross, M. C. (2009). *Reviews of Nonlinear Dynamics of Complexity*, Wiley-VCH Verlag GmbH & Co. KGaA.

Shulaker, M. M., Hills, G., Patil, N., Wei, H., Chen, H.-Y., Wong, H.-S. P., & Mitra, S. (2013). Carbon nanotube computer. *Nature*, *501*(7468), 526–30.

Stuart, S. J., Tutein, A. B., & Harrison, J. a. (2000). A reactive potential for hydrocarbons with intermolecular interactions. *The Journal of Chemical Physics*, *112*(14), 6472.

Treacy, M., Ebbesen, T., & Gibson, J. (1996). Excetionally high Young;s modulus observed for individual carbon nanotubes. *Nature*, *381*, 678-680.

Ustünel, H., Roundy, D., & Arias, T. a. (2005). Modeling a suspended nanotube oscillator. *Nano Letters*, *5*(3), 523–6.

Verbridge, S. S., Shapiro, D. F., Craighead, H. G., & Parpia, J. M. (2007). Macroscopic Tuning of Nanomechanics : Substrate Bending for Reversible Control of Frequency and Quality Factor of Nanostring Resonators. *Nano Letters*, *7*(6), 0–7.

Viani, M. B.,Schaffel, T. E., Chand, A., Rief, M., Gaub, H. E., & Hansma, P. K. (1999). Small cantilevers for force spectroscopy of single molecules. *Journal of Applied Physics*, *86*(4), 2258.

Villanueva, L. G., Kenig, E., Karabalin, R. B., Matheny, M. H., Lifshitz, R., Cross, M. C., & Roukes, M. L. (2013). Surpassing Fundamental Limits of Oscillators Using Nonlinear Resonators. *Physical Review Letters*, *110*(17), 177208.

Volder, M.D., Tawfick, S.H., Park, S.J., Copic, D., Zhao, Z., Lu, W., Hart, A. J. (2010), Diverse 3D microarchitectures made by capillary forming of carbon nanotubes, *Advanced Materials* 22 (39), 4374-89

Volkov, A. N., & Zhigilei, L. V. (2010a). Scaling Laws and Mesoscopic Modeling of Thermal Conductivity in Carbon Nanotube Materials, *Physical Review Letters, 104, 215902*.

Volkov, A. N., & Zhigilei, L. V. (2010b). Structural stability of carbon nanotube films: the role of bending buckling. *ACS Nano*, *4*(10), 6187–95.

Waggoner, P. S., & Craighead, H. G. (2007). Micro- and nanomechanical sensors for environmental , chemical , and biological detection. *Lab Chip*, *7*, 1238–1255.

Wang, H., Schütte, C., & Site, L. D. (2012). Adaptive Resolution Simulation (AdResS): A Smooth Thermodynamic and Structural Transition from Atomistic to Coarse Grained Resolution and Vice Versa in a Grand Canonical Fashion., *Journal of Chemical Theory and Computation*. 8, 2878-2887.

Wang, L., & Hu, H. (2005). Flexural wave propagation in single-walled carbon nanotubes. *Physical Review B*, *71*(19), 1–7.

Warner, J. H., Young, N. P., Kirkland, A. I., & Briggs, G. A. D. (2011). atomic level. *Nature Materials*, *10*(12), 958–962.

Werner, P., & Zwerger, W. (2004). Macroscopic quantum effects in nanomechanical systems. *Europhysics Letters (EPL)*, *65*(2), 158–164.

Westra, H. J. R., Poot, M., van der Zant, H. S. J., & Venstra, W. J. (2010). Nonlinear Modal Interactions in Clamped-Clamped Mechanical Resonators. *Physical Review Letters*, *105*(11), 117205.

Wilson-Rae, I. (2008). Intrinsic dissipation in nanomechanical resonators due to phonon tunneling. *Physical Review B*, *77*(24), 1–31.

Wilson-Rae, I., Barton, R., Verbridge, S., Southworth, D., Ilic, B., Craighead, H., & Parpia, J. (2011). High-Q Nanomechanics via Destructive Interference of Elastic Waves. *Physical Review Letters*, *106*(4), 1–4.

Won, Y., Gao, Y., Panzer, M.A., Xiang, R., Maruyama, S., Kenny, T.W., Cai, W., and Goodson, K.E., (2013), Zipping Entanglement, and the Elastic Modulus of Aligned Single-Walled Carbon Nanotube Films, *Proceedings of the National Academy of Sciences*, 110, 20426-20430.

Xiao, S. (2004). A bridging domain method for coupling continua with molecular dynamics. *Computer Methods in Applied Mechanics and Engineering*, *193*(17-20), 1645–1669.

Yakobson, B., Brabec, C., & Berhnolc, J. (1996). Nanomechanics of carbon tubes: Instabilities beyond linear response. *Physical Review Letters*, *76*(14), 2511–2514.

Yu, M.-F., Wagner, G., Ruoff, R., & Dyer, M. (2002). Realization of parametric resonances in a nanowire mechanical system with nanomanipulation inside a scanning electron microscope. *Physical Review B*, *66*(7), 1–4.

Zhang, X., Hu, M., & Poulikakos, D. (2012). A Low-Frequency Wave Motion Mechanism Enables Efficient Energy Transport in Carbon Nanotubes at High Heat Fluxes. *Nano Letters*, *12*, 3410–3416.

Zhigilei, L., Wei, C., & Srivastava, D. (2005). Mesoscopic model for dynamic simulations of carbon nanotubes. *Physical Review B*, *71*(16), 165417.

Zhou, M. (2003). A new look at the atomic level virial stress: on continuum-molecular system equivalence. *Proceedings of the Royal Society A: Mathematical, Physical and Engineering Sciences*, *459*(2037), 2347–2392.

Ziman, J. M. (1960). *Electrons and Phonons*. OXFORD, University Press Inc., New York.

Zimmerman, J. A., Webb III, E. B., Hoyt, J.J., Klein, P. A. & Bammann, D. J. (2004), Calculation of stress in atomistic simulation. *Modeling and Simulation in Materials Science and En*gineering, 12(2004), S319-S332.

Appendix I: Derivation of Governing Equation and Fitting Graphs

From the Euler-Lagrangian equation which has the strain energy over this assumption, the non-dimensionalized nonlinear equation for cantilever beam motion is derived as followings:

$$u_{,tt} + \frac{I}{AL^2}(u_{,ssss} - \beta\pi^2 u_{,ss}) - \frac{1}{2}u_{,ss}\int_0^1 \{(u_{,s})^2 + (v_{,s})^2\}ds = 0, \tag{1}$$

$$v_{,tt} + \frac{I}{AL^2}(v_{,ssss} - \beta\pi^2 v_{,ss}) - \frac{1}{2}v_{,ss}\int_0^1 \{(u_{,s})^2 + (v_{,s})^2\}ds = 0, \tag{2}$$

where,

$$s = z/L \qquad \tau = (t\ L)\sqrt{E/\rho} \qquad u = u_0/L \qquad v = v_0/L,$$
$$\beta = \epsilon_0/\epsilon_{cr} \qquad I = \int\int_A y^2 dA$$

Equation for suspended condition with fixed-fixed boundary is identical to above equations. Derivation from the given strain energy is in next sub section. The solution of the above equation of motion has two versions, one is original version from Ho (1976) and the other version, which is reproduced in Sec. 0.2. The analytic solution derivation is introcued as part of dissertation for its integrity and for discussing further works using Eq. (1) and Eq. (2).

1 Governing Equation

The deformation caused by transverse mode is assumed to follow Euler-Bernouill beam model, which makes the displacement along axis x and y are the function of z. The tube axis is z axis. The expression for displacement become:

$$\overline{u} = u(z,t), \tag{3}$$

$$\overline{v} = v(z,t), \tag{4}$$

$$\overline{w} = w(z,t) - xu_z - yv_z, \tag{5}$$

The Green lagrangian strain from the displacement above, becomes as below:

$$\epsilon_{zz} = \overline{w}_z + \frac{1}{2}(\overline{u}_z^2 + \overline{v}_z^2 + \overline{w}_z^2) \tag{6}$$

$$= w_z + \epsilon_0 - xu_{zz} - yv_{zz} + \frac{1}{2}(\overline{u}_z^2 + \overline{v}_z^2).$$

From the strain as Eq. (5), the potential energy can be expressed as part of Lagrangian as below:

$$L = \frac{\mu}{2}\left(u_t^2 + v_t^2\right) - \frac{1}{2}\int E\epsilon_{zz}^2 dA \tag{7}$$

$$= \frac{\mu}{2}\left(u_t^2 + v_t^2\right) - \frac{1}{2}E\left(Iu_{zz}^2 + Iv_{zz}^2 + \frac{1}{4}u_z^4 + \frac{1}{4}v_z^4 + u_z^2 v_z^2\right) dA \tag{8}$$

The momentum along z axis and second order of $w_{,z}$ are ignored. From Lagrangian above, motion of equation is derived from the Euler-lagrangian equation as below:

$$\frac{\partial L}{\partial f_i} + \sum (-1)^j \frac{\partial^j}{\partial x_{\mu_1} \cdots \partial x_{\mu_j}} \left(\frac{\partial L}{\partial f_{i,\mu_1 \cdots \mu_j}}\right) = 0 \tag{9}$$

The full expression for each motion of equation along axis x and y are like followings:

$$\frac{\partial L}{\partial u} - \frac{\partial}{\partial t}\left(\frac{\partial L}{\partial u_t}\right) - \frac{\partial}{\partial z}\left(\frac{\partial L}{\partial u_z}\right) + \frac{\partial^2}{\partial z^2}\left(\frac{\partial L}{\partial u_{zz}}\right) = 0, \tag{10}$$

$$\frac{\partial L}{\partial v} - \frac{\partial}{\partial t}\left(\frac{\partial L}{\partial v_t}\right) - \frac{\partial}{\partial z}\left(\frac{\partial L}{\partial v_z}\right) + \frac{\partial^2}{\partial z^2}\left(\frac{\partial L}{\partial v_{zz}}\right) = 0 \tag{11}$$

$$\frac{\partial L}{\partial w} - \frac{\partial}{\partial t}\left(\frac{\partial L}{\partial w_t}\right) - \frac{\partial}{\partial z}\left(\frac{\partial L}{\partial w_z}\right) + \frac{\partial^2}{\partial z^2}\left(\frac{\partial L}{\partial w_{zz}}\right) = 0 \tag{12}$$

Due to the nonlinear term from Green-lagrangian strain term in Eq. (5), the $w_{,z}$ and $w_{,zz}$ are remained with y and v as below:

$$-\mu u_{\tau\tau} + \frac{1}{2}\left(3u_s^2 u_{ss} + 2w_{ss}u_s + 2w_s u_{ss} + u_{ss}v_s^2 + 2u_s v_s v_s s\right) - \frac{I}{AL^2}u_{ssss} = 0 \tag{13}$$

$$-\mu v_{\tau\tau} + \frac{1}{2}\left(3v_s^2 v_{ss} + 2w_{ss}v_s + 2w_s v_{ss} + v_{ss}u_s^2 + 2v_s u_s u_s s\right) - \frac{I}{AL^2}v_{ssss} = 0 \tag{14}$$

As neglecting the momentum along z axis from Eq. (12), the strain condition of w_z becomes as followings:

$$\left(w_s + \frac{1}{2}u_s^2 + \frac{1}{2}v_s^2\right)_s = 0 \tag{15}$$

As expand above, $w_{,s}$ and $w_{,ss}$ becomes the term of u and v as below:

$$w_{ss} = -u_s u_s s - v_s v_s s, \tag{16}$$

$$w_s = C - \frac{1}{2}u_s^2 - \frac{1}{2}v_s^2, \tag{17}$$

The constant C from the integration is resolved as giving one more integration in Eq. (17) with the thermal expansion ϵ as below:

$$\int_0^1 w_s = \epsilon_0 - 0 = C - \frac{1}{2}\int \left(u_s^2 + v_s^2\right) ds. \tag{18}$$

$$w_s = \epsilon_0 + \frac{1}{2}\int \left(u_s^2 + v_s^2\right) ds - \frac{1}{2}u_s^2 - \frac{1}{2}v_s^2 \tag{19}$$

As substituting Eq. (18) and Eq. (19) to Eq.(13) and Eq.(14), the governing equation as below is completed.

$$\mu u_{\tau\tau} - \epsilon_0 u_{ss} - \frac{1}{2}\int \left(u_s^2 + v_s^2\right) u_{ss} + \frac{I}{AL^2} u_{ssss} = 0, \tag{20}$$

$$\mu v_{\tau\tau} - \epsilon_0 v_{ss} - \frac{1}{2}\int \left(u_s^2 + v_s^2\right) v_{ss} + \frac{I}{AL^2} v_{ssss} = 0. \tag{21}$$

2 Analytic Solution

From Galerkin method, the variables for wave vector and time are separated as below:

$$u = \sum_{m=1}^{\infty} \sin\left(\frac{m\pi}{2}s\right)\xi_m(\tau), \tag{22}$$

$$v = \sum_{n=1}^{\infty} \sin\left(\frac{n\pi}{2}s\right)\eta_n(\tau), \tag{23}$$

,here, m and n are the notation for the displacement caused by mth or nth mode. Substituting above condition into the governing eq. becomes followings:

$$\frac{d^2\xi}{d\tau^2} + P_x\xi + \frac{\pi^4}{4}[\sum_{j=1}^{\infty}(\xi_j^2 + \eta_j^2)j^2]\xi = 0, \tag{24}$$

$$\frac{d^2\eta}{d\tau^2} + P_y\eta + \frac{\pi^4}{4}[\sum_{j=1}^{\infty}(\xi_j^2 + \eta_j^2)j^2]\eta = 0, \tag{25}$$

,here, j is mode number in last nonlinear term. The wave vector higher than 1st transverse mode will be neglected in following lines. Since the motion in 1st mode governs most of the motion, we ignore the interaction between different order of modes. The equation becomes :

$$\frac{d^2\xi}{d\tau^2} + P_x\xi + \frac{\pi^4}{4}(\xi^2 + \eta^2)\xi = 0, \tag{26}$$

$$\frac{d^2\eta}{d\tau^2} + P_y\eta + \frac{\pi^4}{4}(\xi^2 + \eta^2)\eta = 0. \tag{27}$$

As the same approach with Ho 1976, to solve nonlinear differential equations, one can assum very small coeficient ϵ to describe the variable as $\xi = \sqrt{\epsilon}x$ and $\eta = \sqrt{\epsilon}y$ so that the second order of terms can be gathered as ϵ. Then the equation becomes :

$$\frac{d^2x}{d\tau^2} + \omega^2 x + \frac{\epsilon\pi^4}{4}\left(x^2 + y^2 + \frac{4\Gamma_x}{\pi^4}\right)x = 0, \tag{28}$$

$$\frac{d^2y}{d\tau^2} + \omega^2 y + \frac{\epsilon\pi^4}{4}\left(x^2 + y^2 + \frac{4\Gamma_y}{\pi^4}\right)y = 0. \tag{29}$$

Each parameter such as amplitude and phase is defined to be the function of time and suppose the displacements which is not described by this condition has another frequency and note them as the function g and h for X and Y axis, respectively. x and y can be expressed as below:

$$x = a(\tau)\cos\left(\omega\tau + \theta(\tau)\right) + \epsilon g, \tag{30}$$

$$y = b(\tau)\cos\left(\omega\tau + \phi(\tau)\right) + \epsilon h. \tag{31}$$

Although Eq. (31) is not same as what Ho et al.(1976) presented, the result of derivation is identical. As substituting the above two homogeneous solution into the simplified governing equation Eq. (30) and Eq. (31), the terms with ϵ becomes as followings:

$$\epsilon\frac{d^2g}{d\tau^2} + \epsilon\omega^2 g - 2\frac{da}{d\tau}\omega\sin(\omega\tau+\theta) - 2\frac{d\theta}{d\tau}\omega a\cos(\omega\tau+\theta) - \frac{\epsilon\pi^4}{4}a\cos(\omega\tau+\theta)\left(a^2\cos^2(\omega\tau+\theta) + b^2\cos^2(\omega\tau+\phi) + \frac{4\Gamma}{\pi^4}\right) = 0 \tag{32}$$

$$\epsilon\frac{d^2h}{d\tau^2} + \epsilon\omega^2 h - 2\frac{db}{d\tau}\omega\sin(\omega\tau+\phi) - 2\frac{d\phi}{d\tau}\omega b\cos(\omega\tau+\phi) - \epsilon\frac{\pi^4}{4}b\cos(\omega\tau+\phi)\left(a^2\cos^2(\omega\tau+\theta) + b^2\cos^2(\omega\tau+\phi) + \frac{4\Gamma}{\pi^4}\right) = 0 \tag{33}$$

By assuming the periodicity on each parameter, a,b,θ and ϕ, the time derivative for each parameter $da/d\tau$ and $d\theta/d\tau$ is expressed as below in the equation merged with ϵ :

$$da/d\tau = \epsilon A^{(1)}(a,b,\theta,\phi) + \epsilon^2 A^{(1)}(a,b,\theta,\phi)..., \tag{34}$$

$$db/d\tau = \epsilon B^{(1)}(a,b,\theta,\phi) + \epsilon^2 B^{(1)}(a,b,\theta,\phi)..., \tag{35}$$

$$d\theta/d\tau = \epsilon C^{(1)}(a,b,\theta,\phi) + \epsilon^2 C^{(1)}(a,b,\theta,\phi)..., \tag{36}$$

$$d\phi/d\tau = \epsilon D^{(1)}(a,b,\theta,\phi) + \epsilon^2 D^{(1)}(a,b,\theta,\phi)..., \tag{37}$$

The nonlinear term in Eq.(32) can be decoupled from the variable $\omega\tau$ by using following condition:

$$\cos^2(\omega\tau+\phi)\cos(\omega\tau+\theta) = -\frac{1}{4}\sin(2\phi-2\theta)\sin(\omega\tau+\theta) + \frac{1}{4}(\cos(2\phi-2\theta)+2)\cos(\omega\tau+\theta) - \frac{1}{4}\cos(3\omega\tau+2\phi+\theta), \quad (38)$$

In case of Eq.(33), it can be decoupled by following condition :

$$\cos^2(\omega\tau+\theta)\cos(\omega\tau+\phi) = \frac{1}{4}\sin(2\phi-2\theta)\sin(\omega\tau+\theta) - \frac{1}{4}(\cos(2\phi-2\theta)+2)\cos(\omega\tau+\theta) + \frac{1}{4}\cos(3\omega\tau+2\phi+\theta) \quad (39)$$

For both cases, particular trigonometic condition is essential as below:

$$\cos^3(\omega\tau+\theta) = \frac{1}{4}(3\cos(\omega\tau+\theta)+\cos(3\omega\tau+\theta)). \quad (40)$$

As substituting above into Eq. (32), the function g becomes as below :

$$\begin{aligned} \frac{d^2g}{d\tau^2} + \omega^2 g = \\ 2\omega A\sin(\omega\tau+\theta) + 2\omega Ca\cos(\omega\tau+\theta) - \\ \frac{\pi^4}{4}\left(a^3\cos^3(\omega\tau+\theta) + ab^2\cos(\omega\tau+\theta)\cos^2(\omega\tau+\phi) + \frac{4\Gamma}{\pi^4}\right) \\ = (2\omega A + \frac{q}{4}ab^2\sin(2\Phi))\sin(\omega\tau+\theta) + \\ (2a\omega C + \frac{3}{4}a^3 + \frac{q}{4}ab^2(2+\cos 2\Phi))\cos(\omega\tau+\theta) + \\ \frac{1}{4}cos(3\omega\tau+\theta)) + \frac{1}{4}ab^2\cos(3\omega\tau+2\phi+\theta) \end{aligned} \quad (41)$$

As substituting Eq. (39) and (40) into Eq. (33), the function h should be as below :

$$\begin{aligned}\frac{d^2h}{d\tau^2} + \omega^2 h = \\ 2\omega A\sin(\omega\tau+\phi) + 2\omega Ca\cos(\omega\tau+\phi) - \\ \frac{\pi^4}{4}\left(a^3\cos^3(\omega\tau+\phi) + ab^2\cos(\omega\tau+\phi)\cos^2(\omega\tau+\theta) + \frac{4\Gamma}{\pi^4}\right) \\ = (2\omega A + \frac{q}{4}ab^2\sin(2\Phi))\sin(\omega\tau+\phi) + \\ (2a\omega C + \frac{3}{4}a^3 + \frac{q}{4}ab^2(2+\cos 2\Phi))\cos(\omega\tau+\phi) + \\ \frac{1}{4}b^3\cos(3\omega\tau+\phi)) + \frac{1}{4}a^2b\cos(3\omega\tau+2\theta+\phi)\end{aligned} \tag{42}$$

If the bending motion with frequency ω is described by first terms in Eq. (41) and Eq. (42), the components of g and h should be free from $\cos(\omega\tau)$ or $\sin(\omega\tau)$. The condition for each variable to satisfy this are like followings:

$$da/d\tau = \epsilon A = -(\epsilon/8\omega)qb^2a\sin(2\phi-2\theta), \tag{43}$$

$$db/d\tau = \epsilon B = (\epsilon/8\omega)qa^2b\sin(2\phi-2\theta), \tag{44}$$

$$d\theta/d\tau = \epsilon C = (\epsilon/2\omega)\{\Gamma + (3/4)qa^2 + (1/4)qb^2[2+\cos(2\phi-2\theta)]\}, \tag{45}$$

$$d\phi/d\tau = \epsilon D = (\epsilon/2\omega)\{\Gamma + (3/4)qb^2 + (1/4)qa^2[2+\cos(2\phi-2\theta)]\}, \tag{46}$$

From Eq. (43) and Eq. (44), it is shown that the square of a and b should be constant.

$$ada_m/d\tau + bdb_n/d\tau = d(a^2+b^2)/d\tau = 0, \tag{47}$$

$$a^2 + b^2 = c_1^2. \tag{48}$$

From the Eq. (48), Eq. (45) and Eq. (46) become :

$$d\theta/d\tau = (\epsilon/2\omega)\{\Gamma + (3/4)qc_1^2 - (1/2)qb^2\sin^2\Phi\}, \tag{49}$$

$$d\phi/d\tau = (\epsilon/2\omega)\{\Gamma + (3/4)qc_1^2 - (1/2)qa^2\sin\Phi\}. \tag{50}$$

,here, $\Phi = \phi_n - \theta_m$.

By dividing Eq.(45) and Eq.(46) with the $a = \sqrt{C}\cos\chi$ and $b = \sqrt{C}\sin\chi$, then :

$$d\theta\{\Gamma + (3/4)qc_1^2 - (1/2)qa^2\sin^2\Phi\} = d\phi\{\Gamma + (3/4)qc_1^2 - (1/2)qb^2\sin^2\Phi\}, \tag{51}$$

$$d\Phi\{\Gamma + (3/4)qc_1^2\} = -(1/2)q\{b^2d\phi - a^2d\theta\}\sin^2\Phi, \tag{52}$$

The expression $\{b^2d\phi - a^2d\theta\}$in the last term in Eq. (52) are organized with following expressions:

$$b^2d\phi - a^2d\theta = -\frac{\epsilon}{2\omega}\{\Gamma + (3/4)qc_1^2\}\cos 2\chi d\tau \tag{53}$$

With assuming $a = c_1 cos\chi$ and $b = c_1 sin\chi$, where χ is unknown function of τ, $d\tau$ becomes function of χ as below:

$$\begin{aligned} da/d\tau &= \sqrt{C}\sin\chi\frac{d\chi}{d\tau} \\ &= \frac{\epsilon}{8\omega}qC\sqrt{C}\sin^2\chi\cos\chi\sin 2\Phi \\ d\tau &= 8\omega d\chi/\epsilon qC\sin\chi\cos\chi\sin 2\Phi, \end{aligned} \tag{54}$$

Then, finally, the integration of Φ is simplified into one equation:

$$\begin{aligned} &\cot\Phi d\Phi = -2\cot 2\chi d\chi \\ &a^2b^2 = c_2^2\csc^2\Phi, \\ &c_2 = Cc_1^2/2. \end{aligned} \tag{55}$$

From Eq. (55), Subtracting Eq. (43) from Eq.(44) with multiplying a and b is expressed as function of Φ and applicable to be integrated as below:

$$\frac{d(a^2-b^2)}{d\tau} = \frac{q}{2\omega}c_2^2\frac{\sin 2\Phi}{\cos^2\Phi} = \frac{q}{2\omega}c_2^2\frac{2\sin\Phi}{\cos\Phi}. \tag{56}$$

Since (a^2-b^2) is exchangeable with a^2+b^2, $tan\Phi$ becomes like below:

$$(a^2-b^2)^2 = (a^2+b^2)^2 - 4a^2b^2 = c_1^4 - 4a^2b^2 \tag{57}$$

$$\sec^2\Phi = -\frac{1}{4c_2^2}(a^2-b^2)^2 + \frac{c_1^4}{4c_2^2} \tag{58}$$

$$\tan\Phi = (\sec^2\Phi - 1)^{1/2} = (-\frac{1}{4c_2^2}(a^2-b^2)^2 + \frac{c_1^4}{4c_2^2} - 1)^{1/2} \tag{59}$$

We can have the expression of Φ with (a^2-b^2) as subsituting Eq. (57) into Eq. (59).

$$\frac{d(a^2-b^2)}{d\tau} = \frac{q}{\omega}c_2^2\tan\Phi, \tag{60}$$

$$\frac{d(a^2-b^2)}{\tan\Phi} = \frac{d(a^2-b^2)}{\left(-\frac{(a^2-b^2)^2}{4c_2^2} + \frac{c_1^4}{4c_2^2} - 1\right)^{1/2}} = \frac{q}{\omega}c_2^2 d\tau. \tag{61}$$

Integrating Eq. (61) gives us differential equation of $a^2 - b^2$ and τ.

$$\frac{d(a^2-b^2)}{\left(-\frac{(a^2-b^2)^2}{4c_2^2}+\frac{c_1^4}{4c_2^2}-1\right)^{1/2}} = \frac{2c_2 d(a^2-b^2)}{(-(a^2-b^2)^2+c_1^4-4c_2^2)} \tag{62}$$

$$= \frac{2c_2}{(4c_2^2-c_1^4)^{1/2}} \frac{d(a^2-b^2)}{\left(\frac{(a^2-b^2)^2}{c_1^4-4c_2^2}-1\right)^{1/2}} \tag{63}$$

To integrage above equation, let X be like below;

$$X = \frac{(a^2-b^2)}{\sqrt{(c_1^4-4c_2^2)}} \tag{64}$$

Then $a^2 - b^2$ becomes:

$$d(a^2-b^2) = \sqrt{(c_1^4-4c_2^2)}dX, \tag{65}$$

As substituting Eq. (65) into Eq. (61), it becomes the integration along X as following:

$$\frac{2c_2 dX}{\sqrt{X^2-1}} = \frac{q}{\omega}c_2^2 d\tau. \tag{66}$$

Integrating above equation is:

$$\int \frac{dX}{\sqrt{X^2-1}} = \sin^{-1} X = \frac{q}{2\omega}c_2\tau + c_3. \tag{67}$$

Since X becomes function of sin like below;

$$X = \sin\left(\frac{q}{2\omega}c_2\tau + c_3\right), \tag{68}$$

$$= \frac{a^2 - b^2}{\sqrt{(c_1^4 - 4c_2^2)}}.$$

With Eq. (67) (68). we can have function a and b with time variable:

$$a^2 - b^2 = \sqrt{(c_1^4 - 4c_2^2)} \sin\left(\frac{q}{2\omega} c_2 \tau + c_3\right), \tag{69}$$

$$a^2 = \frac{c_1^2}{2} + \sqrt{(c_1^4 - 4c_2^2)} \sin\left(\frac{q}{2\omega} c_2 \tau + c_3\right), \tag{70}$$

$$b^2 = \frac{c_1^2}{2} - \sqrt{(c_1^4 - 4c_2^2)} \sin\left(\frac{q}{2\omega} c_2 \tau + c_3\right). \tag{71}$$

Next is the derivation of θ and ϕ which can be found from the integration of Eq. (49) and Eq. (50). For breif derivation we introcude the derivation of θ only.

Integration of above equation gives following steps:

$$\int \frac{d\theta}{d\tau} d\tau = \int \frac{1}{2\omega} \left(\Gamma + \frac{3}{4} q c_1^2\right) d\tau - \int \frac{q}{4\omega} \frac{b^2}{2} \sin^2 \Phi d\tau \tag{72}$$

$$= \frac{1}{2\omega} \left(\Gamma + \frac{3}{4} q c_1^2\right) \tau - \int \frac{q}{4\omega} \frac{b^2}{2} \frac{1}{\csc^2 \Phi} d\tau$$

$$= \frac{1}{2\omega} \left(\Gamma + \frac{3}{4} q c_1^2\right) \tau - \int \frac{q}{4\omega} \frac{c_2^2 b^2}{a^2 b^2} d\tau$$

$$= \frac{1}{2\omega} \left(\Gamma + \frac{3}{4} q c_1^2\right) \tau - \int \frac{q}{4\omega} \frac{c_2^2}{a^2} d\tau$$

$$= \frac{1}{2\omega} \left(\Gamma + \frac{3}{4} q c_1^2\right) \tau - \frac{q}{4\omega} \int \frac{c_2 C_0}{1 + \sqrt{1 - C_0^2} \sin(q c_2 \tau / 2\omega + c_3)} d\tau$$

$$= \frac{1}{2\omega} \left(\Gamma + \frac{3}{4} q c_1^2\right) \tau - \tan^{-1} \frac{\sqrt{1 - C_0^2} + \tan(q c_2 \tau / 4\omega + c_3/2)}{C_0}$$

$$\int \frac{d\theta}{d\tau} d\tau = \int \frac{1}{2\omega} \left(\Gamma + \frac{3}{4} q c_1^2\right) d\tau - \int \frac{q}{4\omega} \frac{a^2}{2} \sin^2 \Phi d\tau \tag{73}$$

$$= \frac{1}{2\omega} \left(\Gamma + \frac{3}{4} q c_1^2\right) \tau - \tan^{-1} \frac{-\sqrt{1 - C_0^2} + \tan(q c_2 \tau / 4\omega + c_3/2)}{C_0}$$

3 Graphs for Fitting

Some fitting process using angle difference is displayed. The duration of certain motion among planar and non-planar is the key to decide the C_0. The rotation exchange during the planar motion motion period is disregarded. This condition can be easily distinguished from the rotation exchange of analytic solution in which the angle difference is monotomically reducing. The relatively large amount of angle differece is remained to have certain level of value during the planar motion range, for instance in $0 \sim 10$ ns in Fig. 1 (b). From Fig. 1 to Fig. 8, the comparison between MD simulation and analytic solution is presented as the result of fitting C_0.

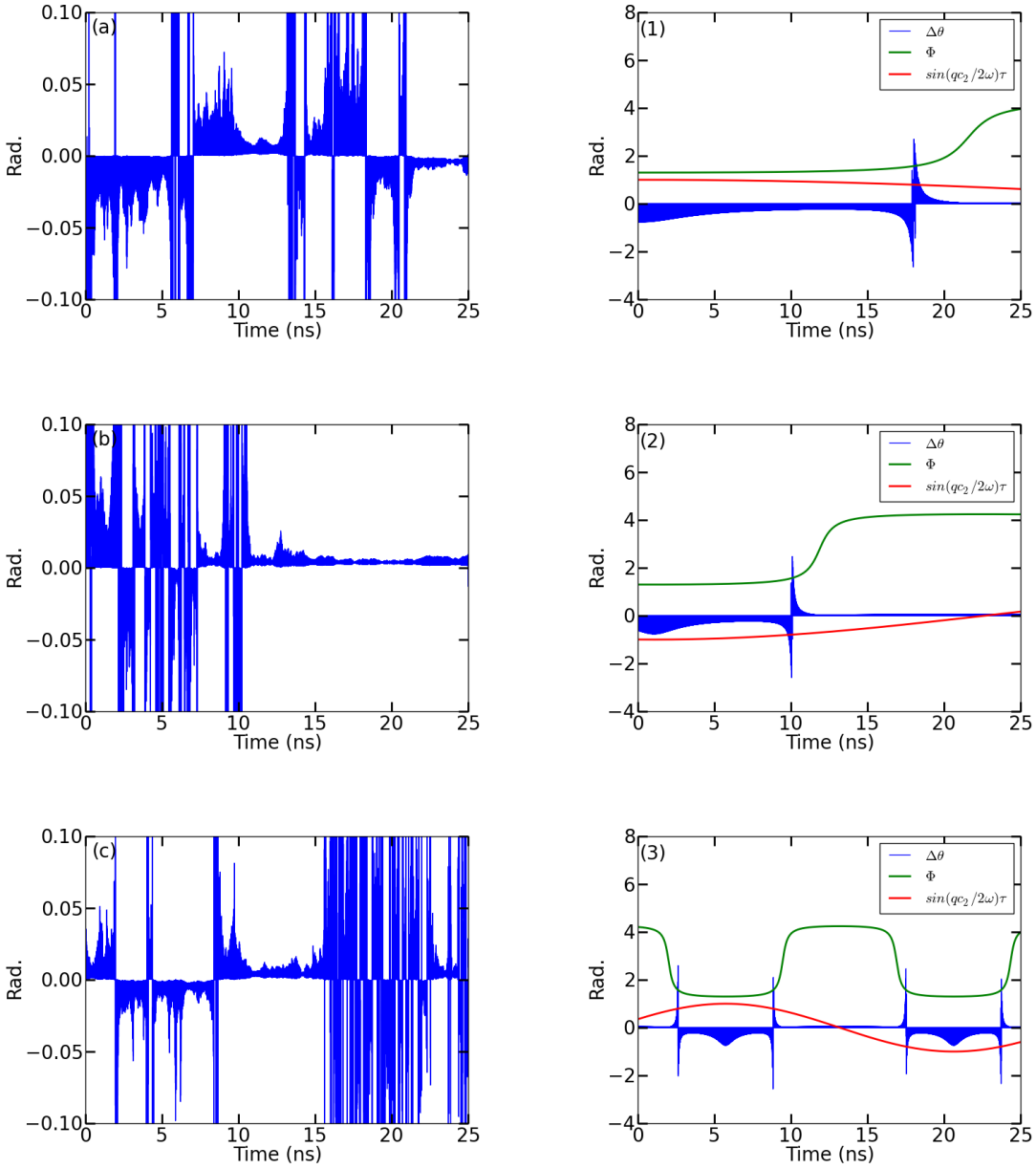

Figure 1: Fitting of (5,5) 4.28 nm, (a)∼(c) are rotation measured from MD simulation and (1)∼(3) are measured result from analytic solution, green line is the phase difference between x and y axis and red line is beating term for the amplitude of $a(\tau)$ and $b(\tau)$; (a,1) 50 K, (b,2) 100 K (Middle) and (c, 3) 300 K.

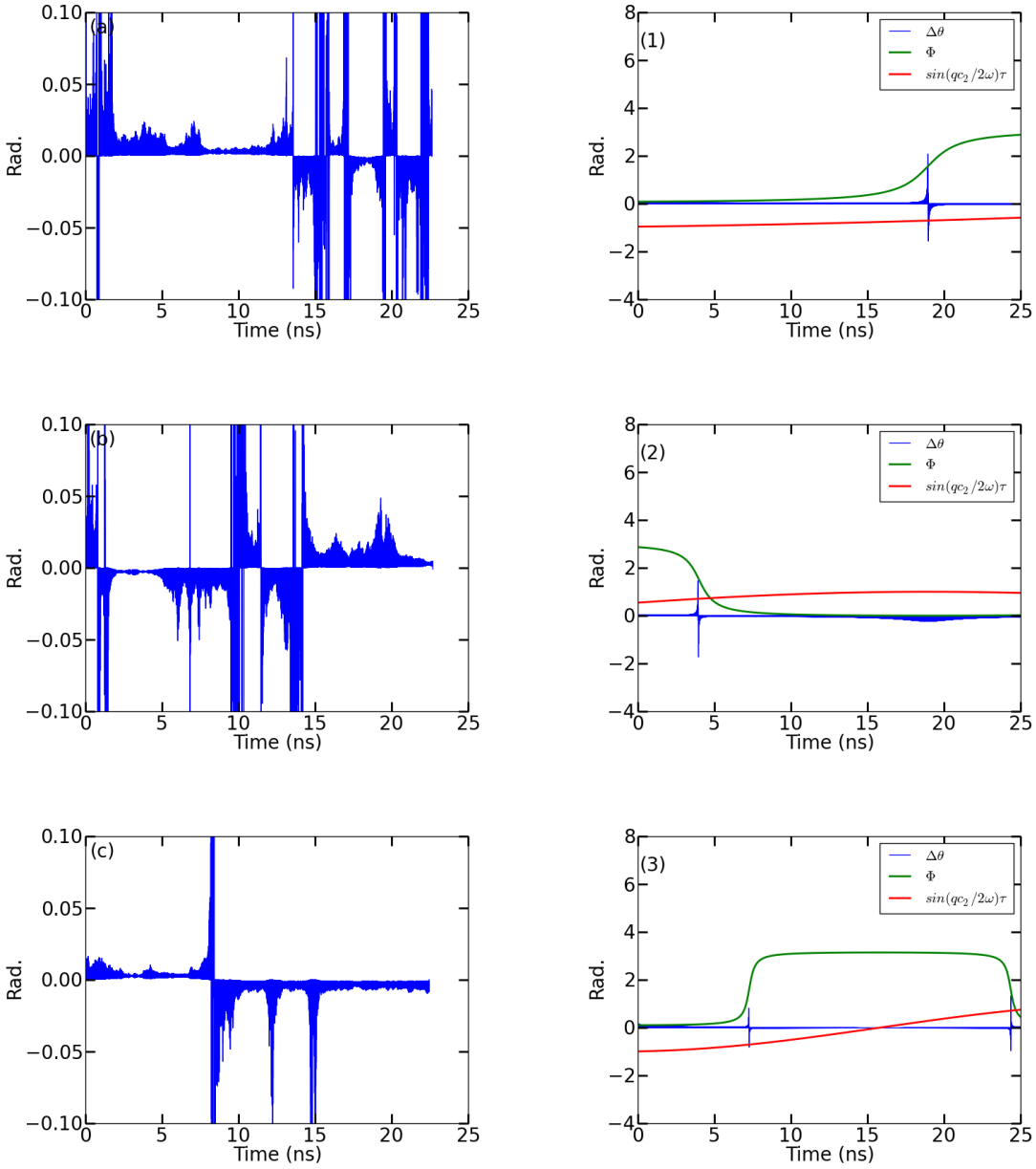

Figure 2: Fitting of (5,5) 5.58 nm, (a)∼(c) are rotation measured from MD simulation and (1)∼(3) are measured result from analytic solution, green line is the phase difference between x and y axis and red line is beating term for the amplitude of $a(\tau)$ and $b(\tau)$; (a,1) 50 K, (b,2) 100 K (Middle) and (c, 3) 300 K.

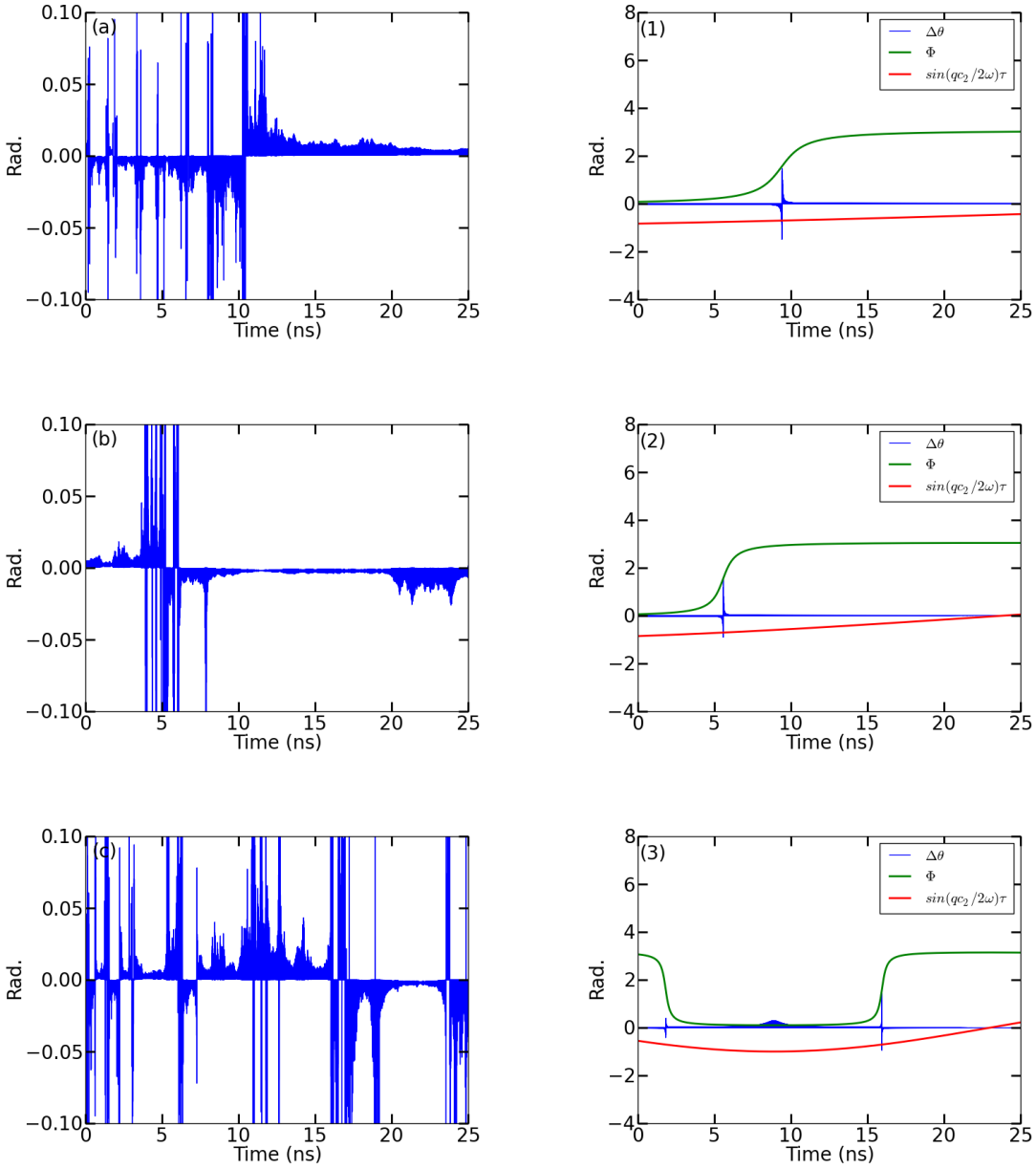

Figure 3: Fitting of (5,5) 6.56 nm, (a) (c) are rotation measured from MD simulation and (1) (3) are measured result from analytic solution, green line is the phase difference between x and y axis and red line is beating term for the amplitude of $a(\tau)$ and $b(\tau)$; (a,1) 50 K, (b,2) 100 K (Middle) and (c, 3) 300 K

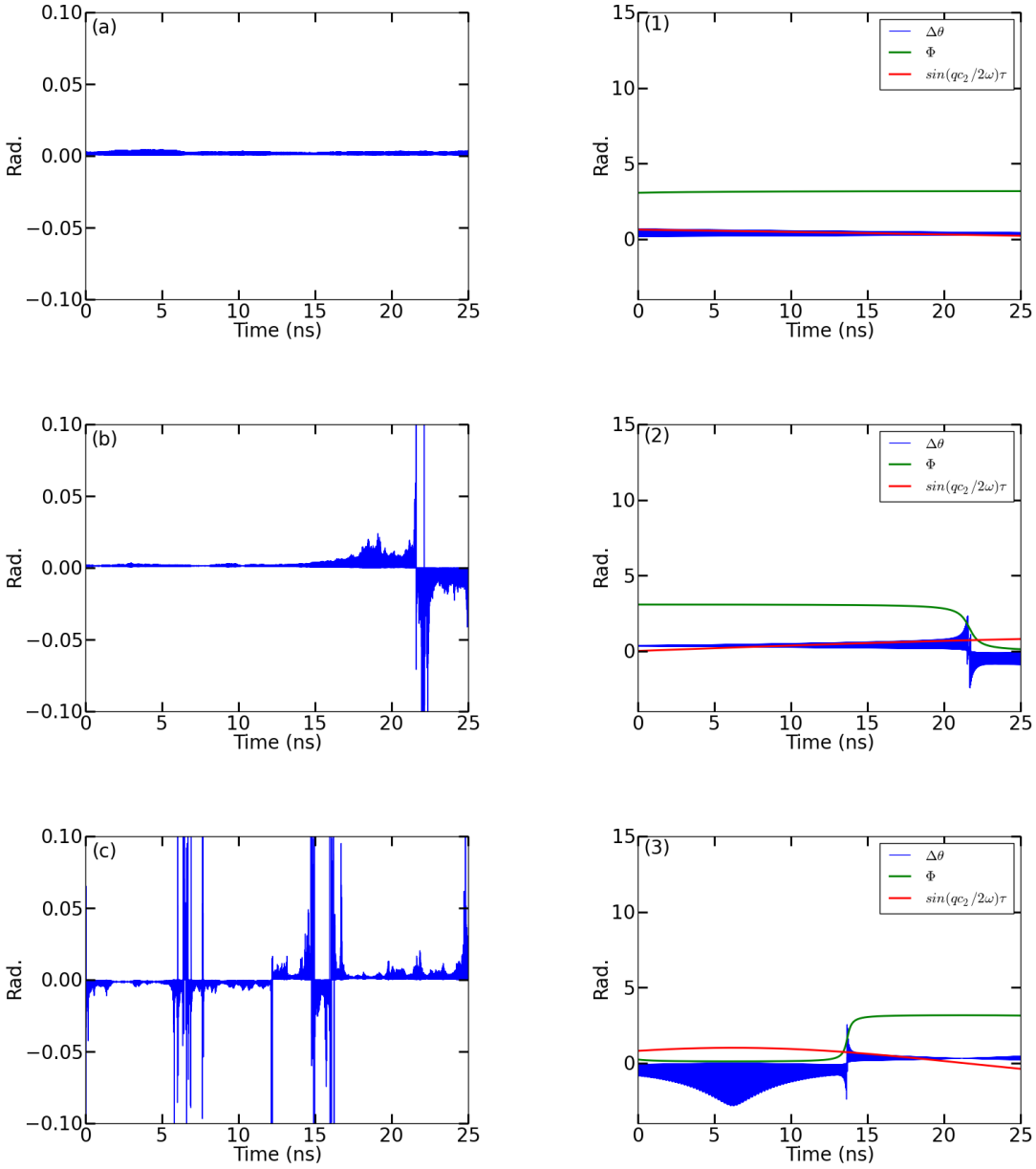

Figure 4: Fitting of (5,5) 7.6 nm, (a)∼(c) are rotation measured from MD simulation and (1)∼(3) are measured result from analytic solution, green line is the phase difference between x and y axis and red line is beating term for the amplitude of $a(\tau)$ and $b(\tau)$; (a,1) 50 K, (b,2) 100 K (Middle) and (c, 3) 300 K

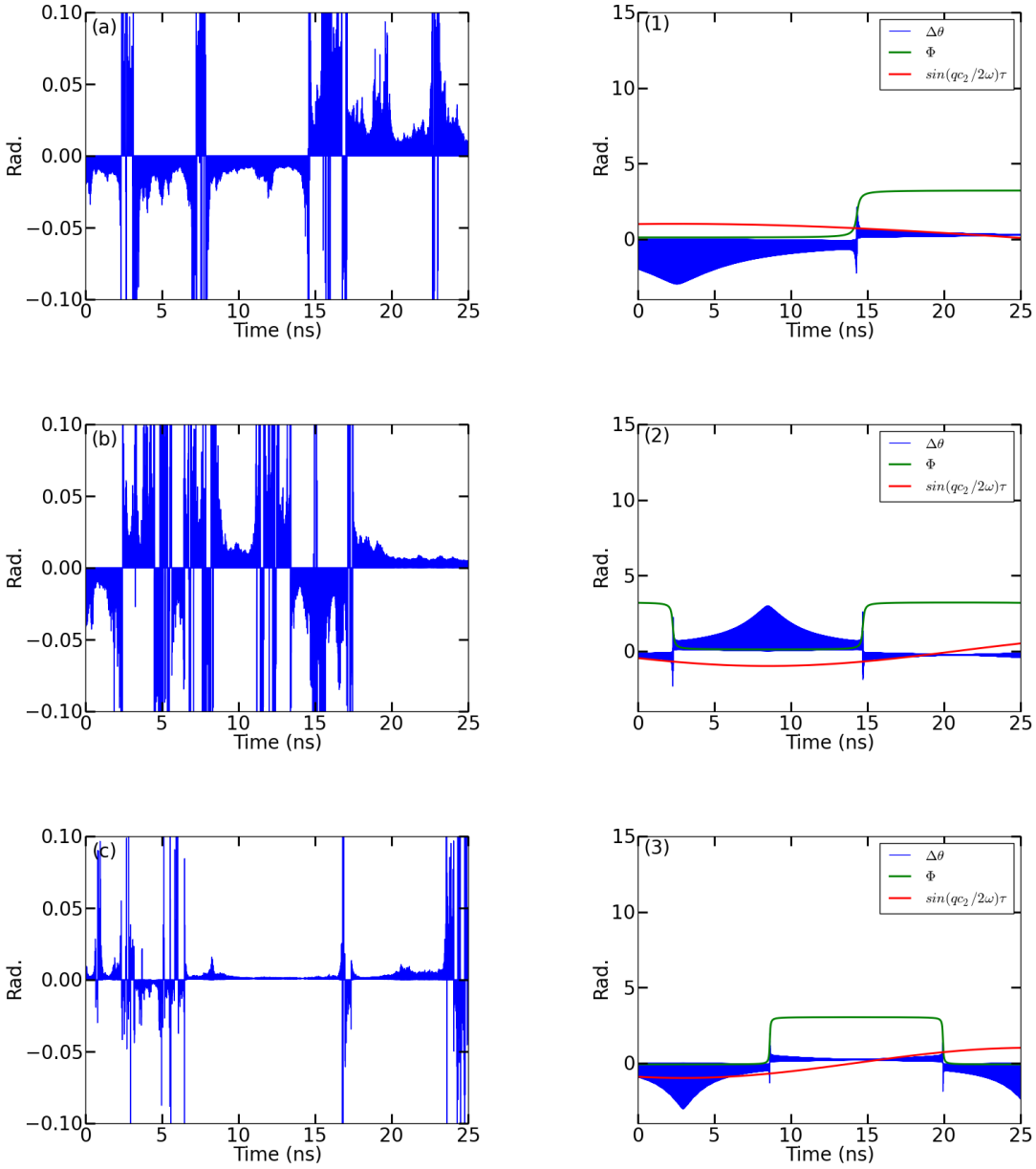

Figure 5: Fitting of (5,5) 9.8 nm, (a)∼(c) are rotation measured from MD simulation and (1)∼(3) are measured result from analytic solution, green line is the phase difference between x and y axis and red line is beating term for the amplitude of $a(\tau)$ and $b(\tau)$; (a,1) 50 K, (b,2) 100 K (Middle) and (c, 3) 300 K

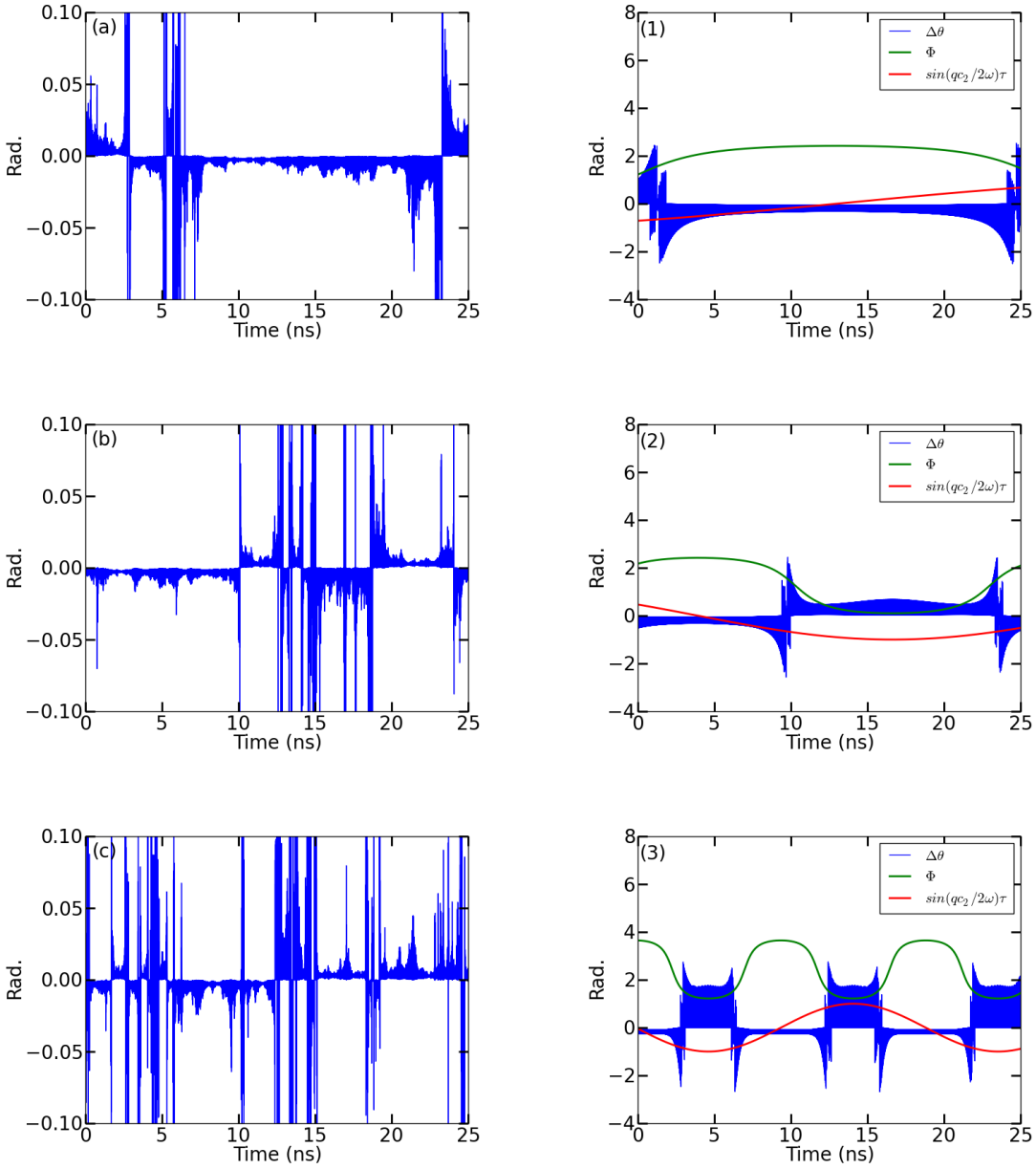

Figure 6: Fitting of (10,10) 7.6 nm, (a)∼(c) are rotation measured from MD simulation and (1)∼(3) are measured result from analytic solution, green line is the phase difference between x and y axis and red line is beating term for the amplitude of $a(\tau)$ and $b(\tau)$; (a,1) 50 K, (b,2) 100 K (Middle) and (c, 3) 300 K

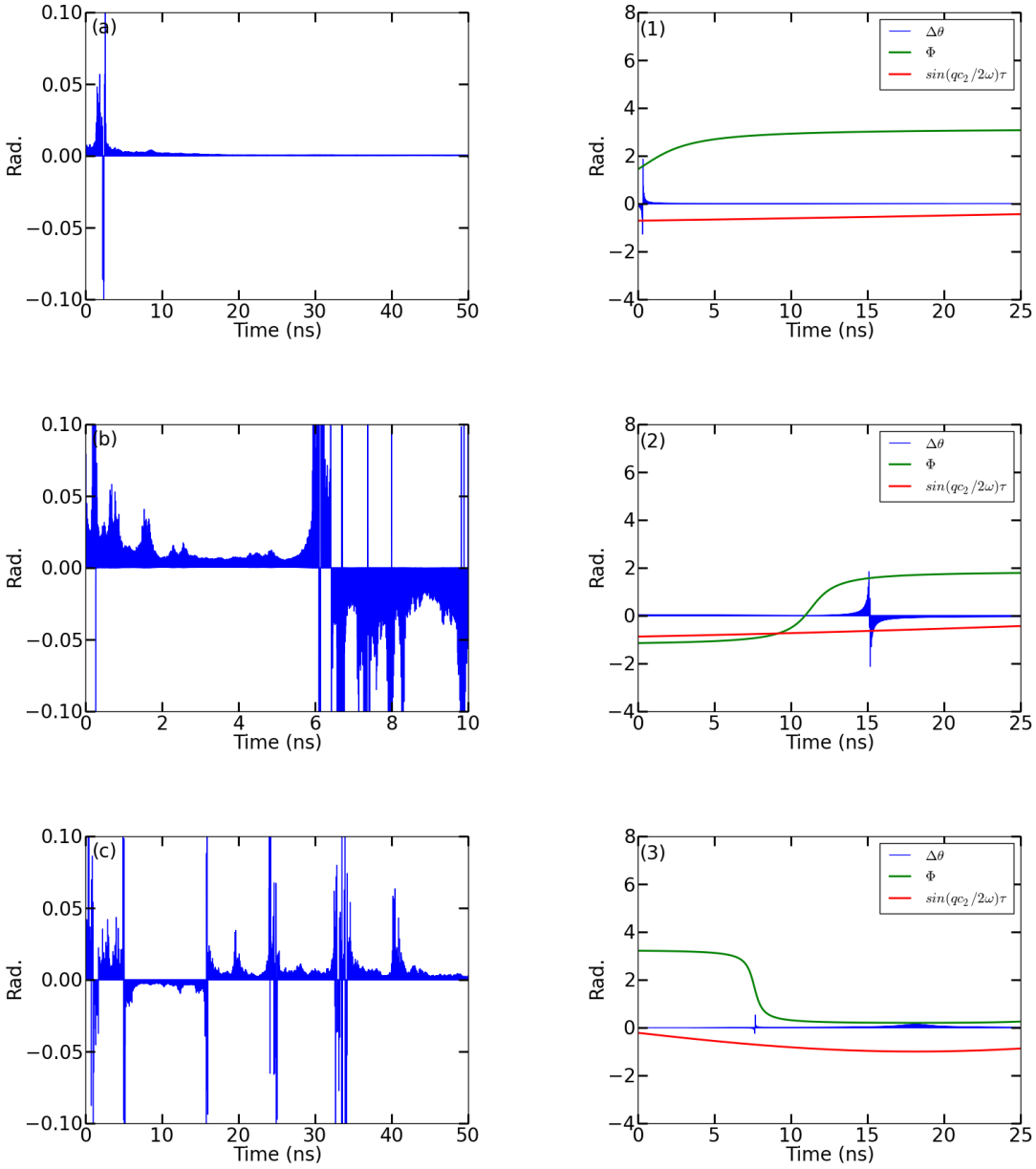

Figure 7: Fitting of (10,10) 23.5 nm, (a)∼(c) are rotation measured from MD simulation and (1)∼(3) are measured result from analytic solution, green line is the phase difference between x and y axis and red line is beating term for the amplitude of $a(\tau)$ and $b(\tau)$; (a,1) 50 K, (b,2) 100 K (Middle) and (c, 3) 300 K

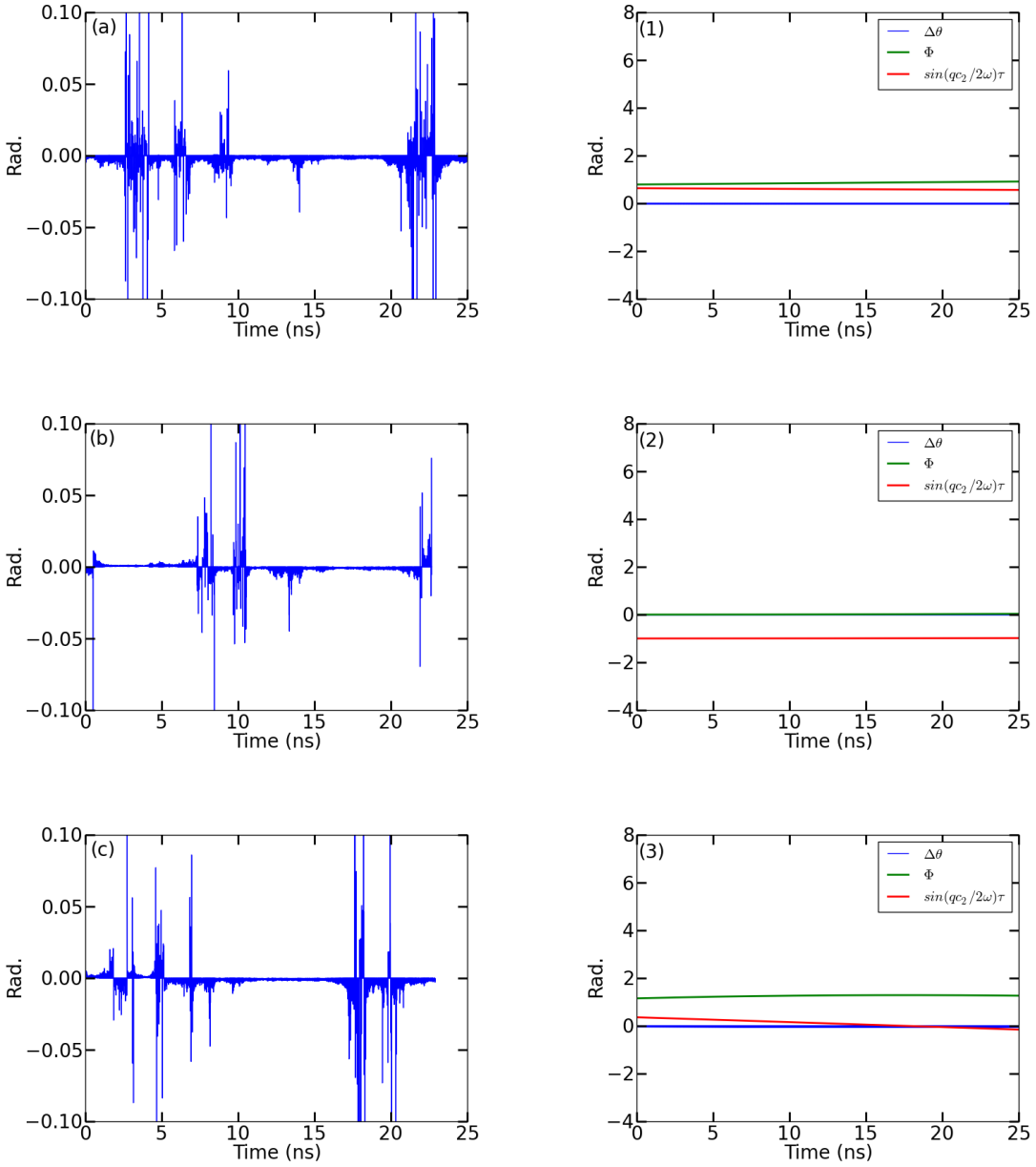

Figure 8: Fitting of (20,20) 23.5 nm, (a)∼(c) are rotation measured from MD simulation and (1)∼(3) are measured result from analytic solution, green line is the phase difference between x and y axis and red line is beating term for the amplitude of $a(\tau)$ and $b(\tau)$; (a,1) 50 K, (b,2) 100 K (Middle) and (c, 3) 300 K

Appendix 2. Preparation of initial condition from beads model for CGMD simulation

As the motion of SWNT is explained from continuum mechanics, a model with averaging the displacement and velocity of each unit cell has been examined with conventional CGMD algorithm so that the thermal vibration dictated by harmonic motion with two kinds of spring.

The purpose is to check the most simplified model, which is simplified into one string without its volume, has enough the degree of freedom for free thermal vibration of molecular system.

The beads model is come from 300K of (5,5) 7.6 nm SWNT. The displacement and velocity at every atom in SWNT should be conserved with same time step. It is 50 fs in this thesis. After averaging the displacement and velocity for each node, typically a half unit cell in this thesis, its node length is calculated. As mentioned, the structure in certain temperature does not follow the length from energy minimized molecular structure. If the node length calculated from minimized energy condition, the Poincare map for CGMD simulation becomes as shown in Fig. A2.1.

Its average value of each node length is in Fig. A2.2. The node length at the bottom and top ring is shorter than rest of nodes due to the influence of lack of sp^2 bonding for boundary atoms.

For 50 K and 300 K, as shown in Fig. A2.3. fluctuation at the boundary rings is ignored and simply averaged value is adapted. This is how the node length is measured and prepared as the condition for CGMD simulation.

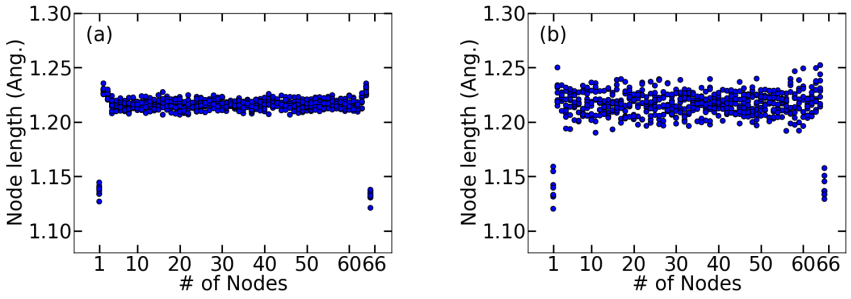

Fig. A2.2. Node length of averaged model of (5,5) SWNT at 50K and 300K.

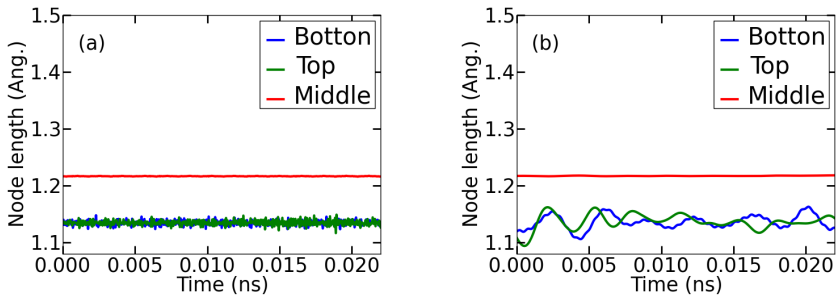

Fig. A2.3 Node lengths measured during couple of ns. Blue line is measured for bottom node, green is from top node and red is the average length of rest. (a) 300K, (b) 50K.

Acknowledgement

During 4 years in Japan, many things have been changed. I feel very thankful about the time I allowed to spend on my interest of research. The question on continuum mechanical regime and its applicability to the molecular system has been an issue, which captured me from senior year of undergraduate school. Although many trials are still in the rest in hard drive, I am satisfied with what I could learn from this opportunity and the possibility of the result to be applied to the next level of understandings.

The most important result of this thesis could be bolstered by the data from Dr. Eichler at CIN2 in Barcelona, I remain a huge appreciation to his kindness. And I also leave the message of gratitude for Dr. Shiga and Dr. Cannon who had helped me a lot for the computing skills, and GMSI Office who supports me with salary and the stay in University of Texas during two months. I also thanks to Prof. Jayathi, Prof. McGaugehey and Prof. Li Shi in University of Texas at Austin for interesting discussions and their kindness. Prof. Shiomi has taught me how to do MD simulation and Prof. Chiashi gave wonderful discussions time to time. I note my gratefulness on them in this acknowledgement. I am also deeply appreciating to Prof. Maruyama for letting me focus to study for the first year of Ph.D period and spending another year to finish the thesis with meaningful result on CGMD.

Lastly, thanks to my family who keep me from a panic and supports with their love, and a special friend who makes me grow a lot during this preparation of Ph.D. I love you all.